An investigation into the fundamentals of trapping and sensing in microstructured photonic crystal fibers

Shinoj Vengalathunadakal Kuttinarayanan

2012

Shinoj, V. K. (2012). An investigation into the fundamentals of trapping and sensing in microstructured photonic crystal fibers. Doctoral thesis, Nanyang Technological University, Singapore.

https://hdl.handle.net/10356/49896

https://doi.org/10.32657/10356/49896

NANYANG TECHNOLOGICAL UNIVERSITY

AN INVESTIGATION INTO THE FUNDAMENTALS OF TRAPPING AND SENSING IN MICROSTRUCTURED PHOTONIC CRYSTAL FIBERS

SHINOJ VENGALATHUNADAKAL KUTTINARAYANAN
SCHOOL OF MECHANICAL AND AEROSPACE ENGINEERING

2012

AN INVESTIGATION INTO THE FUNDAMENTALS OF TRAPPING AND SENSING IN MICROSTRUCTURED PHOTONIC CRYSTAL FIBERS SHINOJ V. K. 2012

AN INVESTIGATION INTO THE FUNDAMENTALS OF TRAPPING AND SENSING IN MICROSTRUCTURED PHOTONIC CRYSTAL FIBERS

SHINOJ VENGALATHUNADAKAL KUTTINARAYANAN

School of Mechanical and Aerospace Engineering

A thesis submitted to the Nanyang Technological University in partial fulfilment of the requirement for the degree of Doctor of Philosophy

2012

Acknowledgement

I take this opportunity to thank my supervisor, Associate Professor V M Murukeshan, for providing me the resources and valuable guidance in conducting this thesis. He continuously inspired me and showed me the right direction to get things on track.

I acknowledge the collaboration with SBIC through Dr. Parasuraman Padmanabhan. I would like to express my sincere thanks to Dr. Saraswathi Padmanabhan for the timely help. I would like to extend my thanks to all the staffs of PAM lab, MEMS lab, PEN centre and Materials Lab-A for arranging lab facilities for the thesis.

I acknowledge the research student support received through NTU. Also, I acknowledge the funding support received through MOE (ARC3/08) and A*STAR-SERC towards the completion of this thesis.

I am deeply indebted to my family for giving their blessings and support for my higher studies. At last, my thanks to my friends in the research circle for their help and encouragement during the course of the thesis project.

Abstract

Ultra sensitive optical manipulation and detection techniques employing specialty fiber optics and tailor made coherent lasers have huge potential in research and development of new generation medical diagnosis systems. Photonic crystal fiber (PCF) is one such specialty fiber that has emerged prominent in recent years and has found to be an efficient medium for sensing or other micro manipulation such as optical trapping or tweezing and promises a noninvasive, non-contact methodology with minimum damage to the living cells. A hollow-core PCF (HC-PCF) can achieve guidance in air by using the Bragg reflection from the periodic fiber cladding structure, and has the potential of being a medium for efficient biosensing application due to the increased light-matter interaction in the hollow-core.

In this perspective, the main objective of the thesis focuses on the research and development of relevant concepts and optical system configuration for:

- detection of target analytes/particles from an extremely low fluorescent sample volume using such microstructured fibers, and
- multifunctional analysis system to perform optical trapping, position sensing, and spectral characterization sequentially and simultaneously.

An efficient fluorescence detection scheme is proposed and illustrated using hollow-core photonic crystal fibers (HC-PCFs) by applying the refractive index (RI) scaling law. Further, an optical method for the recognition of specific protein based on immuno binding is demonstrated using HC-PCF. In this study, estrogen receptor (ER) from a MCF-7 breast carcinoma cell lysates immobilized inside a hollow core photonic crystal fiber was detected using anti-ER primary antibody with either Alexa^{TM} Fluor 488 (Green fluorescent dye) or 555 (Red Fluorescent dye) labeled Goat anti-rabbit IgG as secondary antibody. The fluorescence fingerprints of the ER-alpha protein were observed under fluorescence microscope and its fluorescent signature characteristics were analyzed. It is able to detect $\approx$ 20 pg of ER alpha protein in 50 nL sample volume.

Another set of numerical and experimental investigations are performed on optical trapping applications of HC-PCFs with a transversely probed beam. The

transmission intensity distribution at the central core of liquid filled HC-PCFs are monitored for both TE and TM modes with illumination in the Γ-M direction. Forces acting along the transverse direction on a sphere located inside liquid-filled central core of HC-PCF are calculated using FDTD and Maxwell Stress Tensor based method. An optical trapping system is designed where a near-infrared laser light is focused using a microscope objective to create an optical trap across a liquid-filled HC-PCF. Based on the above principle, a novel multi-functional optical system is developed that is capable of trapping, manipulating, imaging and performing spectral signature characterizations from a micron sized fluorescent sample.

The results of this thesis will enable future HC-PCF based Lab-On-a-Chip (LOC) devices with the ability to potentially trap and detect single biomolecules such as proteins in an extremely low sample volume. Since the system deals with trapping, manipulation, imaging and spectral analysis of micro size particle in aqueous medium, it can be used for studying biochemical changes, single cells, etc. targeting early stage disease diagnosis. Suggestions for extending the application of the developed system by incorporating additional elements are mentioned as future research guidelines at the end of the thesis. It is envisaged that the outcome of this thesis can enable future research and development based on microstructured fibers, such as HC-PCF, for future applications of translational medical applications.

Contents

List of Figures

List of Tables

List of Symbols

Symbol	Definition
a	Core radius
α	Absorbance
σ	Scattering cross-section of the sphere
α^1	Fiber loss
c	Speed of light in vacuum
θ	Angle of incidence
ε	Angle of refraction
ϵ	Electric permittivity
F_{ax}	Axial force
$F_{gradient}$	Gradient force
$F_{scatter}$	Scattering force
$F_{restoring}$	Restoring force
F_{tr}	Transverse force
λ	Wavelength
λ_0	Central wavelength
μ	Magnetic permiability
R	Fresnel coefficient of reflection
ρ	Density of sphere
T	Fresnel coefficient of refraction
n_a	Ambient refractive index
n_b	Background index
n_{co}	Core refractive index
n_{cl}	Cladding refractive index
n_2	Nonlinear refractive index
n_m	Refractive index of medium

γ	Interaction coefficient
I_0	Incoming intensity
I	Transmitted intensity
ν	Frequency
A_{eff}	Effective fiber area
ω_0	Central frequency
$\beta_n s$	Dispersion coefficients at central frequency
h_R	Temporal Raman response
L	Fiber length
P	Laser power
$\vec{P}$	Momentum
$\vec{S}$	Poynting vector
$\vec{T}$	Maxwell stress tensor
$\vec{V}$	Velocity

List of Abbreviations

Abbreviation	Description
2D	Two Dimensional
2D-FDTD	Two Dimensional FDTD
AFM	Atomic Force Microscopy
BS	Beam Splitter
BFP	Back Focal Plane
CCD	Charge Coupled Device
CMOS	Complementary Metal Oxide Semiconductor
CW	Continuous Wave
DEP	Dielectrophoretic
DPSS	Diode-Pumped Solid-State
DC-PCF	Double-Clad Photonic Crystal Fiber
ELISA	Enzyme Linked Immuno Sorbent Assay
EM	Electromagnetic
ESM	Endlessly Single Mode
ER	Estrogen Receptor
EW	Evanescent Wave
FDTD	Finite-Difference Time Domain
GFP	Green Fluorescent Protein
GRIN	Graded Index
HC-PCF	Hollow-Core Photonic Crystal Fiber
IHC	Immunohistochemistry
IR	Infrared
LOC	Lab-On-a-Chip
MO	Microscope Objective
MOF	Microstructured Optical Fiber
μTAS	Micro Total Analysis System

OT	Optical Trap
PBG	Photonic Bandgap
PCF	Photonic Crystal Fiber
QE	Quantum Efficiency
QPD	Quadrant Photodiode
RI	Refractive-Index
RO	Ray Optics
SC	Supercontinuum
SEM	Scanning Electron Microscope
SHG	Second Harmonic Generation
SMF	Single Mode Fiber
STM	Scanning Tunnelling Microscope
TE	Transverse Electric
TIR	Total Internal Reflection
TM	Transverse Magnetic

Chapter 1

Introduction

The chapter begins with the back ground and motivation for undertaking this thesis followed by a brief review on the optical manipulation and detection techniques for biomedical applications. A short note on the limitations of the current methods will be given along with the advantages of the proposed methods incorporating specialty photonic crystal fibers. The scope and main objectives of this thesis will be discussed followed by a block diagram representation of the whole research roadmap planned for meeting the desired objectives of the thesis. The chapter concludes with the organization of the whole thesis.

1.1 Background

Biomedical research mainly focuses on detection, diagnosis, prevention and treatment of disease which ultimately leads to better health. Ultra sensitive detection and imaging methods are enabling current technologies to evolve into a new generation of medical diagnosis techniques [1, 2]. For example, screening for specific antibodies, antigens, hormones, or particular nucleic acid sequences with high sensitivity is of fundamental importance in the early stage diagnosis of bacterial or viral infection and in the detection of genetic disorders or early-stage tumour development. 'Lab-on-a-chip' (LOC) or 'micro total analysis system' (μTAS) is a total analysis system introduced in the early nineties which miniaturized large analytical devices [3, 4]. Here, all sample handling steps are happens extremely close to the place of measurement. The LOC field has developed and diverged with many different applications, such as single cell processing and analysis, biological and chemical analysis, point of care testing and medical diagnostics.

The main component of a miniaturized cell-based 'Lab-on-a-Chip' can be divided mainly into two groups: manipulation and detection units [5]. The ma-

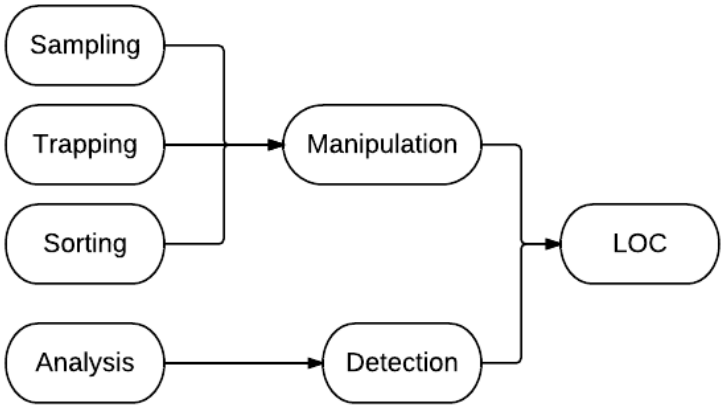

Figure 1.1: Main components of a Cell-based 'lab-on-a-chip' design.

nipulation principally involves the cell sampling, cell trapping and sorting steps. Whereas, the detection module involves chiefly the cell analysis step. In general, microfabricated needles are chosen to be the key component in the cell sampling stage. Cell trapping and sorting is executed by mechanical, electrical, magnetic or optical means, frequently united with flow cytometry systems. Hence, the basic cell-based 'lab-on-a-chip' system can be depicted as in figure 1.1.

Micromanipulation of individual cells is usually carried out using tapered glass micro-pipettes. Such a contact micromanipulator for manipulating a microbe is not only difficult but also has a high risk of damage. Also, it is not possible to use such micropipettes to manipulate cells in a sealed microfluidic device. Hence, the development of non-contact micromanipulation techniques is of high significance for positioning, trapping, and classifying micro objects without damaging them. A number of noncontact micromanipulation techniques have already been proposed [6, 7, 8]. The most promising one is the dynamic micromanipulation using a laser beam with one or more focal points, known as Optical trapping (OT) method. Optical trapping is a non-invasive, non-contact way of manipulation technique that does not cause any damage to the living cells [9, 10]. After the first demonstration of the OT in 1970 [9], it has been successfully used to study biological systems in combination with optical diagnostic techniques like two photon fluorescence and Raman spectroscopy [11]. The applicability of optical tweezers

for cell manipulation has also been shown in other works [12, 13]. Though these systems offer favourable methods for cell manipulation and cultivation, these do not have high-throughput or they require complex setups.

Among the potential detection methods and principles, optical detection is the most common tool in modern chemical and biochemical analysis. Specifically, fluorescence detection establishes to be superior regarding sensitivity and reachable limits of detection [14]. Fluorescent biomarker molecules available in the market can be specifically attached to the relevant sample molecule so as to perform the quantification analysis using fluorescence spectroscopy. Ultrasensitive detection is gaining more potential with the development of the single-molecule detection technique, a laser-based method that allows the detection of single fluorophores in solution [15]. These studies can possibly provide fundamental new information about biological processes and are critical for a better understanding of cellular functions. It is obvious that combining optical trapping (OT) and single-molecule fluorescence would offer a powerful approach to monitor spatial or conformational changes in a temporal manner at the single molecule level. On the other hand, the addition of OT to a single molecular fluorescence experiment can provide the ability to transfer a macromolecule to an area optimized for fluorescence excitation, reducing the background light formed by neighbouring fluorophores [16].

1.2 Motivation

Typically, the micromanipulation and detection tasks require heavy, bulky and/or expensive equipments that involve need for highly qualified personnel. Such a system is not suitable for use in small diagnostic and research laboratories and for distributed point-of care testing. The need for accurate, portable and low cost analytical/diagnostic tools motivates the research and development of LOC. There had been significant advances in LOC technologies in the last two decades, and LOC applications can be regarded as one of the key growth industries of the 21st century. The present work aims to provide new tools for the optical

manipulation and detection of biological samples by integrating optical trapping and microstructured photonic crystal fiber. By incorporating novel principle, the thesis aims to increase the analytical performance of a conventional total analysis system. Furthermore, the reduction in size significantly reduces the consumption of the reagents and makes possible simultaneous multi-functional monitoring with a single device. In the following paragraphs, a short description about the advantages of specialty fiber optics, such as photonic crystal fiber, for Optical Trapping (OT) and detection techniques is given.

The developments in specialty fiber optics and tailor-made coherent lasers have opened up a wide range of applications for trapping, imaging and analysis of biological molecules. The advent of miniaturization of optical and opto-electronic components facilitates the incorporation of novel concepts in trapping and imaging for various biomedical applications. In this background, the thesis focuses on research and investigation into novel multifunctional optical trapping techniques employing specialty microstructured photonic crystal fibers (PCFs). PCFs are one of the most promising specialty fibers that have emerged in recent years and could be engineered to have vastly different properties compared to conventional fibers. Its guiding mechanism is based on the photonic bandgap formed due to its high index contrast (commonly silica and air in optical region) and from the wavelength scale microstructure. The mode propagation properties strongly depend on wavelength, which in turn depends on the design configuration and the geometry of air holes. Unlike conventional fibers, photonic crystal fibers are made of pure silica glass (SiO_2) without any doping. Hence it is biocompatible and chemically inert.

The hollow-core photonic crystal fibers (HC-PCFs) are a class of silica waveguides distinguished by a microstructured cladding of periodic air holes surrounding a hollow air core where the guidance is based on photonic bandgap. It has better sensitivity of samples, arising from high light-matter interaction in the central hollow-core which in turn reduces the sample consumption rate. Apart from sensing applications, the HC-PCF is utilized in another technology known as optoflu-

idics [17], where the photonic structures which are filled with microscopic volumes of fluid provide a different refractive index difference in contrast to the air which naturally fills the voids of the PCF. It promises HC-PCF as an ideal medium for optical trapping studies. So far, most of the work in optofluidic HC-PCFs has been carried out by infiltrating homogenous fluids in the fiber. An important extension to this is the introduction of discrete solid particles into the HC-PCF of varying scales ranging from individual cells to group of microspheres. This may lead to consider HC-PCF as being ideal platform for the investigation into optical manipulation and detection of micron-scaled inorganic or biological species inside the central core.

In this context, the thesis focuses on research and investigation into novel optical trapping and imaging techniques employing specialty microstructured photonic crystal fibers (PCFs) [18]. The main objective is to develop novel multi-functional optical system capable of trapping, manipulating, imaging and spectra analysing using fiber optics. These are expected to overcome the bulk nature of conventional optical trapping methods. Furthermore, the new generation fibers, such as PCFs, allow guiding beyond the optical window of conventional fiber.

1.3 Objective

It can be inferred based on the previous sections that realization of new optical trapping, imaging and spectroscopy techniques based on microstructured waveguides such as photonic crystal fiber is one of the latest research thrust areas. The thesis aims to explore the hollow-core PCF as an efficient nanohole array targeting detection of fluorescent sample in an extremely low sample volume. The fundamental focus of the thesis then aims at the research and development of new optical trapping methods and the combination of it with novel imaging and detection techniques to trap and analyse by exploring the properties of microstructured photonic crystal fiber. The major objectives of this research thesis in this context can be summarized as:

- ⇨ Investigation into the research and development of an efficient biosensing medium to detect target analytes in an extremely low sample volume. The properties of micro-structured hollow-core photonic crystal fibers (HC-PCFs) are explored to meet this objective.

- ⇨ Research and development of a transverse trapping that enable multi-functional analysis such as trapping, imaging, position sensing and fluorescent signature characterization (either sequentially or simultaneously).

These are expected to increase the analytical accuracy and overcome the bulk nature of conventional optical trapping based diagnostic methods.

The following section outlines the scope of the research work carried out to meet these desired objectives.

1.4 Scope

In the case of optical trapping methods or optical tweezers, it was shown that the radiation pressure forces of a focused optical beam can hold and even levitate a small particle, or living cell, in a fluidic medium without physical contact [6]. The method does not involve any mechanical contact, thus avoiding any risk of contamination. Hence it is a minimally invasive/non-invasive method of manipulation that does not cause any damage to the living cells. Thus a living cell can be optically trapped and manipulated without affecting its survivability. The use of optical forces for deflecting particles or living cells through a fluidic channel was first proposed [19] soon after the first demonstrations of optical trapping of living cells [20]. With the growing interest in optical manipulation techniques within fields such as microbiology and medicine, the need to combine the optical tweezers with advanced imaging techniques has increased. It is obvious that combining optical trapping (OT) and single-molecule fluorescence would offer a powerful approach to monitor spatial or conformational changes temporally at the single molecule level. The developments of specialty fiber optics and tailor made coherent lasers

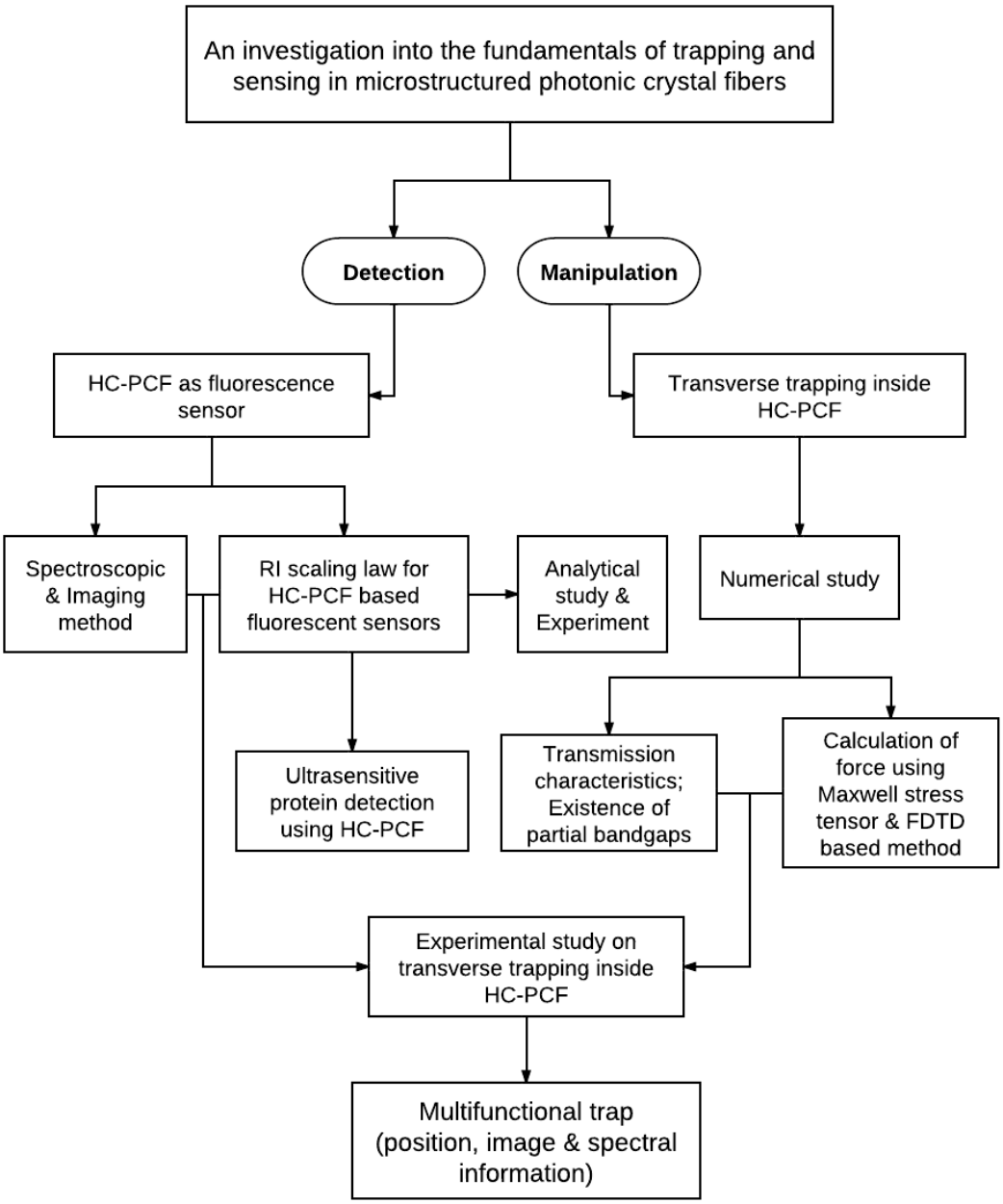

Figure 1.2: The block diagram representation of the whole research methodology implemented for the research thesis.

have opened up a wide range of applications for trapping imaging and analysis of biological molecules. The advent of miniaturization of optical and opto-electronic components facilitates the incorporation of novel concepts in trapping and sensing for various biomedical applications.

The major scope/ expected research contributions can be explained as follows:

1. Investigation on the influence of central wavelength shift on the fluorescence emission intensity in common fluorescence sensing studies employing HC-

PCFs based on refractive index (RI) scaling law.

2. Research and development of a simple optical method for the specific protein detection from extremely low sample volume employing immobilization inside the HC-PCF.

3. Fundamental analysis on the transverse optical trapping mechanism inside the hollow core PCF using Maxwell stress tensor (T) and Finite Difference Time Domain (FDTD) method.

4. Numerical investigation on presence of transverse partial bandgaps in HC-PCF and its influence on the central wavelength and infiltrated material index. The choice of fiber for optical trapping experiment is based on this analytical study.

5. Design and implementation of an optical trapping experimental set up for transverse optical trapping inside HC-PCF.

6. Development of multi-functional analysis system for trapping, imaging, position sensing and fluorescent signature characterization sequentially or simultaneously from a micron sized fluorescent sample.

The block diagram (Figure 1.2) sum ups the research methodology executed for this thesis.

1.5 Organization of report

The whole thesis is divided into five chapters. Each chapter starts with a short note, which reflects on the main contents of that chapter.

Chapter 1 is an introduction chapter which gives a brief outline about the present status of the research problem considered here. The main motivation, scopes and objectives of the thesis are discussed here. A summary regarding the limitations of current optical manipulation and detection techniques are briefly discussed highlighting the need for a new system surpassing the current limitations. A

block diagram representation of the proposed thesis project explaining its methodologies is also presented. The organization of the whole thesis is given in the last section of the chapter.

Chapter 2 gives an overview of the various optical manipulation and detection techniques for the biomedical applications. Detailed description about the optical trapping, detection and manipulation methods are provided along with the theoretical background. The current restriction of these methods is also given. Furthermore, it presents background to the photonic bandgap materials especially photonic crystal fibers. It further discusses the ultrasensitive detection capability of these photonic bandgap fibers. With a view to consider these fibers for optical trapping applications, the transverse propagation in these fibers is also discussed based on the reported works. The outcome of literature review is discussed briefly towards the end of this chapter.

In chapter 3, an efficient fluorescence sensing approach using hollow-core photonic crystal fibers based on refractive index (RI) scaling law is illustrated numerically and experimentally. The variations in the central wavelength for different filling material indices are demonstrated for most commonly available HC-PCFs that have cladding made of pure fused silica with array of air holes running along the entire length of the fiber. The proposed concept is verified by immobilizing fluorescent microsphere samples inside two HC-PCFs of different central wavelengths and the quantification of fluorescence inside the fibers is performed through spectroscopic analysis. The sensitivity has been compared for similar fiber with different dispersed media and different fibers with same dispersed medium. The hollow-core fiber based evanescent sensing is performed for different standard fluorophores followed by sensitivity analysis at various concentrations. The method is then extended to recognize specific protein in extremely low volume of sample based on immune binding.

Chapter 4 illustrates a numerical investigation and experimental study carried out for optical trapping applications with transversely probed HC-PCFs. The

transmission intensity distribution at the central core of liquidfilled HC-PCFs are monitored for both TE and TM modes with illumination in the Γ-M direction. Further experiments are performed on the optical manipulation and detection of micron sized fluorescent sample using optical trapping and HC-PCF is described. An optical trapping system is developed where a near-infrared laser light is focused to create an optical trap across a liquid-filled HC-PCF. The particle is trapped into the system where it undergoes optical analysis. Also it is possible to track the particle into a different medium, again using optical trap created by the same system. Further, a multi-functional optical system is developed using fiber optics that is capable of trapping, manipulating, imaging and spectra-analysing.

Chapter 5, is the last chapter of the thesis, gives the conclusion for the whole thesis along with the guidelines for future works. It explains the important original research contributions made as part of the submitted thesis. All the theoretical and experimental works associated with the proposed research for fulfilling the required objectives are concluded here. Also, certain suggestions are provided for extending the applications areas of the proposed system by incorporating additional elements.

The next chapter overviews the state of the art literature survey relevant to the proposed research topic to identify the potential research gap and required improvement.

Chapter 2

Literature Review

This chapter reviews the earlier work done in the related areas that are relevant to the proposed thesis. The chapter starts with descriptions on various optical manipulation methods with theoretical background. Subsequently, information about the detection methods and the combination of optical manipulation methods with fluorescence detection methods is also given with perspective on employing the system for biomedical applications. Also, it provides background to the photonic bandgap materials especially photonic crystal fibers. It further explains potential applications of these photonic bandgap fibers in ultrasensitive detection. With a view to consider these fibers for optical trapping applications, the transverse propagation in these fibers is also discussed based on the reported works. The outcome of literature review is discussed briefly towards the end of this chapter.

2.1 Introduction

Biomedical research is mainly focused on detection, diagnosis, treatment and prevention of diseases that ultimately leads to better health. Ultrasensitive detection techniques have an important role in many of the biomedical fields such as molecular biology, medical diagnosis, and forensic analysis. For example, screening for specific antibodies, antigens, hormones, or particular nucleic-acid sequences with high sensitivity is of fundamental importance in the early stage diagnosis of bacterial or viral infection and in the detection of genetic disorders or early-stage tumour development.With the advances in the single molecule detection techniques and their importance in biomedical areas, there is a great interest in the mechanical behaviour of single proteins and other biological molecules. The examination of how individual cells operate, function and interact with each other can reveal invisible processes such as single cell gene expression. The combination of opti-

cal manipulation methods with the popular detection techniques will be having a greater importance in the future translational medicine.

2.2 Manipulation methods

Two major types of techniques have been developed for manipulation of single cells: one is scanning probes such as atomic force microscope (AFM) and scanning tunnel microscope (STM) and the other is field gradient traps such as optical tweezers (OT), magnetic tweezers (MT) and dielectrophoretic (DEP) traps. The conventional scanning probe microscopes require a macroscopic mechanical device that guides the probe across the object. They were well suited for the characterization of the outer membrane of the living cell. However the living cells are objects with complicated 3D structures which have to be prepared elaborately before characterization with conventional scanning probe. Also the cell needs to adhere tightly to a surface.The mechanical restrictions of the conventional scanning probes can be overcome in the field gradient traps which are the noncontact way of manipulating micro/nano size particle. The combined ability to noninvasively trap and manipulate microscopic particles and to measure forces of the order of piconewtons rapidly led to the use of optical tweezers in a variety of biological and other fields. The biological application includes the measurement of mechanical properties of cells, the kinetics and properties of important biological molecules, and measurements of forces acting on particles in colloidal suspensions. When compared to existing light microscopes, the microscopes based on trapping principle works without diffraction limit and gives access to mechanical properties of the sample not accessible by conventional light microscopy.

2.2.1 Optical trapping (OT): An introduction

The trapping and manipulation of matter by light is one of the major research areas in biomedical field. The impact of the light-matter interaction has also occurred

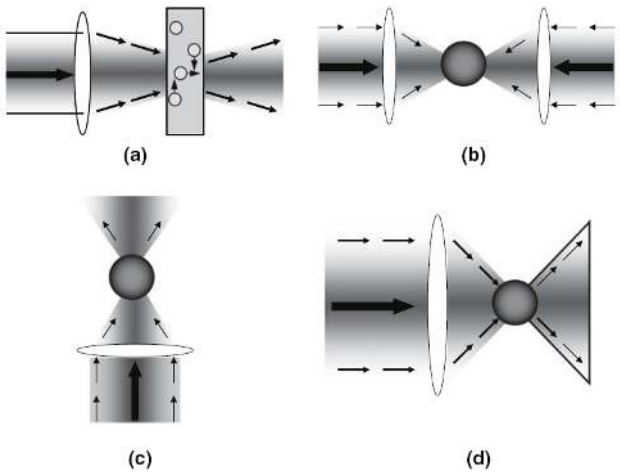

Figure 2.1: A schematic illustration of optical trapping and manipulation of a microparticle suspended in water. (a) Transverse confinement and axial driving by a mildly focused laser beam; (b) three-dimensional trapping in a counter-propagating dual-beam trap; (c) optical levitation by a mildly focused laser beam pointing upward balancing against the weight of the particle; (d) three-dimensional trapping by a strongly focused (numerical aperture NA>0.6) laser beam [21].

on scales larger than that of the atomic regime: the pioneering work of Ashkin led to the development of optical trapping of microscopic particles including biological specimens such as cells [9, 21, 22]. An optical trap is usually built by modifying a commercial microscope. The basic requirement of a trapping laser is that it delivers a single mode output (typically, Gaussian TEM_{00} mode) with excellent pointing stability and low power fluctuations into the back aperture of microscope and is focused by the objective mounted on the microscope into the trapping microchamber that contains samples suspended in aqueous solution. The parameters of objective such as NA, transmittance, working distance and immersion medium play an important role in the trapping experiment (Some typical specification of objective are: NA=0.65-1.4, magnification= 40-100X). In general, the trapping chamber is placed on a 3D stage for the convenience of focusing and movement of sample after trapping. The non-invasive and sterile nature of optical trapping methods makes them good candidates for use with biological particles. Complete process integration is possible if we could utilize optical radiation for both identifying target cells and sorting them.

The group led by Ashkin demonstrated:

- A weakly focused laser beam in a sample chamber containing micron-size polystyrene beads suspended in water could attract the bead transversely towards the beam axis and drive the bead to move along the beam axis in the direction of beam propagation (figure 2.1a).

- A pair of weakly focused laser beams aligned coaxially and propagating in opposite direction with approximately equal optical power could trap a bead (suspended in water) in a three-dimensional space in a stable manner(see figure 2.1b). In this work,the particle suspended in liquid was stabilized axially at the location where the scattering forces of the two weakly focused laser beams balanced each other. Here the scattering forces of two beams balanced each other.

- A weakly focused laser beam directed vertically upward can levitate a bead in a stable manner by balancing the radiation pressure against the weight of the bead in water (figure 2.1c).

- A single laser beam alone when strongly focused with high numerical aperture (NA>0.6) could stably trap micron-sized polystyrene bead in water [23](see figure 2.1d).

Out of which, the strongly focused single-beam configuration, also known as single-beam gradient-force or optical tweezers, has attained tremendous interest in the scientific community due to its relative simplicity in the experimental set up. In the single-beam gradient force trap, the beam was strongly focused to a diffraction-limited spot by a high-numerical-aperture objective. This laser beam trapping method is considered to be useful for manipulation of biological object because of non-invasive technology. Optical Tweezers use light to manipulate microscopic objects as small as a single atom. The small biochemical particles or cells are trapped at the waist of a focused laser beam due to the gradient force, which is derived from the change in momentum of light. A sharp focal point is created using a laser and when a small particle comes into contact with the focus it remains

trapped. In general, the particle is pulled towards the more intense light because it has a greater index of refraction than the surrounding medium. In most practical situations, an optical tweezer is made up of two individual set ups, one that uses white light to image the particles, while the other uses an appropriate laser to trap the particle.

2.2.2 Theoretical Models for the Optical Forces in OT

The forces acting on microparticles in optical traps have been calculated theoretically mainly using two models - Ray-optics (RO) and Electromagnetic (EM) models [24, 25, 26]. When the sizes of the particles are larger than the wavelength of trapping beam, the RO model represents the better model. EM model provides good approximation for the cases where the particle size is smaller than wavelength of trapping beam. For particles with size comparable to wavelength of trapping beam, the calculation is much more complex and the results are often less accurate. The RO & EM models are discussed briefly below in this section.

2.2.2.1 The Ray-Optics (RO) Model

In the RO model, one may calculate the total force applied on a particle by calculating the forces of single rays that strike the particle and then integrating the forces of all the rays of the beam acting on the particle. In accordance with Fresnel laws of refraction and reflection, a ray incident upon a particle will be partly transmitted and partly reflected at the surface. The refraction and reflection will transfer momentum and resultant force on particle. Schematic representation of RO model is shown in figure 2.2.

The major correlation between the force (F) exerted on the particle and the laser power (P) is:

$F = QnP/c$

, where 'n' is the refractive index of the surrounding medium, 'P' is the laser power, and c is the velocity of light in free space. 'Q' is a normalized trapping

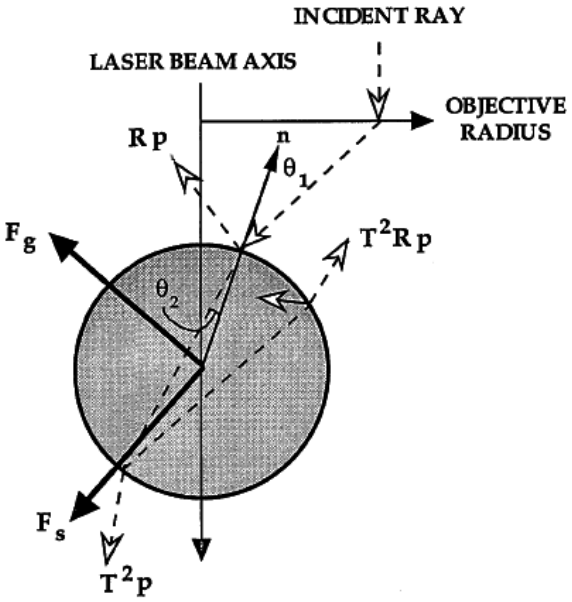

Figure 2.2: The ray optics (RO) model for optical trapping (dashed line shows the beam path). The scattering force F_s points in the light propagation direction and the gradient force F_g points to the intensity maximum (adapted from [25]).

force (trapping efficiency), it represents the fraction of photon momentum per second associated with the trapping beam that is converted into the net trapping force. According to Ashkin, the force exerted by a single ray on a bead can be divided into two parts: a ray-scattering force parallel to the incident ray and a ray-gradient force perpendicular to the incident ray [25]. The gradient and trapping forces can be expressed as follows [25]:

$$\begin{aligned} F_{gradient} &= \frac{\Delta P}{\Delta t} = \left(\frac{n_m P Q_g}{c}\right) \\ &= \left(\frac{n_m P}{c}\right)\left\{R\sin 2\theta_1 - \frac{T^2\left[\sin\left(2\theta_1 - 2\theta_2\right) + R\sin 2\theta_1\right]}{1 + R^2 + 2R\cos 2\theta_2}\right\} \end{aligned} \tag{2.1}$$

The scattering force,

$$\begin{aligned} F_{gradient} &= \frac{\Delta P}{\Delta t} = \left(\frac{n_m P Q_s}{c}\right) \\ &= \left(\frac{n_m P}{c}\right)\left\{1 + R\cos 2\theta_1 - \frac{T^2\left[\cos\left(2\theta_1 - 2\theta_2\right) + R\cos 2\theta_1\right]}{1 + R^2 + 2R\cos 2\theta_2}\right\} \end{aligned} \tag{2.2}$$

where n_m, P, c, θ_1 and θ_2 are the refractive index of medium, laser power, speed of light, angle of incidence and angle of refraction respectively. The quantities R and T are the refractive and reflective Fresnel coefficients. 'Q' is dimensionless angle-dependent factor, which is different for gradient and scattering force.

For a particle in a focused Gaussian beam, the total optical force exerted on the particle is determined by integrating the force components associated with each ray over all solid angles in the half sphere that the beam is incident from. The total optical force can also be decomposed into two parts: the gradient and scattering forces. The scattering force is along the beam propagation direction, drives the particle in the forward direction. If the particle is off the beam axis, the lateral gradient force will attract the particle back to the beam axis. While the particle is laterally centered on the beam axis but away from the beam waist, the component of the gradient force along the beam propagation direction will try to attract the particle back to the beam waist. To achieve a stable three dimensional (3D) trap, the gradient force component in the beam propagation direction must balance the scattering force. This necessitates the laser beam to have a very large gradient in the propagation direction. This can be obtained by focusing the beam with a high numerical aperture (NA) objective lens. The stable particle position will be slightly moved from the beam waist in the beam transmission direction.

2.2.2.2 EM model

When the trapped particle is much smaller than the wavelength ($a \ll \lambda$) of the trapping laser (also known as Rayleigh particle), the optical forces can be calculated by treating the particle as a point dipole that is dynamically polarized by the incoming field as in figure 2.3.

Since the particle is much smaller than the wavelength of the trapping beam, the electric field is more or less uniform within the particle. Then the dipole moment of the particle is [26]:

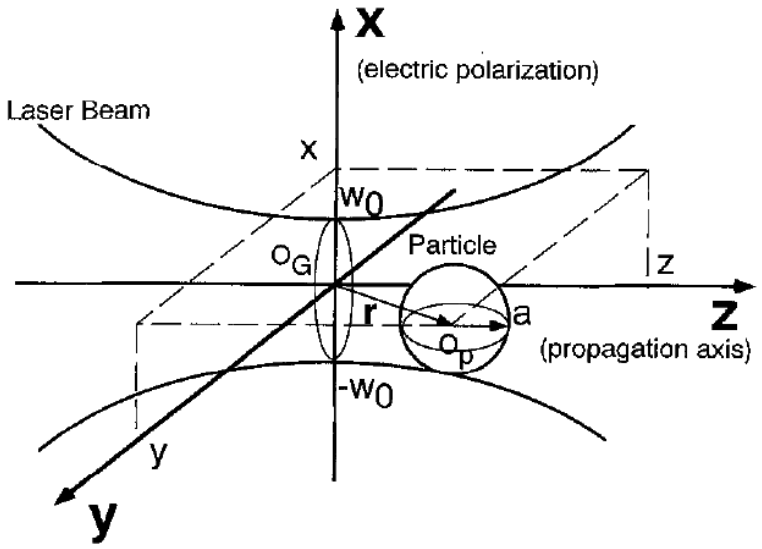

Figure 2.3: Schematic representation of Rayleigh (EM) model [26].

$$\vec{P}_{dipole} = 4\pi n_1^2 \varepsilon_0 a^3 \left(\frac{m^2-1}{m^2+2}\right) \vec{E}(t) \tag{2.3}$$

$$\vec{P}_{dipole} = \varepsilon_0 \chi \vec{E}(t) \tag{2.4}$$

,where $m = n_1/n_2$, the ratio of the refractive indices of the particle and the medium and χ the polarizability of the particle in the medium. The instantaneous gradient force applied on the point dipole arises from the interaction of the dipole with the inhomogeneous field and can be expressed as [26]:

$$\vec{F}_g(t) = \left(\vec{P}_{dipole} \cdot \vec{\nabla}\right) \vec{E}(t) + \frac{d\vec{P}_{dipole}}{dt} \times \vec{B}(t) \tag{2.5}$$

From equation (2.4) and equation (2.5)

$$\vec{F}_g(t) = \varepsilon_0 \chi \left[\frac{1}{2} \nabla E^2(t) + \frac{d}{dt}\left(\vec{E}(t) \times \vec{B}(t)\right)\right] \tag{2.6}$$

The time average of the gradient force is given by,

$$\begin{aligned} \vec{F}_g = \langle \vec{F}_g(t) \rangle &= \frac{2\pi n_1 a^3}{c} \left(\frac{m^2-1}{m^2+2}\right) \nabla I \\ &= \alpha \cdot \frac{4\pi a^3}{3} \cdot \nabla I \end{aligned} \tag{2.7}$$

Where, $I = \frac{cn_1\varepsilon_0}{2}|\vec{E}|^2$ is the laser intensity in absence of particle and $\alpha = \frac{3n_1}{2c}\left(\frac{m^2-1}{m^2+2}\right)$, is the force constant for unit volume.

From equation (2.7), it is clear that direction of the gradient force depends both on the intensity gradient and the ratio of the refractive indices between the particle and the medium. In general, the particle's refractive index is larger than that of the medium surrounded by the particle. Then the particle will be attracted to the intensity maxima. A lower index particle will be repelled away from the intensity maxima.

The scattering force is due to absorption and reradiation of light by the dipole. The scattering force acts along the light propagation direction and is proportional to the intensity of light [26, 27].

$$F_s = \frac{n_1}{c} \cdot \frac{8}{3}\pi \left(\frac{2\pi}{\lambda}\right)^4 a^6 \left(\frac{m^2-1}{m^2+2}\right)^2 \cdot I \tag{2.8}$$

Hence to obtain a 3D stable trap for a Rayleigh particle, the particle's refractive index has to be bigger than that of the medium. The laser beam must also be focused tightly enough in order that the gradient force overcomes the scattering force. Also, from Equation (2.7) and Equation (2.8), it is obvious that gradient force is linear in the particle volume whereas the scattering force is proportional to the square of the particle volume. Thus, it is easy to trap a smaller particle in 3D than a bigger one without considering the Brownian motion of the particle.

RO and EM models allow one to calculate forces in two particle size regions which are respectively bigger and smaller than wavelength of trapping beam. But, the most practical case involves particle with sizes similar to the light wavelength. The Lorentz-Mie scattering theory has been developed to calculate the optical forces in this regime [28]. However, the procedures are found to be very tedious and are valid only if the particle is in homogeneous medium. Though the ray optics and Rayleigh models are not accurate for estimating the optical force in this region, they are still useful in calculating the value of the force.

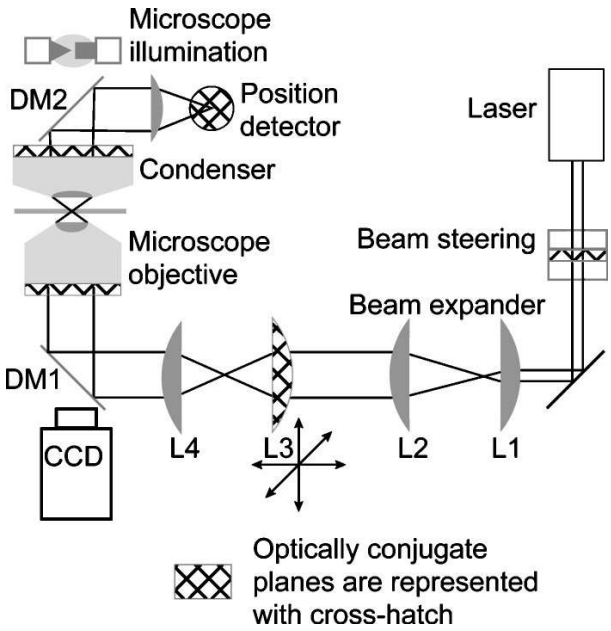

Figure 2.4: Typical Optical trap set up.

2.2.3 Typical Optical trap system

Figure 2.4 shows schematic of a typical optical trap set up [29]. The necessary elements required for a typical optical trapping set up are as follows:

- A trapping laser
- Beam expansion and steering units
- A high NA focusing lens
- Sample chamber
- One or more methods to observe trapped sample

An optical tweezer is generally built in an inverted microscope configuration such that laser beam is introduced into the optical path before the focusing objective lens. Microscopic configuration provide a good platform for generating optical trap since it provides high numerical aperture objectives and imaging system for visualising trapped objects. The fundamental requirements in a microscope-based optical tweezer are:

1. A single-mode laser must be launched into the microscope such that it does not affect the basic microscope function and it is brought into a tight focus at the specimen plane with a high NA objective lens.

2. The optics should be in order such that the optical trap is within the specimen focal plane so that the trapped objects are imaged using the microscope's imaging system [30].

The selection of objective lens decides the efficiency of optical trap since the trapping force is dependent on the NA. Normally, objective lenses used in optical trap have numerical apertures NA$\geq$1. In order to construct a stable and consistent optical trap, the output of trapping laser should be continuous wave (CW) with single mode laser beam (typically, Gaussian TEM_{00} mode). Also, it should have low power fluctuations and good pointing stability. The effective beam diameter ($1/e^2$ of the Gaussian beam diameter) of the laser spot have to be tuned to exactly fill or slightly overfill the back aperture of the microscope objective [31]. This makes the incident beam converges to a tight, diffraction-limited spot. This will maximize the intensity gradient at the focused spot to obtain optimal trapping force. The beam diameter can be adjusted using a beam expander before it reaches the objective lens. To move and control the trapped object, the optical trap has to move in the specimen plane. Beam steering elements are used for this in most of the optical trapping setups.

2.2.4 Position Measurement for OTs

Figure 2.5 represents the schematic representation of circuit to obtain position information out of a quadrant photodiode [32]. It has four stages such as photodiode, current-to-voltage conversion, differential and summing. In the first stage, the output current from each quadrant is converted to a voltage. This gives a linear relation between the incident light intensity and output voltage. The voltage signals from each adjacent pair of quadrants are compared by a differential amplifier. The signals for each axis are then added by a summing amplifier. Hence, the amplified

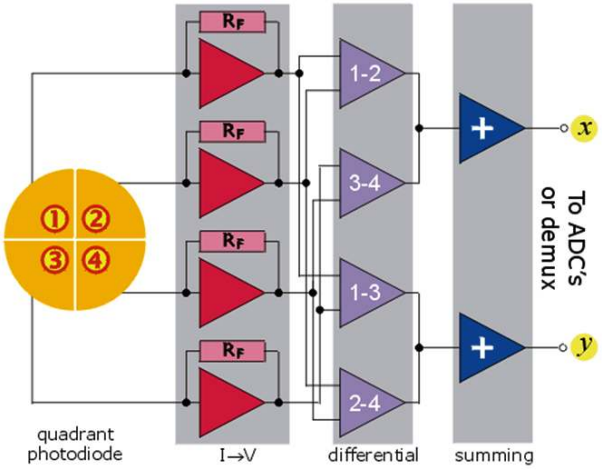

Figure 2.5: Schematic of circuit to acquire position signals from a quadrant photodiode (adapted from [32]).

voltage signal is then transmitted to the analogue electronics which process them into x and y position signals.

In order to provide necessary forces to trap a particle in optical tweezers, the laser beam has to be focused with a high NA (1-1.2) objective lens and the back aperture of the objective lens has to be overfilled as shown in figure. The trapping laser is required to be continuous wave (CW) and Gaussian TEM_{00} mode with high pointing stability and low power fluctuation (<1%). In optical trapping experiment, the position information of the particle relative to the center of the trap is very important. Distance also gives information on the force that the trap exerts since the force is linearly related to the distance from the trap's center. In order to observe the motion of particle trapped, two types of detection schemes are generally used: video based detection method and photodetector based detection method.

Video based detection are traditional methods of position detection which utilizes video camera mounted on a translational stage [33]. But, the video acquisition rates, which are typically ≈10 full frames per second (fps), are the key drawback of video camera based position detection methods. Hence the obtained resolution is limited to several hundred nanometers which depends on optical diffraction and camera chip pixels. The standard CCD camera has low resolution of the order

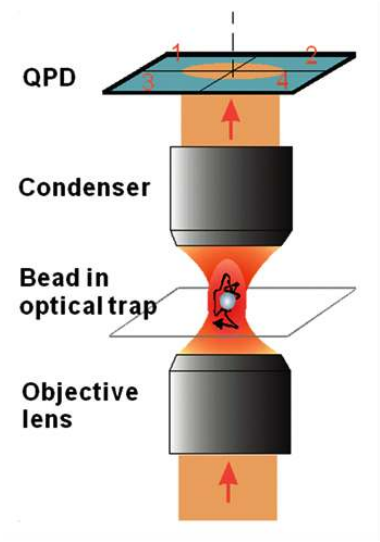

Figure 2.6: The BFP position detection configuration using QPD.

of ≈25-120 Hz which makes them insufficient for many of the optical trapping applications that have faster dynamism. Hence the video based detection system is limited to track the Brownian motion of the trapped bead with a bandwidth exceeding hundreds of Hz in general. There are video cameras with faster acquisition rates such as the complementary metal oxide semiconductor (CMOS) and electron multiplying charge coupled device (EMCCD) based cameras. But the actual imaging rates are still limited by signal to noise ratio, memory capacity and data processing speed. Furthermore, the data processing is so slow that the results cannot be obtained in real time.

Photodiodes allows improved temporal resolution. Here, the position resolution is defined as the least measurable displacement of a spot of light on the detector active area. The achievable resolution is restricted by the signal to noise ratio of the system. It also depends on light intensity, detector noise, and electronics bandwidth. The Quadrant photodiode detectors (QPDs) belongs to family of position sensitive light detectors [34, 35]. QPDs consist of four separate photodiodes. In general, the four photodiodes share a common cathode (which connected to ground) and have separate anodes. Figure 2.6 shows the schematic of position measurement of optically trapped particle using the quadrant photodiode detector (QPD). QPD can achieve much better temporal resolution of the order of ≈5000 kHz [36]. It

allows them to be better devices for position detection system in optical tweezers. QPD is placed at the back focal plane (BFP) of the condenser [37, 38]. Since the same laser is used for the position measurement and optical trapping, the BFP detection provide detection of the displacement of the trapped particle with respect to the center of the optical tweezers. By calculating the intensity difference of its four elementary chips, the lateral displacement of the particle can be calculated.

2.2.5 Potential Biomedical Applications of OTs

Optical trapping techniques were also demonstrated to be useful in medical fields. The optical trapping and manipulation of viruses and bacteria in aqueous solution through single-beam gradient force was demonstrated in 1987 [20]. The option of noncontact and noninvasive measurements could lead to a new concept for considering the physiology and the pathology of living cells with potential clinical applications. It allows one to measure visco-elastic property and to compare this with its physiological condition through trapping and stretching experiment. The method is readily adaptable for living cell imaging and manipulation. By trapping two cells, the cell-cell interaction can be measured. It can be associated with laser spectroscopy and microscopic methods for single cell measurements. One can monitor in real-time the dynamics of molecular binding or of biological forces associated with molecular interactions to examine the functions of the biomolecules.

2.2.5.1 Selection of Laser for trapping biological sample

A drawback of optical trapping has been the damage induced by the intense trapping light. In practice, such damage limits the exposure time for trapped specimens and has proved to be a significant problem for some optical trapping studies, particularly those *in vivo*. Some practical progress has been made toward decreasing photodamage in optical trapping systems, primarily through the choice of trapping lasers with wavelengths in the near-infrared (NIR) region. It corresponds to the region of optical transparency of the particle to avoid the absorption of light. The

visible light is completely absorbed by the biological material, while IR light is absorbed by the water.

There are numerous reports on the wavelength dependent damage on the biological sample. Both continuous and pulsed NIR lasers have been employed and both linear and two photon processes have been studied. The NIR laser for trapping biological sample was first recommended by Ashkin [6]. Followed by that, several groups have studied the extent of damage on different biological sample by using NIR laser sources. The effects of NIR trapping is studied by using NIR CW laser with wavelength 790-1064 nm on Escherichia coli (*E. coli*) bacteria [39]. Photodamage exhibited on sample is found to be minimum at 830 and 970 nm and maximum at 870 and 930 nm. Comparable results have been obtained by another group; they considered cloning efficiency of Chinese hamster ovary cells after optical trapping [40]. It is also reported that the dependence of photodamage in a timeshared trap depended weakly on the NIR wavelength (840-930 nm) but linearly on the peak laser power [41]. Another group has monitored the influence of damaging effects of NIR CW light on a living organism [42]. It was found that the 700-760 nm wavelength regions is not suitable for trapping biological sample while the 810 nm laser was found to be less damaging. Though photoinduced damages reduce at higher wavelengths, the heating effects do increase. An outline of studies about the laser induced optical damage on trapping biological specimen is given in Table 2.1.

2.3 Detection Techniques

Radioactive labeling methods [45] are often used for the detection of trace amounts of nucleic acids and proteins, mainly because of their sensitivity, which extends down to the Pico gram range [46]. However, because of the difficulties associated with the handling and disposal of radioactive reagents, the development of other nonradioactive detection methods has been a field of immense interest in recent years [15]. Among the broad diversity of nonradioactive analytical methods, fluo-

Table 2.1: Damage induced by the trapping laser to the biological specimens.

Biological System	**Laser and Power**	**Observed Damage**
E. Coli under anaerobic conditions [39]	Continuous NIR from 790-970 nm, 88-100 mW	Minima at 830 nm and 970 nm. Maxima at 870 nm and 930 nm.
Chinese hamster ovary cells [40]	Continuous NIR from 700-990 nm, 100 mW	Maximum clonability at 950-990 nm and least clonability at 740-760 nm and 900 nm.
E. coli [41]	Time-shared optical tweezers 840-930 nm	Weak dependence on λ, linear dependence on power. Lethal energy dose for *E. coli* is 5 J.
Red blood cells [43]	CW laser at 1064 nm, 80-120 mW	The observed photodamage due to heating is found to be linearly dependent on the laser power. It can be reduced with a flow of cold buffer.
C. elegans with heat shock promoter [42]	CW laser from 700-1064 nm, 100 mW	Maxima below 760 nm, at higher Λ less photochemistry but an increase of heating.
Red blood cells [44]	CW laser at 830 nm, 120 mW	No noticeable influence on the laser power after 20 minutes of trapping.

rescence based techniques for molecular detection are the most promising because of high specificity and sensitivity. Fluorescence occurs when certain molecules generally known as fluorophores or fluorescent dye absorbs light. This raises its energy to a brief higher level (excited state). From this excited state, it decays to lower level by emitting fluorescent light. Fluorescence techniques are sensitive and quantitative method that is widely used in molecular biology and biochemistry laboratories for a variety of experimental, analytical, and quality control applications [47]. Other main advantages of fluorescence techniques over other detection methods are multi-colour detection (hence multiple targets), stability, low hazards, commercial availability and low cost.

2.3.1 Fluorescence based detection

Ultrasensitive detection techniques with single-molecule detection technique, a laser-based method that allows the detection of single fluorophores in solution, can possibly provide fundamentally new information about biological processes

and are critical for a better understanding of cellular function [15]. The development of new optical techniques for quantifying the fluorescence is crucial in cancer diagnosis. Currently, the analysis of fluorescently labelled molecules in tumour is mainly based on surgery or biopsy [48]. These methods have tremendous power and hence are ubiquitous in the laboratory, but they suffer from a serious shortcoming: neither of these methods can be used for *in vivo* measurements [49]. In microscopy, fluorescent dyes are used to label specific sub-cellular components, which are then optically imaged. Flow cytometry requires the extraction of isolated cells from tissue, and confocal microscopy can image only through thin slices of tissue because of the strong scattering of the excitation light and the emitted fluorescence.

Detection at molecular level such as reporter assays and gene expression studies are achieved by extremely high techniques using Fluorescent Proteins as biomarkers [50]. The method of 'micro-sensing and imaging' began the use of optical discoveries to perceive biological function become more significant. Green fluorescent protein (GFP) and Red fluorescent protein (RFP) are, naturally occurring fluorescent proteins, widely used as a reporter molecule for variety of studies such as protein localization, protein binding events, and gene expression [51]. GFP contains a choromophore which absorbs blue light and allows the emission of green light. The stability and the easy application of these fluorescent proteins permit us to use as an experimental system in the fields ranging from cell biology research to biomedicine. Fluorescent protein labelling as a cancer marker improved the visualized detection of cancer cells when exposed to organs and tissues down to the single cell level [52]. Another major advantage of fluorescent protein markers are that imaging is possible without any preparative procedures, contrast agents and substrates.

Detection of small amount of biological threats will be enhanced with possible development of simple inexpensive methods that give brightest possible fluorescence for detection using high throughput suspension arrays [15]. Moreover, many biomolecules are not available in large quantity; in which case reagent use is limited.

Also, viewing and detection of viable cell with the required fluorescence characteristics from a large heterogeneous population is very important [53, 54]. It is therefore important to develop bioelements or biosystems which can be made efficiently in small quantities and used repeatedly. There has been a growing interest in using optical fibers for biosensing purposes [55].

The conventional fiber optic evanescent wave sensors have low mode field overlap of light with samples. When using conventional solid optical fibers for evanescent wave sensing, the protective fiber coating and cladding needs to be removed to ensure an overlap between the optical field and the sample it probes. Furthermore, conventional fiber based chemical sensors have found limited applications due to small mode overlap and high loss. The emergence of microstructured optical fibers (MOFs) opens up new opportunities for novel evanescent wave biosensor design, which can solve the problems encountered in conventional biosensors [56]. Microstructured optical fibers (MOFs) are characterized as having a plurality of air holes running along the entire length of the fiber. The optical properties of this class of fibers are determined by the geometry, size, and relative position of the air holes. By varying these parameters, MOFs with strong evanescent fields in the air holes can be designed and fabricated [57]. The majority of MOFs produced worldwide are based on silica, the standard basis material for the fabrication of optical fibers. Photonic crystal fibers (PCFs) are one of the most promised MOFs that have emerged in recent years that could be engineered to have vastly different properties compared to conventional fibers [58].

2.4 Combination of OT with Fluorescence detection techniques

For meaningful single-cell studies, the combination of optical manipulation techniques with powerful detection techniques is crucial. Fluorescence or Raman spectroscopic techniques are most suitable optical methods. Raman techniques are

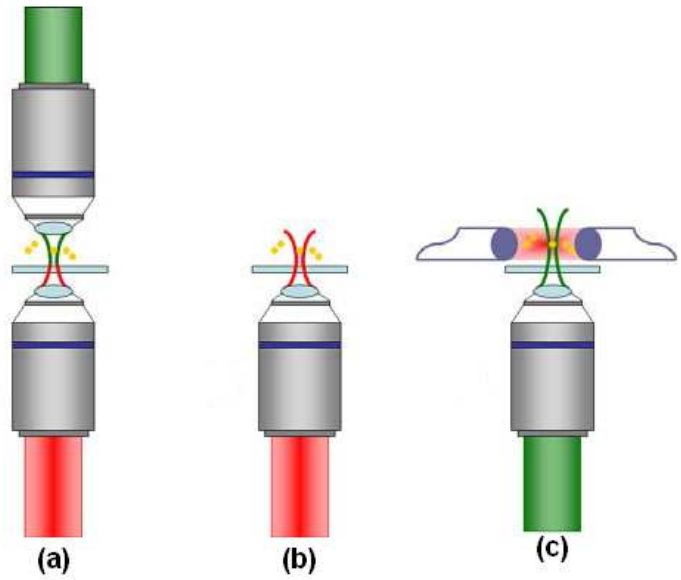

Figure 2.7: Typical microscope objective based configurations for combined optical trapping and optical detection.

comparatively lower sensitive and require high concentrations of compound to be monitored. Also, visible lasers are often used that can cause photodamage to the biological sample. Fluorescence techniques are easy and comparatively cost effective. Also, it is very easy to realize with optical trapping methods as they are contact free and readily performed under microscope. Also many cellular mechanisms of a cell can be studied concurrently if many laser lights are employed. Commonly used fluorescent techniques are wide-field, confocal laser scanning and multiphoton fluorescent microscopic techniques. Most molecules of interest to be studied are not fundamentally fluorescent. But, by explicitly tagging cellular components with fluorescent dyes, fluorescence based detection can be carried out on a wide range of systems. Most of the researches in these fields are heading for the development of specific fluorophores such as the green fluorescent protein (GFP) or quantum dots [59].

In the majority of the fluorescent spectroscopic techniques, visible or ultraviolet light sources are used since most optical properties of molecules lie in this region. Wavelength is an important parameter when biological samples are to be trapped and the near infrared region (790-1064 nm) is favoured since the photodamage

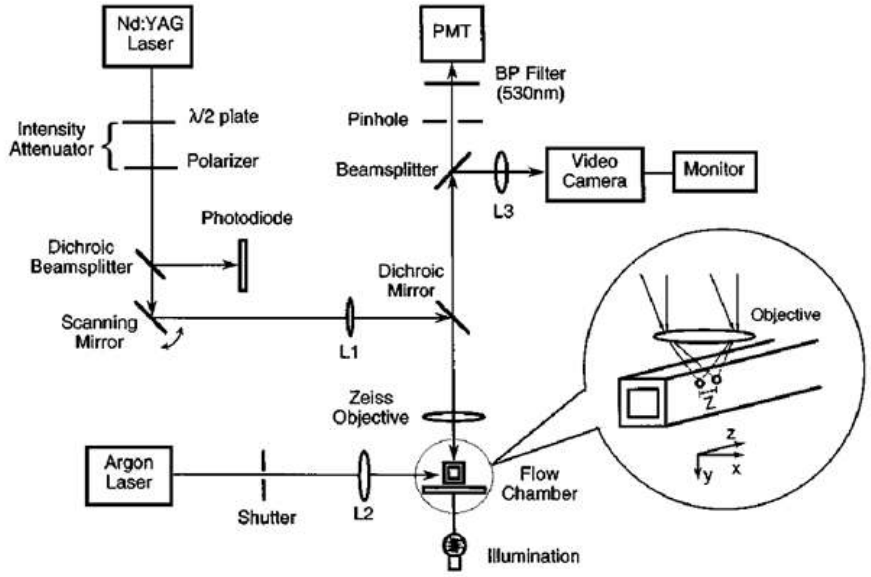

Figure 2.8: Schematic of the optical setup employed for simultaneous optical trapping and fluorescence detection [61].

is minimal. Hence as a minimum of two lasers are essential and system needs to be outfitted with appropriate filters in order to guide the proper wavelengths either towards the sample or into the detector. It also requires different microscope objectives. For example, long working distance objectives are required while the sample is positioned in a deep vessel at a moderately long focal distance. The long working distance objectives are inappropriate for stable optical trapping. In such cases, double-microscope configurations where two separate objective lenses facing each other are used [43]. Three different geometries that have been used to combine the trapping and detection laser beams are shown in figure 2.7 [60]. In figure 2.7(a), two objective lenses are used for trapping and fluorescent detection. Whereas a single objective lens is used for optical trapping and fluorescent detection in figure 2.7(b). In this case either one laser or two different lasers are employed for both trapping and detection. In some cases (figure 2.7(c)) a dual-fiber based optical trapping is performed where the detection is carried out through a microscope objective.

Optical trapping using an IR laser and off-axis fluorescence emission detection is simultaneously realized in a laminar flow system [61]. The optical system employed

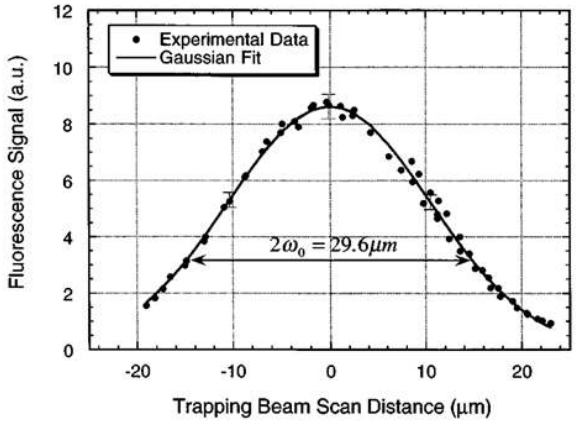

Figure 2.9: The change in fluorescence signal with particle displacement off the trapping beam axis [61].

in this study is shown in figure 2.8. Two micron sized fluorescent dyed microspheres in laminar flow is considered here and the measurement of particle escape velocity, trapping efficiency, and fluorescence intensity are performed. The magnitude of fluorescence signal as a function of particle position is shown in figure. Here, optical trap is formed by light from a continuous wave (CW) Nd:YAG laser with wavelength 1064 nm. Simultaneously a CW argon laser with wavelength 488 nm is focused by an objective lens mounted on a multi-axis translation stage is used to irradiate, and excite fluorescence from the trapped sample. Fluorescence is collected along the axis parallel to the trapping beam by the same objective lens used to form the trap.

The magnitude of fluorescence signal along the flow direction as a function of particle position is measured with respect to the trapping beam origin as shown in figure 2.9 [61]. Gaussian fit to the above data yield a 1/e half-width of 14.8 μm (ω_0) which is approximately same as the diffraction-limited beam width of the excitation laser beam focused using the same objective lens. This confirmed that in the confocal geometry, the fluorescence collection efficiency is not degrading with off-axis sample displacement.

This proposal investigates research into Photonic bandgap (PBG) material, specifically photonic crystal fiber, based optical manipulation and detection methods. Photonic bandgap materials is briefed in the next section.

2.5 PBG materials

Since their invention in 1987, Photonic crystals have gained immense interest from the optics society-both the academic and industrial. Photonic crystals or PBG materials are three-dimensional periodic dielectric structures that possess one or more complete photonics stop or photonic bandgap (PBG) bands in the transmission spectrum for propagation of electromagnetic waves [62]. The periodic modulations of refractive index in the photonic crystals make them conceptually equivalent to the two- and three-dimensional periodical electronic crystal structures found in semiconductors and semimetals suggesting an analogous band gap for photons [63]. Because of the dependence of the photonic stop bands on the crystallographic axis, certain frequencies cannot propagate along the direction of the periodic structure in such photonic bandgap structures, and this property is useful in controlling the electromagnetic radiation. The relationship between wave vector and frequency can be determined via band structure calculations employing numerical techniques such as plane wave method.

PBG materials exhibit a rich range phenomena which makes them advantageous for device applications. Since the wavelengths that lie within the bandgap are prohibited from propagating through material, it can be applied as wavelength filters and for light confinement [64, 65]. The wavelengths outside bandgap perhaps strongly dispersed leading to the supeprism effect [66]. Another application is the fabrication of lossless dielectric mirrors and resonant cavities for optical light [64]. One of the most exciting applications of photonic bandgap is the photonic bandgap fibers where the light guidance is possible in hollow-core. In this proposal, most of the studies are focused on these photonic crystal fibers. PBGFs are formed by introducing a low index defect in a 2D photonic crystal structures, hence they are able to support guidance in air. Since the cross sectional geometry in a photonic crystal fiber is 2D photonic crystal, 2D-photonic crystal is considered in the next section.

2.5.1 2D photonic crystal

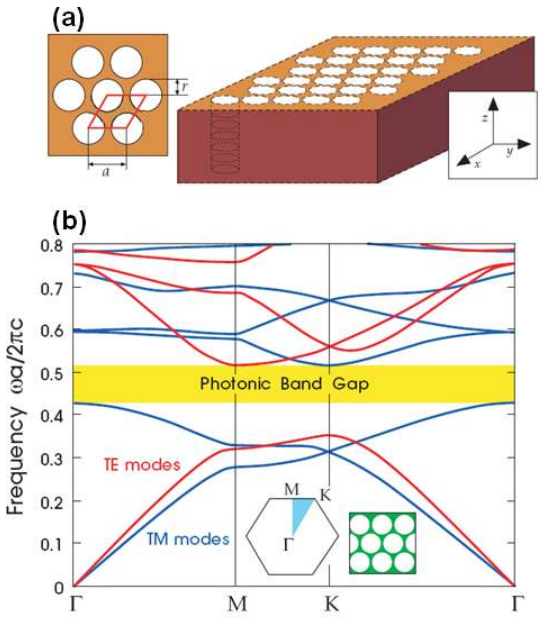

Figure 2.10: (a) A 2D photonic crystal formed by triangular array of air column in a dielectric substrate and (b) band structure of 2D photonic crystal formed by triangular array of air column drilled in dielectric substrate (adapted from ref. [62]).

A two-dimensional photonic crystal is periodic along two of its axes as the name implies and homogeneous along the third axis. It is easier to study photonic crystals in two dimensions theoretically, since in that case the wave propagation can be analysed separately for two different polarizations transverse magnetic (TM) where the electric field is perpendicular to the plane defining the structure and transverse electric (TE) where the magnetic field is perpendicular to the plane defining the structure whereby the original vector problem can be reduced to two scalar problems. If the band gaps for two different polarizations overlap, a combined band gap is created which is known as an absolute (full or complete) photonic band gap.

Several structures are known to possess photonic band gaps for one of these polarizations and for both polarizations simultaneously at certain wavelengths, as studied systematically for high values of refractive-index ratio in the two-dimensional geometry [67]. A typical 2D photonic crystal is former by triangular lattice of air

columns in a dielectric substrate which is extended in z-direction as shown in figure 2.10(a) [62]. The column have a dielectric constant, ε=1. Band structure for the lattice is shown in figure 2.10(b) [62]. Obtained band diagram is for particular radius of column (r) and lattice constant (a) such that r/a=0.48 and dielectric constant ε=13. We can observe 18.6% complete photonic bandgap for both TE and TM polarization.

2.5.2 Specialty fibers

Recently there has been a growing interest in using optical fibers for biosensing purposes [55, 68]. The conventional fiber optic evanescent wave sensors have low mode field overlap of light with samples. When using conventional solid optical fibers for evanescent wave sensing, the protective fiber coating and cladding needs to be removed to ensure an overlap between the optical field and the sample it probes. Further, Conventional fiber based chemical sensors have found limited application due to small mode overlap and high loss. The emergence of microstructured optical fibers (MOFs) opens up new opportunities for novel evanescent wave biosensor design, which could solve the problems encountered in conventional biosensors [69, 56]. Microstructured optical fibers (MOFs) [18] are characterized by having a plurality of air holes running along the entire length of the fiber. The optical properties of this class of fibers are determined by the geometry, size, and relative position of the air holes. By varying these parameters, MOFs with strong evanescent fields in the air holes can be designed and fabricated (Cordeiro, C.M.B., et al., 2006). The majority of MOFs produced worldwide are based on silica, the standard basis material for the fabrication of optical fibers.

2.5.3 Photonic Crystal Fibers (PCFs)

Photonic crystal fibers are fundamentally 2D photonic crystals in the transverse geometry that extend longitudinally along the length of the fiber. Photonic crystal fibers (PCFs) are one of the most promised microstructured optical fibers (MOFs)

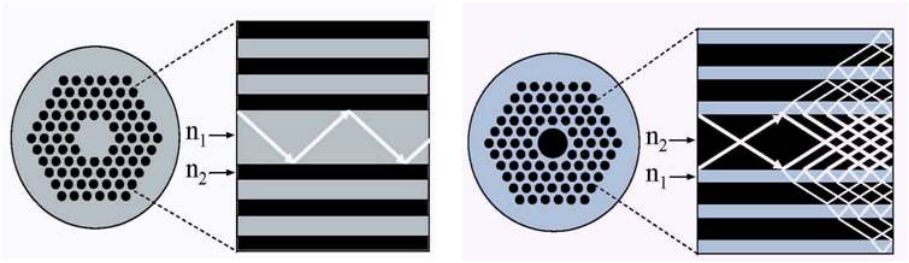

Figure 2.11: Illustration of (a) Index guidance and (b) Bandgap guidance in photonic crystal fiber, $n_b = 1.45$ (silica) and $n_a = 1$ (air).

that have emerged in recent years and could be engineered to have vastly different properties compared to conventional fibers [58, 18]. In 1996, Russell and his coworkers demonstrated the first Photonic crystal fibers (PCF) [70], compromising fine silica fibers with an array of air holes running down their length with central region where a air hole absent acting as guiding core. Since then, the field of PCF has developed rapidly and has attracted attention from research communities from whole over the world. A common way to classify photonic crystal fibers is based on guiding mechanism. Holey fibers consist of a central solid core surrounded by cladding region laced with air holes, which acts as index-decreasing elements. In this case light is guided by modified form of total internal reflection, since the refractive index of core is greater than effective index of surrounding cladding region. Another class of fibers known as photonic bandgap fibers (PBGFs), where light within certain wavelength bands is prevented from propagating through cladding region due to bandgap effects. PBGFs are formed by introducing a low index effect in a 2D photonic crystal structures, hence they are able to support guidance in air [71]. The illustration of guiding mechanism in hollow and solid core fiber is as shown in figure 2.11.

Photonic crystal fibers (PCFs) come in many shapes and forms with exhibits different characteristics which are unattainable using conventional fibers. The mode propagation properties strongly depend on wavelength, which in turn depends on the design configuration and the geometry of air holes. This dramatic broadening of the performance landscape for optical fibers arises from the combination of a very high refractive index contrast (most common PCFs use both silica and air in

the optical region) and from the introduction of wavelength-scale microstructure, whether periodic or not. The photonic crystal fiber technology offers new types of fiber with large mode area and endless single mode by accurately controlling the hole size and distribution. In a large mode area PCFs (LMA-PCFs), the core diameter can be as large as 35 μm with single-mode guidance for any wavelength at which silica is transparent. Thus LMA-PCFs reduce nonlinearity significantly. The lower spectral broadening of LMA-PCFs compared to conventional fibers has been experimentally proved [72].

The double-clad fiber is another type of photonic crystal fiber, where the central single mode core is surrounded by a lower index cladding region which is further surrounded by a region of even lower refractive index so that light can be confined and propagated. With its unique properties - the single-mode central core and the high NA multimode inner cladding - the double-clad PCFs have gained attention in the research for improvement in signal level in the fields of biosensing and endoscopy [73, 74]. The LMA core of the fiber is placed in a microstructured inner cladding, offering the single-mode guidance for near infrared beam and reducing nonlinearity significantly for excitation. The inner cladding has a high NA up to 0.6 and a diameter of hundreds of micrometer to propagate light in visible and near infrared wavelength ranges with a high efficiency. The high NA of the inner cladding is achieved by separating the inner and outer claddings with a web of silica bridges that are substantially narrower than the wavelength of the guided light. The use of double-clad fiber allows the single-mode operation of near infrared light (excitation) through the small diameter core and multimode guidance in the visible wavelength range (collection) using the larger diameter inner cladding. It leads to the possibilities of nonlinear optical imaging for internal organs with flexible fiber-optic endoscopes. The usage of double-clad PCFs in a nonlinear optical microscope has been demonstrated to improve the detection efficiency significantly by two orders of magnitude compared to that achieved by a standard SMF [75].

Another class of PCFs known as highly nonlinear PCFs which combines small

core sizes (diameters down to 1 μm) with a very large core/cladding index contrast (up to 0.4). The speciality of such fibers is its highly enhanced nonlinear properties. Additionally it is possible to design with zero-dispersion wavelengths over a wide range in the visible and near infrared spectra. It makes them ideal medium for application like four-wave mixing, Raman amplification, optical parametric amplification and supercontinuum generation for metrology, optical coherence tomography (OCT) or spectroscopy. The broad bandwidth and highly spectral brightness of generated supercontinuum source based on nonlinear PCFs have been applied to a number of imaging modalities, including optical coherence tomography, confocal and TPEF microscopy.

2.5.3.1 Hollow-core PCFs (HC-PCFs)

The hollow-core PCFs (HC-PCFs) are comprised of an air core with a cladding that consists of a two-dimensional (2-D) periodic array of air inclusions in silica [71, 58]. Here light within certain wavelength bands is prevented from propagating through cladding region due to bandgap effects. As indicated by their name, HC-PCFs guide light in the air core within certain bandgaps, which manifest as transmission windows in the transmission spectrum. The photonic bandgap (PBG) property of the fiber is a function of both its geometry and the refractive-index (RI) contrast [58]. HC-PCFs are formed by introducing a low index effect in a 2D photonic crystal structures, hence they are able to support guidance in air. The intrinsic need for a two-dimensional (2D) photonic bandgap (PBG) requires that the fiber cladding contain a near-perfect periodic array of air holes (the photonic crystal) with a high air-filling fraction and a small pitch (the distance between adjacent holes in the lattice). As the light guidance is through air, hollow-core PCFs can avoid material nonlinearity associated with self phase modulation (SPM). By properly designing the size and distribution of air-holes, the dispersion profile of hollow-core PCFs can change from normal to anomalous in the transmission window. The zero-dispersion wavelength of the hollow-core fiber can be shifted from the conventional 1310 nm

(zero-dispersion wavelength for bulk silica) to a shorter wavelength, such as 800 nm or down to a visible wavelength.

2.5.4 PCF based sensors

It has been proved experimentally that light can be made to interact with fluid samples in a controlled manner. The normal evanescent wave sensors have low mode field overlap of light with samples. Conventional fiber based chemical sensors have found limited application due to small mode overlap and high loss. For several years there has been discussion on using photonic crystal fibers for sensing application [76] such as detection of trace chemicals in gas or liquid samples. Photonic crystal fibers (PCFs) consist of periodic patterns of air holes running along the entire length of the fiber. Most promising property of microstructured photonic crystal fiber as sensor is the possibility to infiltrate sample materials into the holes, where it can interact with the guided light. In contrast photonic crystal fibers can be designed in such a way that a consistent fraction of optical field propagates in the holes surrounding the core [77]. By suitable choices of fiber parameters such as the separation between holes (Pitch, Λ) and the air-hole diameter 'd', a large fraction of optical field can propagate through the fiber as evanescent wave. As the process of sensing is carried out in the air holes, PCF allow micro volume of liquid sample to be incorporated inside the fiber which allows it to be used a sensitive optical sensor. The microstructure greatly enhances the specific area of sensing.

When the holey regions of HC-PCFs are filled with aqueous solution, the transmission window shows a blue shift [78, 79, 80, 81]. This approach is in analogous with the well-known scaling laws that describe the shift in the PBG edge which is derived from scalar waveguide approximation [78]. An experimental demonstration of the shift in the PBG edge due to refractive-index scaling using D_2O-filled HC-PCFs has been reported based on the above approximation [79]. The application of HC-PCF as a refractive index sensor based on RI scaling laws has also been reported [80]. Recently, the dependence of PBG edge shift on the physical

measurands such as strain, temperature, curvature, and twist are studied [81].

Unlike conventional fibers, photonic crystal fibers are made of pure silica glass (SiO_2) without any doping. Hence it is biocompatible and chemically inert [82]. Both solid core PCFs [83] and hollow PCFs [77, 57] based sensors have been used for a variety of biochemical detection techniques including fluorescence and absorption measurements. The PCF-based device has two major advantages. One is the robustness of the fiber sensor element itself. In a PCF, the air holes allow the sample to be brought into contact with the fiber core. There is hence no need to remove the coating and the fiber remains robust while still being able to function as an evanescent wave sensor. Secondly, capillary tubes present in the PCFs have a good surface-to-volume ratio. The PCF-based sensor hence utilizes the available sample volume much more efficiently.

In short, PCF based sensor has following advantages over conventional fiber based evanescent sensors. They are:

- Photonic crystal fibers can transmit broader bandwidths and access wavelength regimes that would be difficult to explore using conventional solid-core fibers. This increases their applications in remote sensing and other bio-imaging studies.

- In the conventional fiber, it is required to remove the outer coating and cladding to make the evanescent wave field to be detected. This reduces the robustness of fiber

- Due to the better coupling of sample and evanescent field wave, the interaction length or probing length can be reduced in PCF when it is used to detect the aqueous samples

- PCF based sensor can be used to detect micro and sub micro litre volume of sample along with sub micro molar concentration by properly choosing the PCF parameters such as lattice pitch 'Λ' and air hole diameter 'd'

- The response time is even faster since such smaller volumes fill up faster.

The light-matter interaction is evanescent in the case of solid core fiber [84], where light is index guided within the higher dielectric and a small portion of field penetrates into the sample volume. The hollow core fiber, where the guiding mechanism is photonic bandgap effect can avoid this drawback. Majority of photonic crystal fiber based biosensors makes use of the advantage of the unique possibility to position a given biological sample inside the air holes in close proximity to the fiber core. Also in PCF based evanescent sensors, both cladding and coating is on which ensures the robustness of the system. In hollow core fiber, where light guidance is through the central hole bandgap confinement from the surrounding smaller cladding holes. Thus a much higher interaction of field energy and sample materials can be achieved. In this way both gas and the liquid samples can be sensed. In air-guiding HC-PCFs as much as 99% of optical field is typically located in air; allowing extremely efficient interaction if a material is directly placed into the core [85]. With low transmission losses, photonic crystal fibers can provide long interaction length (hence high sensitivity) thus offering a substantial improvement as compared to systems based on bulk cells and unguided beam of light. This is attractive in the case of detection of trace chemicals or biomolecules. Also it would be highly applicable when the sample volume is extremely small or expensive. In HC-PCF ectromagnetic field from light propagating through the fiber is mostly confined to the glass. But because of the wave nature of electromagnetic waves an exponential tail of the optical field will penetrate into cladding holes of the HC-PCF and thereby probe any sample placed there. Hence, the HC-PCF acts as a highly advanced capillary tube with strong sample-light interaction.

In MOF based sensing, there are mainly three configurations according to the mechanism of guidance and the location of materials to be probed. They are:

1. In the case of solid core MOFs, the cladding holes filled with the materials to be sensed [83]. Here transmittance window is broad but being limited by material loss. A small fraction of optical field (the evanescent field) travels in the material to be sensed.

2. Hollow core PBG fibers, can be completely filled with gas or low refractive index liquid keeping the same guiding mechanism [86]. Here the light-matter overlap is very high.

3. Another class of microstructured fibers known as Liquid core photonic crystal fibers. Here the central hollow-core is filled by the solution to be detected so that the light-matter interaction will be increased. It belongs to the family of total-internal reflection (TIR) fibers [57]. This approach requires a high air filling fraction cladding and a (selectively filled) liquid core. Here, the light-liquid overlap is very strong.

2.5.5 Partial bandgaps in PCFs

Majority of the studies on PCFs is guiding light along the length of the fiber. i.e., propagation occur mostly perpendicular to the photonic crystal structure. Of late, few groups are investigated the bandgap property of the solid core PCFs by probing transversely to the length of the fiber. Nguyen et.al, investigate the manipulation of light by propagating transversely across the fiber [87]. The considered geometry is depicted in figure 2.12. Here, light penetrates the PCF from side is interacted with the photonic crystal microstructures and is diffracted to various orders on the right. The band diagram is studied for both TE and TM polarizations. For TM polarization electric field is oriented parallel to the cylinder whereas for TE it is perpendicular to the cylindrical axis. The propagation is considered is along the Γ-M direction as shown in figure 2.12. The obtained band diagram is shown in figure 2.13. Each band in band diagram represents a mode, for which the spatial parity in the in-plane direction normal to Γ-M (i.e., parallel to M-K axis. See Fig 2.12) may be either odd or even [88]. In figure2.13, solid and dashed lines correspond to bands with even and odd parity. The shaded horizontal region corresponds to the photonic partial bandgaps.

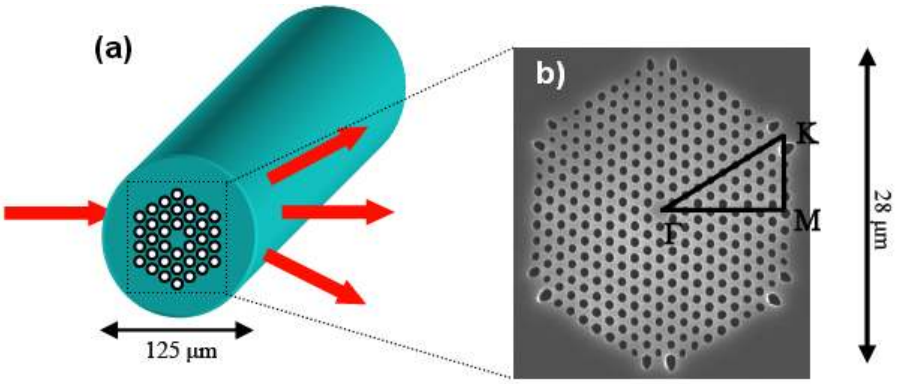

Figure 2.12: (a) Schematic representation of the transverse fiber concept (b) SEM image of the end-face of the fiber (high-symmetry points of the Brillouin zone mapped onto the actual PBG structure) [88].

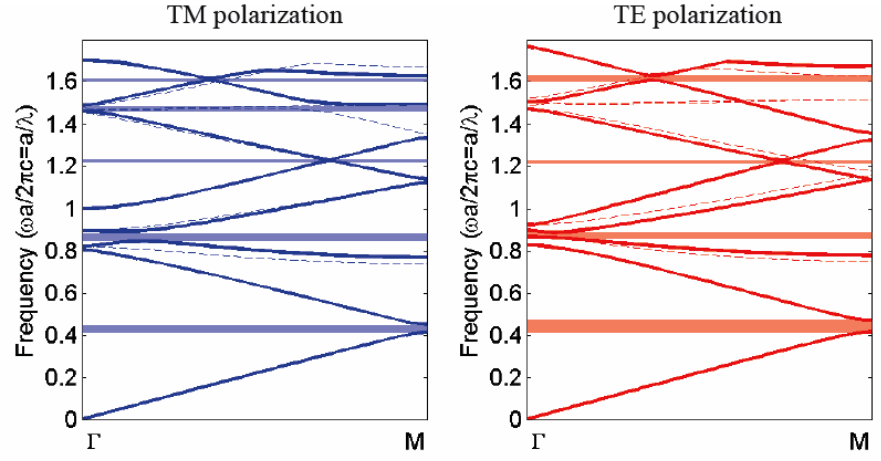

Figure 2.13: Band structure along Γ-M axis, for TM (left) and TE (right) polarizations (shaded rectangles that span horizontally represent partial photonic bandgaps) [83].

2.6 Outcome of Literature Review

The research and development of accurate, portable and low cost analytical/diagnostic tools is one of the growing areas in the biomedical industry. The combination of optical manipulation and detection units is the key element in such systems. Optical trapping methods are powerful tools for optical manipulation of biological samples because of the non-invasive, non-contact way of manipulation that does not cause much damage to the biological samples. Fluorescence techniques are most suitable since these are fast, simple and sensitive ways of detection. Fluorescence methods can be easily combined with optical trapping techniques as these also are

contact-free and can be readily carried out under the microscope.

Microstructured optical fibers (MOFs) consist of a two-dimensional periodic matrix of air inclusions that run along the length of the fiber. Hollow core photonic crystal fibers (HCP-CFs) are special class of MOFs where light is guided within the central hole that is surrounded by smaller cladding holes which provide the bandgap confinement [71]. High light-matter interaction cross section of the field energy and the sample material can be achieved with these fibers. Because of these, HC-PCFs have been widely used for evanescent wave sensing or highly efficient sensing of biomolecules, such as DNA, enzymes, antigen, antibodies, and proteins in the recent past [77, 82, 57]. A further improvement in fluorescence sensitivity by applying refractive index (RI) scaling law is yet to be explored.

A few groups have examined the possibility of various ultra-small optical devices by transversely probing light across the length of microstructured HC-PCF [89, 90]. Transverse guidance through a solid-core photonic crystal fiber is already reported, numerically and experimentally, and the presence of partial bandgaps are observed [91]. The use of HC-PCF to transmit light within a liquid-core and to levitate dielectric particles is demonstrated [17]. The presence of fundamental and higher order partial bandgaps is not investigated yet in HC-PCF and such results will be beneficial in choosing the right laser wavelength for transverse trapping studies using these fibers. The influence of filling material and polarization of trapping beam will be particularly important in these studies. Further, a multi-functional trap can be developed using these HC-PCFs which will be highly advantageous in terms of manipulation and detection of extremely low sample volume. The multi-functional optical trap may have much functionality: trapping, motion control, position sensing and signature characterization from a cell-like particle to mention a few.

In short, researchers have been exploring various optical manipulation and detection methods and techniques for reliable, fast and minimally invasive diagnosis of properties, functioning or interactions of individual cell like structures. In this con-

text, the proposed research work aims at developing multi-functional optical trap employing microstructured photonic crystal fiber that can find potential biomedical applications. Based on the literature review, it can be said that the microstructured hollow-core photonic crystal fiber has a bright future in the 'Lab-on-a-chip' applications. However, the research will be facing challenges in integrating the above mentioned properties to develop a multi-functional trap using HC-PCF and further optimization in terms of theoretical formulation and simulation for better performance.

Chapter 3

HC-PCFs for Fluorescence Sensing Applications

This chapter illustrates numerically and experimentally an efficient fluorescence sensing approach using hollow-core photonic crystal fibers (HC-PCFs) and by applying refractive index (RI) scaling law. The variations in the central wavelength for different filling material indices are demonstrated for most commonly available HC-PCFs that have cladding made of pure fused silica with array of air holes running along the entire length of the fiber. The proposed concept is verified by immobilizing fluorescent microsphere samples inside two HC-PCFs of different central wavelengths and the quantification of fluorescence inside the fibers is performed through spectroscopic analysis. The sensitivity has been compared for similar fibers with different dispersed media and for different fibers with same dispersed medium. Later the HC-PCF based evanescent sensing is performed for different standard fluorophores followed by sensitivity analysis at various concentrations. The method is then extended to recognize specific protein based on immune binding with extremely low volume of sample.

3.1 Introduction

It is reported that the sensitivity of detection of small amount of biological threats can be enhanced with simple inexpensive methods which can give brightest possible fluorescence for detection using high throughput suspension arrays [15]. Moreover, many biomolecules are not available in large quantities which limit the usage of reagents. It is therefore important to develop bioelements or biosystems which can be made efficient and potent in small quantities and can be used repeatedly. The use of optical fibers for various sensing purposes has been reported [55]. The emergence of microstructured optical fibers (MOFs) opens up new opportunities

for novel fluorescent biosensor design, which can solve the problems encountered in conventional biosensors [69, 92]. MOFs are characterized as having a plurality of air holes running along the entire length of the fiber. The optical properties of this class of fibers are determined by their geometry, size, and relative position of the air holes.

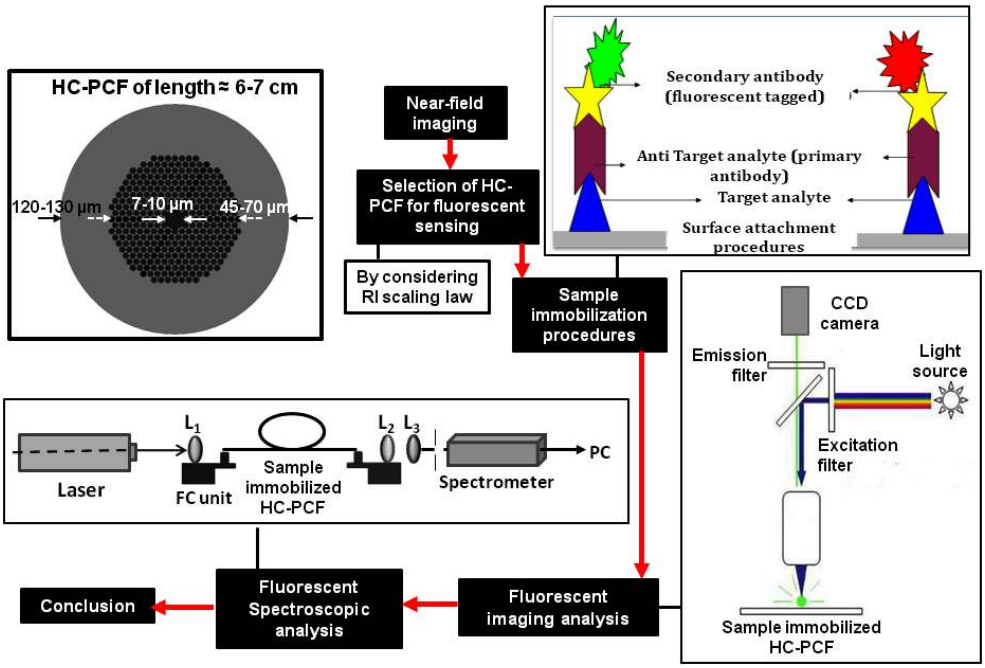

Figure 3.1: The schematic representation of key procedures implemented in this chapter.

Photonic crystal fibers (PCFs) are one of the most prominent MOFs that have emerged in recent years that could be engineered to have vastly different properties compared to conventional fibers [18]. Its guiding mechanism is based on the photonic bandgap formed due to its high index contrast (commonly silica and air in optical region) and from the wavelength-scale microstructure. The mode propagation properties strongly depend on wavelength, which in turn depends on the design, configuration and geometry of air holes [93]. Unlike conventional fibers, photonic crystal fibers are made of pure silica glass (SiO_2) without any doping. Hence it is biocompatible and chemically inert. Further, the capillary tubes present in the PCFs have a good surface-to-volume ratio. The PCF-based sensor hence utilizes the available sample volume much more efficiently. Figure 3.1 shows the key

methods/ system in operation employed in this chapter.

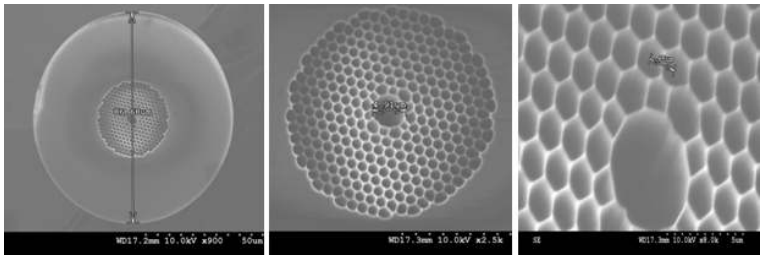

Figure 3.2: SEM images of the hollow-core Yellow fiber (HC-580).

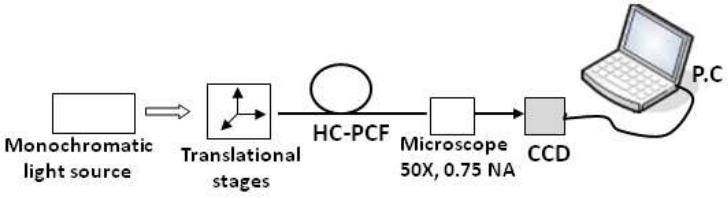

Figure 3.3: Experimental set up for the observation of near field intensity pattern at the output of hollow core PCF at various wavelengths.

3.2 Near-field imaging of HC-PCF end face

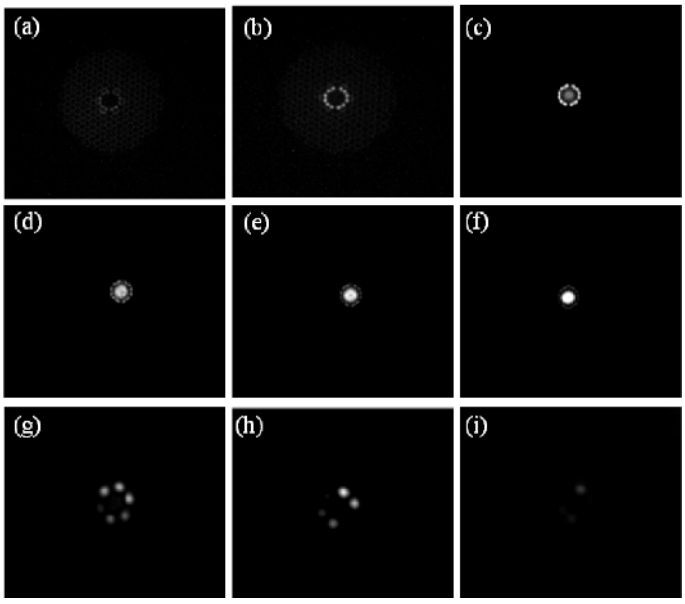

Figure 3.4: Near-field intensity patterns of HC-PCF (with central wavelength 580 nm) at different wavelengths such as: (a) 450 nm, (b) 475 nm, (c) 500 nm, (d) 550 nm, (e) 575 nm, (f) 600 nm, (g) 650 nm, (h) 700 nm and (i) 800 nm.

The near field imaging of hollow-core fiber is carried out in order to understand

the intensity profile of guided light in the core and micro structured cladding. The fiber employed in the study has its characteristic central wavelength at 580 nm (HC-580) having core diameter of 4.9 μm and acrylate coating diameter of 220 μm. The fiber has loss <1 dB/m at wavelengths between 510 and 590nm and <1.5 dB/m at wavelengths between 590 nm and 610 nm.The SEM image of HC-580 is given in figure 3.2. The basic experimental set up for the near field imaging of photonic crystal fiber is shown in figure 3.3. A monochromatic light source consisting of a monochromator at the output of halogen lamp, is used as the light source. Light output can be varied from 200-800 nm with a resolution of 1 nm. The monochromatic light source is coupled to the HC fiber using standard bare fiber SMA adapter. Transmitted light from the other end of fiber is coupled to an objective lens mounted on an X-Y-Z translational stage, which can be controlled using a piezoelectric actuator. The transmitted light is imaged using a CCD camera.

The near-field images of the HC-580 at different wavelengths and the corresponding surface intensity plots are given in figure 3.4 and figure 3.5 respectively. From the near-field images, it is evident that light is confined almost in the central core or in first few rings of cladding over a range of wavelengths around central wavelength. The guidance of light along the silica walls of the fiber is observed at above and below the transmission band. The penetration of light into the cladding region over a range of wavelength allows better coupling of light with the filled chemical samples. This is very important in the case of evanescent wave (EW) sensing application of this fiber where the guidance through silica walls allows the penetration of light into the cladding and core holes and thereby probe the sample placed there. This efficient light-matter interaction makes HC-PCFs suitable medium for highly efficient evanescent sensing. Further discussion about the EW sensing application of HC-PCF is given in the next section. The variation of transmission intensity with wavelength is also carried out for the same fiber (HC-580) by replacing the CCD camera in figure 3.3 with a spectrometer. The obtained output is given in figure 3.6.

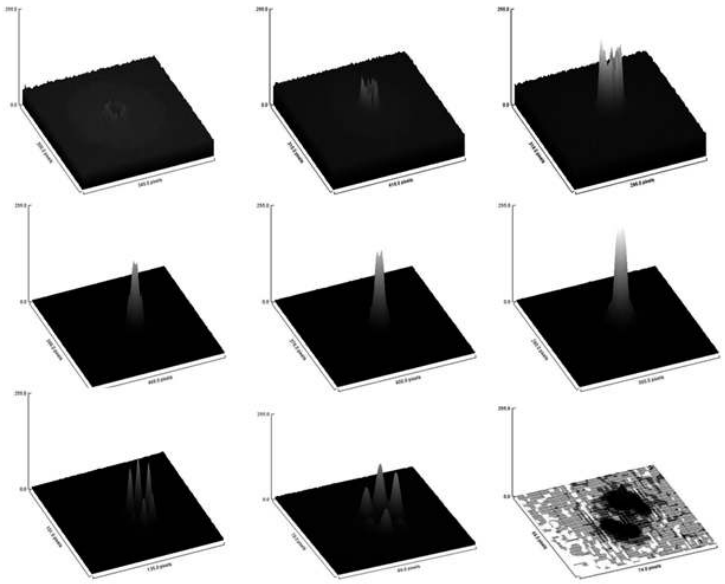

Figure 3.5: Surface intensity plots of HC-PCF (with central wavelength 580 nm) at different wavelengths such as: (a) 450 nm, (b) 475 nm, (c) 500 nm, (d) 550 nm, (e) 575 nm, (f) 600 nm, (g) 650 nm, (h) 700 nm and (i) 800 nm

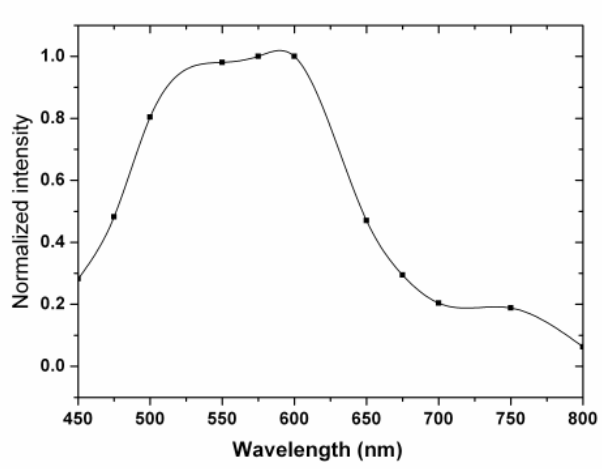

Figure 3.6: Variation in near-field transmission intensity with wavelength for HC-PCF with central wavelength 580 nm.

3.3 Evanescent wave sensing using HC-PCF

The efficiency of these evanescent wave (EW) based biosensors depends on the interaction length and large overlap between excitation light and fluorescent dye-labeled analytes. The conventional fiber based EW sensing relies on the penetration of the EW of a totally internally reflected light into the fiber cladding where a chemical species absorbs/scatters the EW or is excited by the EW to give a sensing signal. Here, one needs to remove the optical fiber's jacket as well as the cladding that

will make fiber fragile and difficult to handle. Additionally, only a few centimeters of the cladding can be replaced and this limits the sensitivity of the conventional fiber based EW sensors. The emergence of photonic crystal fibers (PCFs), especially hollow-core photonic crystal fibers (HC-PCFs), opens up new opportunities for EW biosensor design which could solve the problems encountered in conventional biosensors. The capability of the air holes in the HC-PCF to hold analyte liquid sample and the penetration of the guided mode into the air holes makes PCFs appealing for evanescent-wave sensing devices. HC-PCF based EW sensors can remain with both the cladding and the coating on, thereby ensuring a robust device.

In the case of evanescent wave biosensors, only part of the guided light interacts with the sample. For fiber optic evanescent sensors, the effective optical path length is determined by the fiber length (l) and the sensitivity coefficient (r). Here the fiber efficiency is a measure of the effective interaction length L_{eff}, which is the section of fiber where the light and the sample have 100% overlap. For a given optical fiber with length l [94],

$$L_{eff} = l \times r \tag{3.1}$$

The sensitivity coefficient 'r', describing the overlap between the light and the sample, is an important parameter in quantifying the fiber efficiency. In the case of hollow-core PCF, the sensitivity coefficient can be expressed as [84]:

$$r = \frac{n_r}{n_{eff}} \times f \tag{3.2}$$

where 'n_r' is the refractive index of the sensed material,'n_{eff}' is the modal effective index, and 'f' is the percentage of optical power in the holes and can be calculated by integrating the optical power inside the air-holes and dividing it by the total power of the mode.

Hollow-core Photonic crystal fibers (HC-PCFs) are characterized as having a

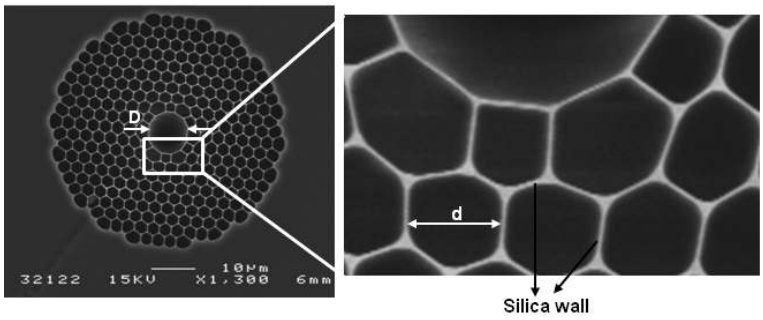

Figure 3.7: The SEM image of the HC-PCF end face and enlarged view of the region enclosed by the rectangular box.

hollow-core (of diameter 'D') surrounded by pattern of air holes (of diameter 'd') running along the entire length of the fiber. As indicated by their name, HC-PCFs guide light in the air core within certain bandgaps, which manifest as transmission windows in the transmission spectrum. The SEM image of fiber end face and an enlarged view of the region enclosed by the rectangular box are shown in figure 3.7. When the entire section of the fiber is illuminated/ excited with a laser light source from one end, the electromagnetic field from light propagating through the fiber is mostly confined to the silica walls (the area between the neighbouring air holes). But due to the wave nature of electromagnetic waves an exponential tail of the optical field will penetrate into the holes of the HC-PCF (core and cladding holes) and thereby probe any sample placed there. The strong evanescent field interaction with the fluorescent sample over several centimetres ensures efficient usage of entire sample volume and the emitted fluorescence is guided along the fiber for subsequent detection at the other end.

3.3.1 Spectroscopic Analysis: Experimental set up

The presence of fluorescence sample inside the HC-PCF is further confirmed spectroscopically and the schematic diagram of the experimental setup is shown in figure 3.8. A continuous wave (CW) diode-pumped solid-state (DPSS) 473 nm laser (output power ≈10 mW) is coupled into the proximal end of PCF immobilized with fluorescence sample using a high precision single mode fiber coupling (FC) unit (*Melles Griot Pte Ltd.*) with a microscope objective (20X, 0.65 NA (L_1).

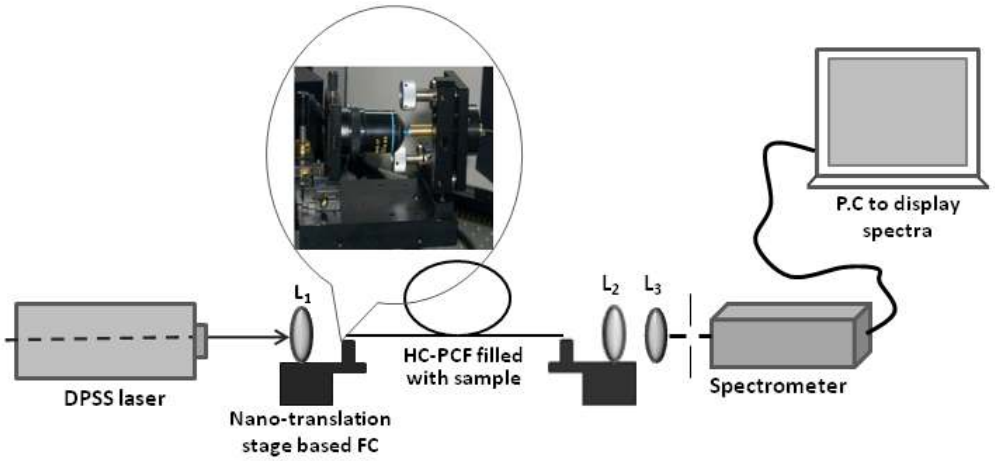

Figure 3.8: Schematic Diagram of the set up used for PCF based EW sensing of samples.

The diverging beam emerging from the distal end of the sample immobilized fiber was allowed to pass through a 2-f lens system, which is configured using two microscope objective (MO) lenses [*Newport* M-20X/0.4 (L_2) and *Newport* M-40X/0.65 (L_3)]. The 2-f lens system focuses the beam onto a high quantum efficiency spectrophotometer (*Ocean Optics*, QE65000). The spectrometer is coupled to a PC which displays the spectrum.

3.3.1.1 EW sensing of standard fluorophores

In order to understand the sensitive detection of bio-chemical solutions using photonic crystal fiber based evanescent-wave sensor, a proof of concept study of the technique was carried out. Understanding of the light leaking in to the micro structured part of HC fiber and the probing of sample inside the holes of fiber using this light is highly significant. This can be carried out by 'absorbing' a test sample in the form of solution in to the air holes of fiber, which acts as the cladding. The electromagnetic field from light propagating through the fiber is mostly confined to the glass, but due to the wave nature of electromagnetic waves an exponential tail of the optical field will penetrate into the holes of the MOF and thereby probe any sample placed there. Therefore, the system acts as a highly advanced capillary tube with strong sample-light interaction.

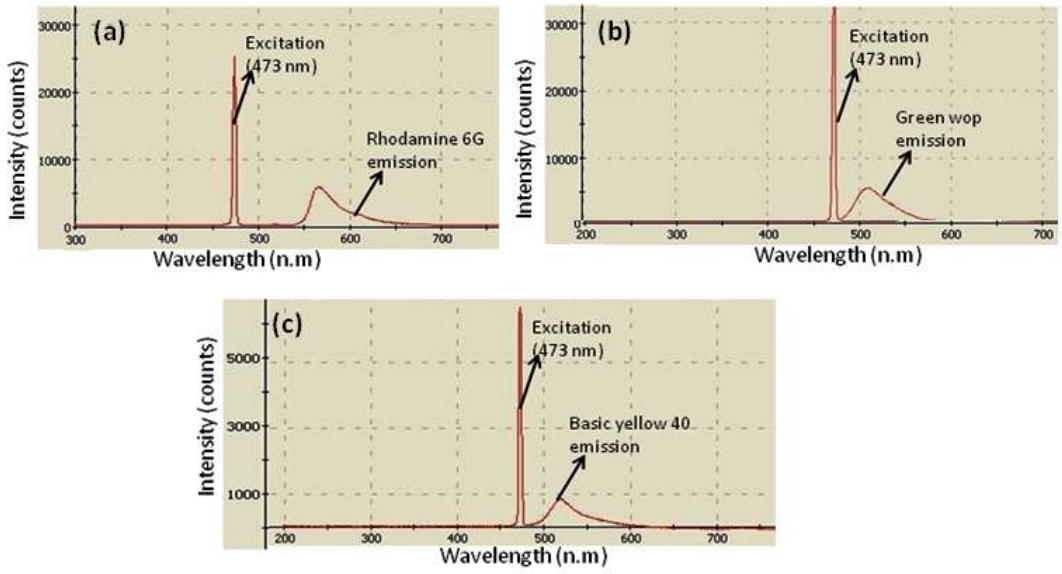

Figure 3.9: Obtained spectra of (a) Rhodamine 6G, (b) Green wop dye and (c) Basic yellow 40 using evanescent sensing inside HC-PCF (central wavelength 830 nm) fiber at 473 nm excitation.

Different commercially available fluorescent dyes such as Rhodamine 6G (Rh 6G), Basic yellow 40 and Green wop in solution form was used to prove the concept of evanescent sensing using photonic crystal fiber. In this study, hollow core fiber with central wavelength 830 nm (HC-800) was used. 1 mM solution of each of these fluorescent dyes was prepared by dissolving in ethanol. One of the ends of the properly cleaved HC fiber was dipped inside this solution for about 1-2 minutes and due to capillary action the fluorophores gets 'absorbed' in to the air holes of the fiber. In order to evaporate the solvent, the fiber is kept as such for few minutes. Then the sample end of the fiber is cleaved. The fiber with fluorescent dye is then aligned as in figure 3.8. By filling all holes with sample material, the light is guided in the fiberwall itself and only an evanescent interaction occurs between sample and light. The obtained spectra of fluorophore such as Rhodamine 6G, Basic yellow 40 and Green wop are shown in figure 3.9.

3.3.1.2 Sensitivity analysis using Rh 6G

Sensitivity studies on infiltrated hollow-core photonic crystal fiber based evanescent system have been carried out at different concentration levels. A Rhodamine 6G

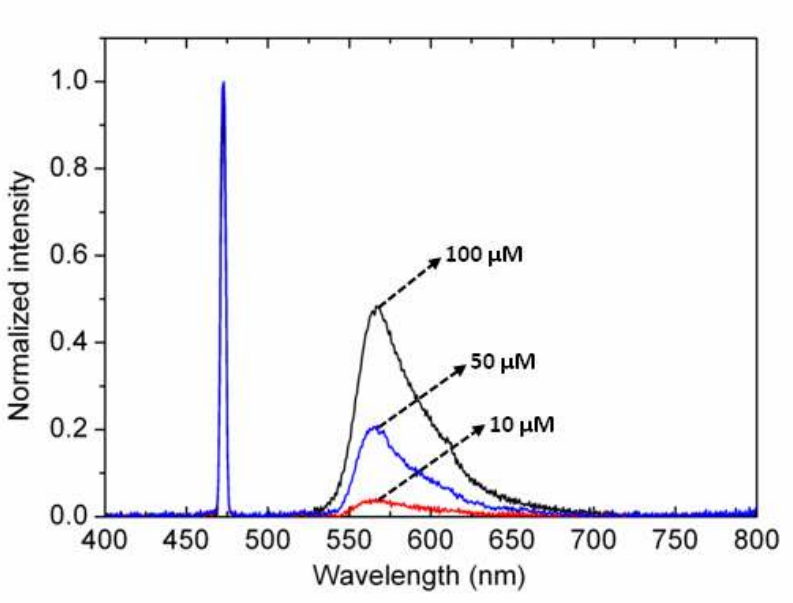

Figure 3.10: Spectra of Rhodamine 6G at different sample concentration.

test solution with a concentration of 100 μM was prepared by dissolving 0.48 mg of Rhodamine 6G fluorescent dyes in 10 ml of ethanol. The test solution is then diluted to 50 μM, and subsequently to 10 μM. Three pieces of hollow core photonic crystal fiber (HC-580), each of length 12 cm, are prepared. Both ends of these fibers are stripped followed by cleaving using a high precision standard cleaver. One end of the fiber is dipped into the prepared Rhodamine 6G test solution of concentration 100 μM for 2 minutes. The solution is filled into the fiber by the process of capillary action. After 2 minutes, the fiber is removed from solution and allowed to dry for a few minutes. The sample end of the fiber is again cleaved. The fiber with sample is then aligned as in figure 3.8. The transmitted light along the length of the fiber is detected using a sensitive spectrometer which is interfaced with a computer to display the spectra. The experiment is repeated for 50 μM and 10 μM solutions. The obtained spectra with 100 μM, 50 μM and 10 μM solutions are shown in figure 3.10.

3.4 RI scaling law for efficient fluorescence sensing

The hollow-core PCFs (HC-PCFs) acts as a highly advanced capillary tube with strong sample-light interaction in the central core. Hence, it can act as a highly efficient sensing medium for fluorescent sample/fluorescent tagged biomolecules in extremely low volume. Filling the holes of such a fiber with liquid will change the refractive index of the holey region and therefore will result in the shift of band gaps and their operational bandwidths. In fluorescence sensing applications, the shift in the photonic band gap (PBG) edge is an important parameter to be considered to make sure that the fluorescent emission signal is well within the transmission window after infiltrating the fiber with the sample. In this background,we investigate the dependence of shift in PBG edge on the background and ambient indices with respect to the parametric optimization of HC-PCF so as to develop efficient fluorescence sensors for low volume samples. Such efficient detection methods promise new photonic bandgap based fluorescence biosensors that can be employed as a diagnostic tool in future translational medicine. Theoretical model and performed numerical studies in this regard are described in the next section.

3.4.1 Theoretical model and simulations

In general, the wave equation for the scalar field distribution in microstructured index-contrast structures is given by [79]:

$$\nabla_{\perp}^{2}\Psi(x,y) + (k^{2}n_{0}^{2} - \beta^{2})\Psi(x,y) = 0 \tag{3.3}$$

, where $k \rightarrow$ free-space wave number,

$n_0 \rightarrow$ the transverse distribution of the refractive index of the structure,

$\beta \rightarrow$ propagation constant of the mode and

$\nabla_{\perp} \rightarrow$ Transverse Laplacian operator

The scalar wave equation is valid for very small index contrast. But it is found to be roughly explain light propagation in high-index contrast microstructures such as HC-PCF as well [78]. Figure 3.11 represents the cross section of a representative HC-PCF. It consists of a hollow-core of diameter 'D' surrounded by cladding holes in triangular lattice. The separation between holes is represented as 'Λ' (pitch) and the air-hole diameter 'd'. The important characteristics of HC-PCFs are the positions and the bandwidths of the photonic bandgap which in turn depends on the fiber geometry and the refractive index contrast between ambient and background media. In scalar approximation for a photonic crystal structure comprising

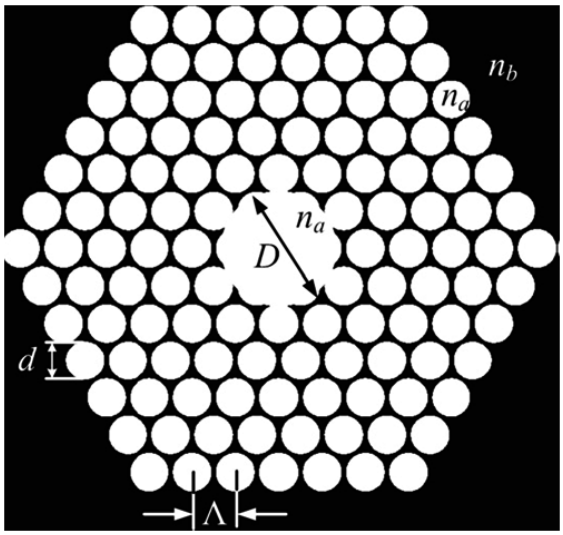

Figure 3.11: HC-PCF with air holes arranged in a triangular lattice. White regions correspond to air.

a material with high index n_1 and a material with low index n_2 with pitch Λ, the photonic states scale so that the quantities such as v^2 and w^2 remain invariant with any changes of parameters k, Λ , n_1 and n_2 [78]. Where,

$$v^2 = k^2\Lambda^2(n_1^2 - n_2^2) \tag{3.4}$$

$$w^2 = \Lambda^2(\beta^2 - k^2 n_2^2) \tag{3.5}$$

The equations (3.4) and (3.5) provide refractive index scaling law that can describe the extent to which the frequency of the photonic state of fiber can shift on changing

the index contrast of the fiber materials. Specifically, consider the case where the low index material (n_2) in an HC-PCF is altered while the high index material remains unchanged. The initial refractive index contrast (N_0= (n_1/n_2)) changes to N. From equation (3.4) and equation (3.5), the bandgap at wavelength λ_0 will shift to a new wavelength λ given by [79]:

$$\lambda = \lambda_0 \left[\frac{1 - N^{-2}}{1 - N_0^{-2}}\right]^{1/2} \tag{3.6}$$

As shown in figure 3.11, in HC-PCF, the ambient refractive index (n_a) represents the refractive index of holey region that consist of both core and cladding holes. The refractive index of back ground material (in general, silica) is symbolized as n_b. The shift in central wavelength from wavelength λ_0 to a new wavelength λ can be expressed as:

$$\lambda = \lambda_0 \left[\frac{n_b^2 - n_m^2}{n_b^2 - n_a^2}\right]^{1/2} \tag{3.7}$$

where, n_m represents the refractive index of filling material. This refractive index scaling law is particularly applicable where the entire air region of HC-PCF needed to be filled with gases or liquids. Filling the holes of fiber with different fluid media will result in the shift of bandgaps and their corresponding bandwidth. This shift in central wavelength and bandwidth can be evaluated using refractive index scaling law, equation (3.7).

In equation (3.7), n_a represents the ambient index inside the holey region which includes the core and the holes inside the cladding. The refractive index of background material and infiltrated material is denoted as n_b and n_m respectively. Also, λ_0 represents the central wavelength of the fiber in air medium (n_0). Hence for hollow-core fibers with similar geometry profile, when the refractive index of the filling material changes from n_0 to n_m, the corresponding wavelength shift of the PBG edge varies from λ_0 to λ. Differentiating Eq. (3.7) partially with respect

to n_m,

$$\frac{\delta\lambda}{\delta n_m} = \lambda_o \left[\frac{(n_b^2 - n_a^2)^{1/2} \frac{\delta}{\delta n_m} \left((n_b^2 - n_a^2)^{1/2} \right)}{(n_b^2 - n_a^2)} \right] \tag{3.8}$$

$$\frac{\delta\lambda}{\delta n_m} = -\frac{\lambda_0 . n_m}{\left[(n_b{}^2 - n_a{}^2)^{1/2} . (n_b{}^2 - n_m{}^2)^{1/2} \right]} \tag{3.9}$$

$$\frac{d\lambda}{dn_m} = -K . \frac{n_m}{(n_b{}^2 - n_m{}^2)^{1/2}} \tag{3.10}$$

where

$$K = \frac{\lambda_0}{(n_b{}^2 - n_a{}^2)^{1/2}}$$

'K' is a positive constant determined by the refractive index of the fiber material and the central wavelength. $(\delta\lambda/\delta n_m)$ represents the refractive index sensitivity and its negative value indicates that the PBG has a blue-shift in wavelength with increase in index of the infiltrated material. $(\delta\lambda/\delta n_m)$ varies with the ambient refractive index (n_a) of the medium, background material index (n_b) and infiltrated material index (n_m) as shown in figure 3.12.

The effect of ambient and background indices on the shift in PBG is studied for different filling material indices values ranging from 1.3 to 1.4. The central wavelength (λ_0) of the considered fiber is 800 nm. Figure 3.12(a) and 3.12(c) represent respective shifts in photonic bandgap edge and refractive index sensitivity change at different ambient indices (n_a = 1, 1.05 and 1.1) but at constant background index (n_b=1.45). Figure 3.12(b) and 3.12(d) correspond to the respective shifts in photonic bandgap edge and refractive index sensitivity change for different background indices (n_b=1.45, 1.475 and 1.5) in the air (n_a = 1) medium. In both cases the wavelength undergoes a blue shift on increasing the index of filling material but the nature of variation is different. In the first case (figure 3.12(a)) where the background index is kept constant (n_b=1.45), it is seen that the central wavelength is shifted to higher values at higher ambient index. But the effect is minor at higher material index. For example, when the filling medium is water

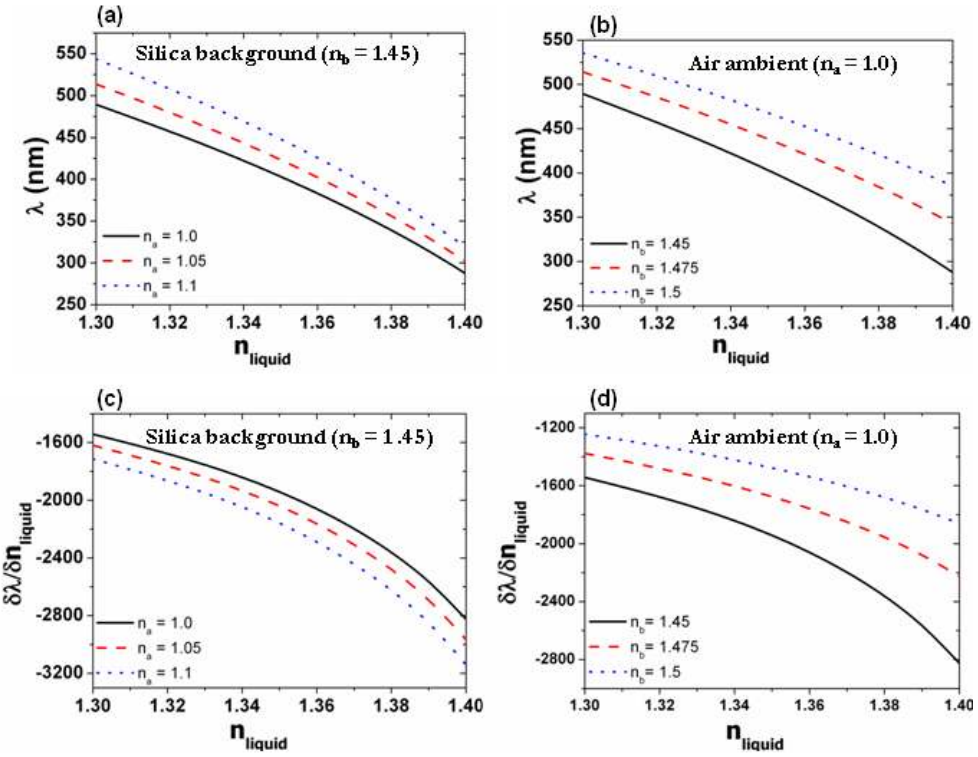

Figure 3.12: (a) Wavelength shift in the falling PBG edge and (c) change in refractive index sensitivity as function of filling liquid index (in the RI range 1.3 to 1.4) for different ambient refractive indices (n_a= 1.0, 1.05 and 1.1) at pure silica (n_b=1.45) background. (b) Shift in PBG edge and (d) change in refractive index sensitivity for different background indices (n_b=1.45, 1.475 and 1.5) at constant ambient index (n_a=1.0, air medium).

(n_m=1.33) with pure silica background (n_b=1.45), the values of central wavelength at n_a=1, 1.05 and 1.1 are 440 nm, 462 nm and 489 nm respectively. In the sec-

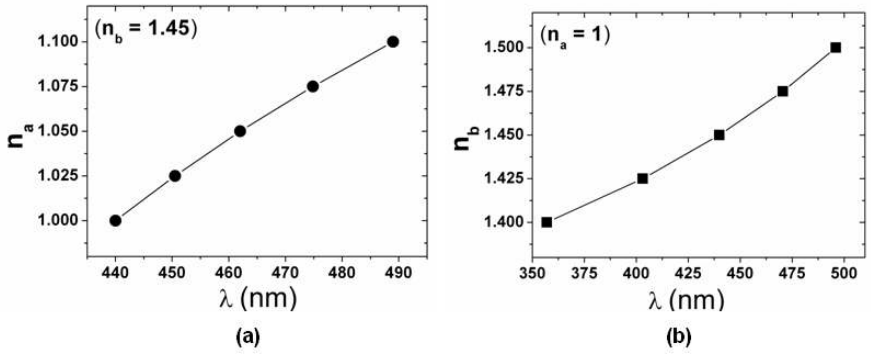

Figure 3.13: Shift in PBG edge for (a) varying ambient index at silica background (n_b=1.45) (solid circles) and (b) for varying background index in air medium (n_a=1.0) (solid rectangles).

ond case (figure 3.12(b)) where the ambient index is kept constant (n_a=1) and the

back ground index varied, it is seen that the central wavelength values increases significantly on increasing the background index when the infiltrated material index is high. For example, when the filling medium is water with air ambient, the respective values of central wavelength at n_b=1.4, 1.45 and 1.5 are 357 nm, 440 nm and 496 nm. In a water filled fiber, the effect of background index on shift in central wavelength (PBG edge shift) is much significant than the ambient index as shown in figure 3.13. Figure 3.13(a) represents the shift in PBG edge for different ambient indices at silica background, whereas figure 3.13(b) corresponds to shift in PBG edge for various background indices in air ambient.

3.4.2 The choice of HC-PCFs

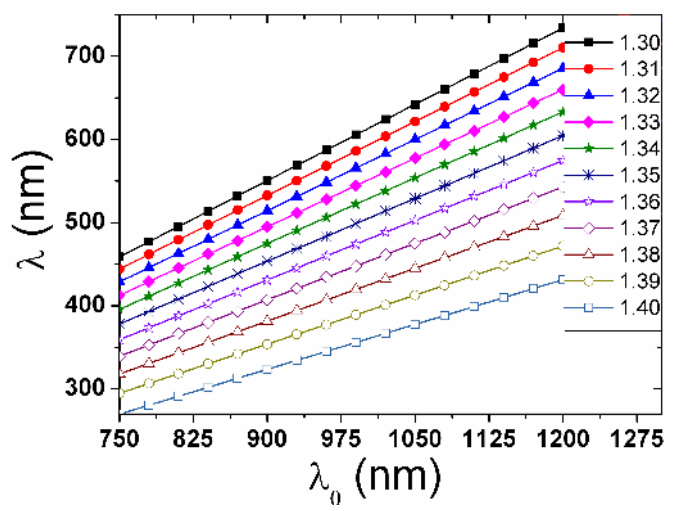

Figure 3.14: The shift in central wavelength (λ_0) of HC-PCFs to the new wavelength (λ) at various filling material indices.

In HC-PCF based fluorescence sensing applications, the sample volume is drawn into the fiber holes using capillary action. In general, the fluorescence samples are dissolved/ dispersed in medium such as methanol, water or ethanol etc. Most HC-PCFs have cladding made of pure fused silica (n_b=1.45) with array of air holes (n_a=1) running along the entire length of the fiber. In HC-PCF based fluorescence sensing applications, the sample volume is drawn into the fiber holes using capillary action. In general, the fluorescence samples are dissolved/ dispersed in medium such as methanol (refractive index, n=1.329), water (n=1.33) or ethanol (n=1.36).

Based on the RI scaling law, for a particular filling material, the shifted wavelength (λ) is proportional to central wavelength (λ_0) of the HC-PCF. The variation of λ with λ_0 is plotted for different filling material indices values ranging from 1.3 to 1.4 in figure 3.14. An experiment has been performed to demonstrate the induced changes in the sensitivity of the HC-PCF based fluorescence sensors due to the shift in wavelength and is explained in the following section.

3.4.3 Materials and methods

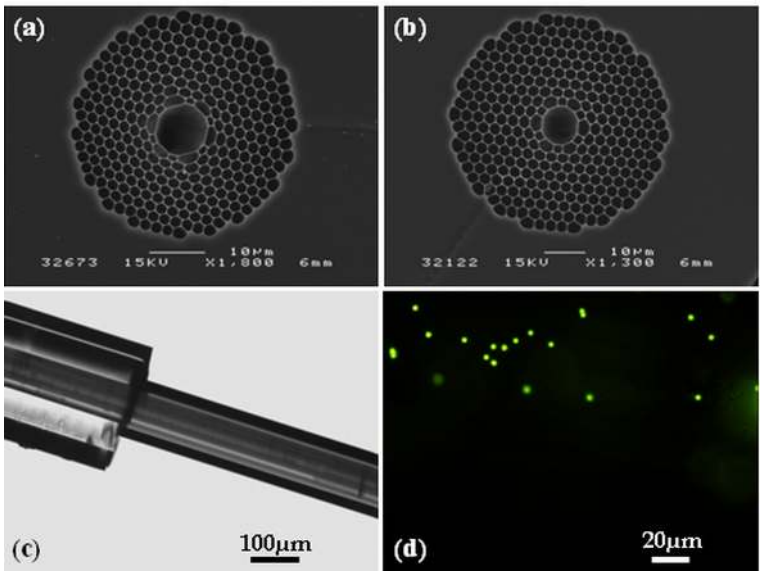

Figure 3.15: SEM images of HC-PCF with (a) central wavelength 830 nm (HC-800) & (b) central wavelength 1060 nm (HC-1060), (c) microscopic side view of a cleaved HC-PCF end (10X/0.3NA objective lens) and (d) microscopic view of the longitudinal section of HC-PCF showing the immobilized green fluorescent microspheres of diameter 2 μm (50X/0.75NA objective lens).

Two hollow-core fibers, HC-800-01 and HC-1060-02 (from *Crystal Fiber A/S*) are selected for the experimental study. The scanning electron micrograph (SEM) images of the HC-PCF facets are given in figure 3.15(a) and figure 3.15 (b). The HC-800-01 has an approximate core diameter of 9.3 μm surrounded by a 40 μm holey region. It operates at a center wavelength of 830 nm and exhibits full photonic bandgap (high transmission range) extending from approximately 770 nm to 890 nm. The attenuation over this range is less than 0.5 dB/m. The HC-1060-02 photonic bandgap presents a band larger than 100 nm centred at 1060 nm. The

hollow core has a centre core size of diameter 10 μm $\pm$ 1μm surrounded by a microstructure comprised of eight periods of hexagonally packed cylinders with a period of 2.75 μm and a filling fraction of around 90%. The cladding diameter is 123 μm $\pm$ 5 μm.

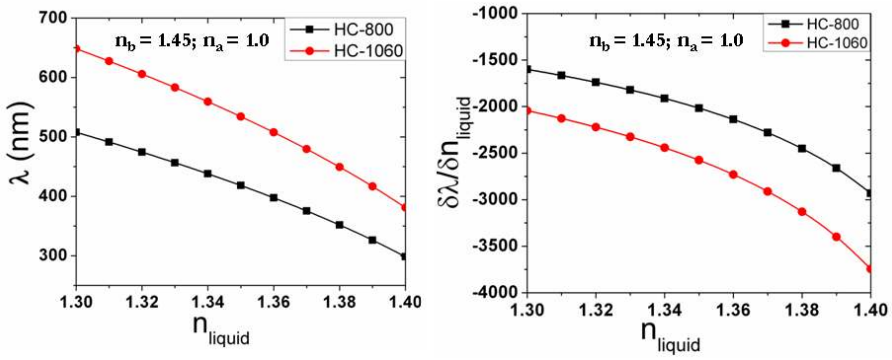

Figure 3.16: (a) Central wavelength plot for HC-1060 (solid circles) and HC-800 (solid rectangles) using equation (3.7) and (b) refractive index sensitivity plot for HC-1060 (solid circles) and HC-800 (solid rectangles) using equation (3.10), for different filling indices between 1.3 and 1.4.

Both the hollow-core fibers are cut into segments of ≈10 cm length and one end of the fiber is cleaved carefully using a fiber cleaver to produce a flat surface. Microscopic side view of the cleaved fiber end is given in figure 3.15(c). Microscope with 10X (0.3NA) objective lens is used for imaging the fiber end. Evaluation of equation (3.7) and equation (3.10) for different filling material indices ranging from 1.3 to 1.4 are performed for the two hollow-core fibers (from Crystal Fiber A/S) with central wavelengths 830 nm (HC-800-01) and 1060 nm (HC-1060-02) which are employed in the experimental study (section 3.4.4). The obtained results given in figure 3.16(a) and figure 3.16(b) denote the variation in the central wavelength and refractive index sensitivity, respectively, for different filling liquid indices.

The green fluorescent microspheres (*Duke Scientific Corp.*) of diameter ≈2 μm, employed in this study are internally-dyed polymer beads. The particles are in a solution of DI water and some surfactants. The green fluorescence labeled microsphere immobilized fiber that gives an emission maximum wavelength at around 508 nm is excited with blue laser light (473 nm). In order to verify the influence of photonic bandgap edge shift on the sensitivity of fluorescence signal, two types of

study has been performed. In the first study, same fiber (with central wavelength 830 nm) has been used for two different dispersion media such as ethanol (n = 1.36) and distilled water (n = 1.33). In the second case, two fibers with different central wavelengths (830 nm and 1060 nm) are considered with sample particles dispersed in same medium (ethanol). The experiment is carried out on both fibers for same values of laser power and similar coupling efficiency in order to compare the fluorescence collection efficiency.

The cleaved end of the HC-PCFs segments were dipped into the sample solution to allow the sample to be drawn into the fiber due to the capillary effect. The microsphere particles have nearly the same density as water (1.05 g/cm^3). Therefore, the particles would follow the fluid flow arising from the capillary force. The fibers are permitted to dry out in room temperature for approximately one hour, after which the microsphere immobilized fibers are ready for the fluorescence imaging and sensing studies. The presence of the microsphere sample inside the fiber is detected using a fluorescence microscope. The flat end facet of the fiber is placed under the microscope for investigation and fluorescent immobilized particle inside the HC-PCF is imaged through a charge-coupled device (CCD) camera (*Sensovation*, Germany, image resolution of 696 x 520 pixels) attached to a microscope (Zeiss, Germany). A mercury lamp connected to the fluorescence microscope with an appropriate filter (excitation wavelength of 436 nm) is used for fluorescence excitation to illuminate the fluorescent tracer particles. The microscope with a 50X (0.75 NA) objective is used here for imaging. The obtained fluorescent microscopic picture of fiber containing fluorescent microspheres is shown figure 3.15(d). The quantification of fluorescence signal from both fibers is performed using spectroscopic analysis as described below.

3.4.4 Spectroscopic Analysis

The spectroscopic analysis is performed using the experimental set up shown in figure 3.8. The fluorescent spectra obtained at identical conditions from HC-800

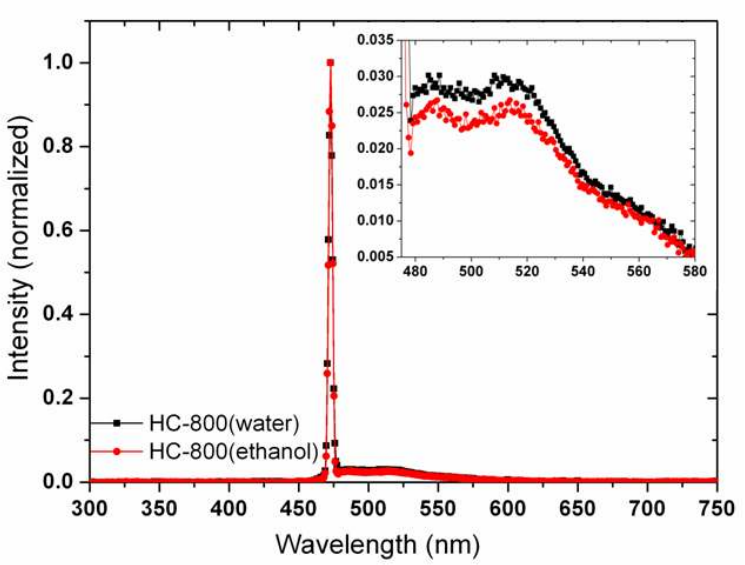

Figure 3.17: The obtained fluorescence spectrum (normalized) for excitation at 473 nm from the HC-PCF with central wavelength 830 nm filled with green fluorescent microparticles dispersed in water (black solid rectangles) and ethanol (red solid circles) [Inset: the wavelength region corresponding to the fluorescence emission is expanded].

fiber segments for ethanol and water dispersed microsphere samples are normalized as shown in figure 3.17. The water dispersed fiber gives better signal for green fluorescence when compared to the ethanol dispersed fiber. This result is in agreement with the result obtained in section 3.4.2 (figure 3.14). For a fiber with central wavelength (λ_0) 830 nm (HC-800), the filling of water causes the shift in central wavelength to an approximate value of 457 nm. But, the filling of ethanol shifts the central wavelength from 830 nm to 397 nm, approximately. Hence the water filled HC-800 has central wavelength nearer to the green region which results in better sensitivity. The results are found to be reproducible for different fiber segments with same central wavelength (830 nm).

Figure 3.18 shows the normalized spectra obtained from fibers with central wavelengths 830 nm and 1060 nm for green fluorescent particles dispersed in ethanol medium. It is vivid that the fiber with central wavelength 1060 nm shows better fluorescent signal when compared with fiber of central wavelength 830 nm. The higher intensity obtained with 1060 nm fiber is also in agreement with the results shown in figure 3.14, corresponding to refractive index 1.36 which is refractive

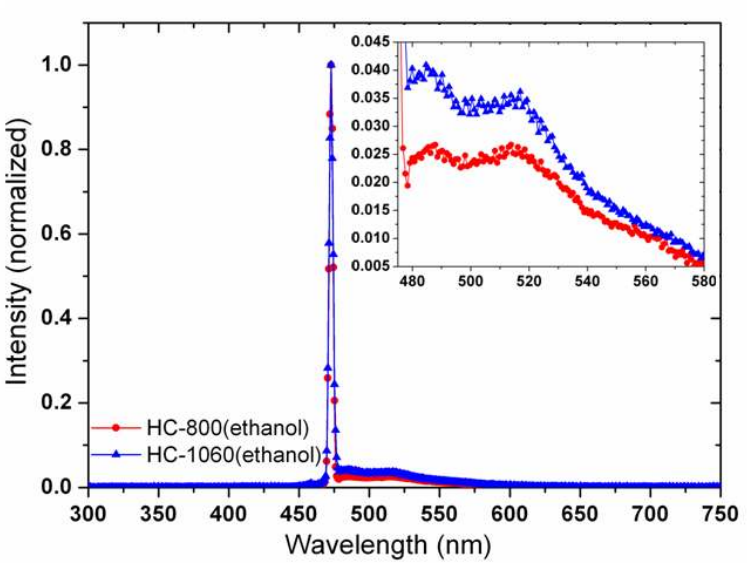

Figure 3.18: The obtained fluorescence spectrum (normalized) for excitation at 473 nm from the HC-PCFs with central wavelengths 830 nm (red solid circles) and 1060 nm (blue solid triangles) filled with green fluorescent microparticles dispersed in ethanol [Inset: the wavelength region corresponding to the fluorescence emission is expanded].

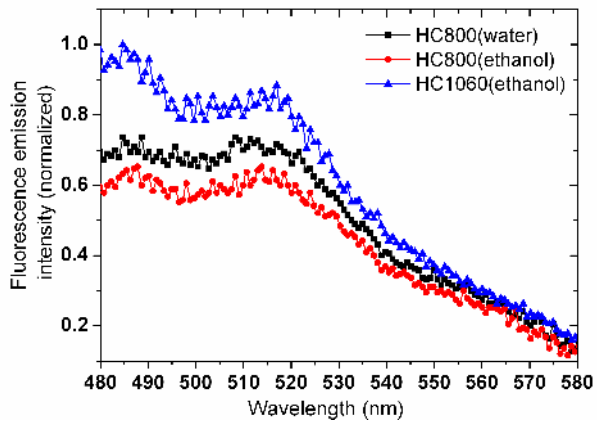

Figure 3.19: Comparison of green fluorescent signals obtained from the HC-800 filled with green fluorescent microparticles dispersed in water (black solid rectangles) and ethanol (red solid circles), and HC-1060 filled with green fluorescent microparticles dispersed in ethanol (blue solid triangles).

index of the dispersed medium (ethanol). From figure 3.14; it can be seen that for a filling material index of 1.36, central wavelength of the HC-1060 fiber will shift from 1060 nm to around 508 nm; whereas in the case of fiber with central wavelength at 830 nm (HC-800), the approximate value of shifted wavelength is 400 nm for the infiltrated material index of 1.36. The results are repeatable for different fiber segments with the same central wavelengths. The fluorescent signals obtained

shown in figure 3.17 and figure 3.18 are normalized and plotted in figure 3.19 for comparison. The obtained results are in accordance with the RI scaling law.

3.5 Ultrasensitive Protein detection technique using HC-PCF

The detection technique based on HC-PCF is further extended to selectively detect ER alpha protein. The method is based on antibody based immunoassay technology [95] that makes use of the binding between an antigen and its homologous antibody in order to identify and quantify the specific antigen in a sample. In this study, estrogen receptor (ER) from a MCF-7 breast carcinoma cell lysates immobilized inside a hollow-core photonic crystal fiber was detected using anti-ER primary antibody with either Alexa^{TM} Fluor 488 (green fluorescent dye) or 555 (red fluorescent dye) labeled Goat anti-rabbit IgG as the secondary antibody. Based on the RI scaling law described formerly in this chapter, two HC-PCFs with central wavelength at 830 nm (HC-800) and 1060 nm (HC-1060) are selected for the detection of green and red fluorescent dye respectively.

3.5.1 Materials and methods

Both MCF-7 and MDA-MB 231 cells are grown to confluence in Dulbeccos Modified Eagle Medium (DMEM)-high glucose supplemented with 10% Fetal Bovine Serum (FBS) and 1% penicillin and streptomycin. The estimated amount of protein in MCF-7 and MDA-MB-231 cell lysates by Bradfords method [96] is found to be 1 μg/μl. The amounts of estrogen receptor (ER) alpha protein immobilized in the fibers are calculated according to the protein quantity in the cell lysate. To confirm the ER protein signal, the cells are analyzed for Western blot using anti-ER-α antibody for cellular ER, and anti-β-actin antibody for β-actin.

The HC-800 has an approximate core diameter of 9.3 μm surrounded by a 40 μm diameter microstructured cladding. It exhibits full photonic bandgap (high

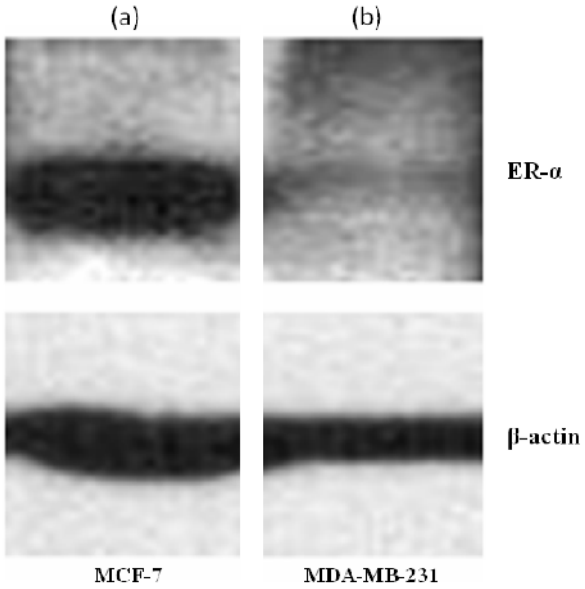

Figure 3.20: Western blot analysis data of ER-α and β-actin in (a) MCF-7 and (b) MDA-MB-231 cells. ER-α was detected using using anti-ER-α antibody and β-actin using a monoclonal anti-β-actin antibody.

transmission range) extending from approximately 770 nm to 890 nm. The attenuation over this range is less than 0.5 dB/m. The HC-1060 has photonic band larger than 100 nm centred at 1060 nm. The hollow core has a centre core size of diameter 10±1 μm surrounded by a microstructure comprised of eight periods of hexagonally packed cylinders with a period of 2.75 μm and a filling fraction of around 90%. The cladding diameter is 123±5 μm. Both the hollow-core fibers are cut into segments of ≈10 cm length and one end of the fiber is cleaved carefully (approximately 1.5-2.0 cm length) using a fiber cleaver to produce a flat surface. The primary step of the experiment is to activate the silica inner core of the fiber to facilitate the detection of ER protein. The tip of the fiber is dipped in the 0.01% Poly L-lysine (*Sigma Aldrich*, USA) solution for 3 minutes and the solution is allowed to get into the fiber by simple capillary forces. The fiber is permitted to dry out in room temperature for approximately one hour. After drying it is washed twice with PBS for 5 minutes. Thus the inner core is prepared for further process.

3.5.2 Results and discussions

3.5.2.1 Western Blot Analysis

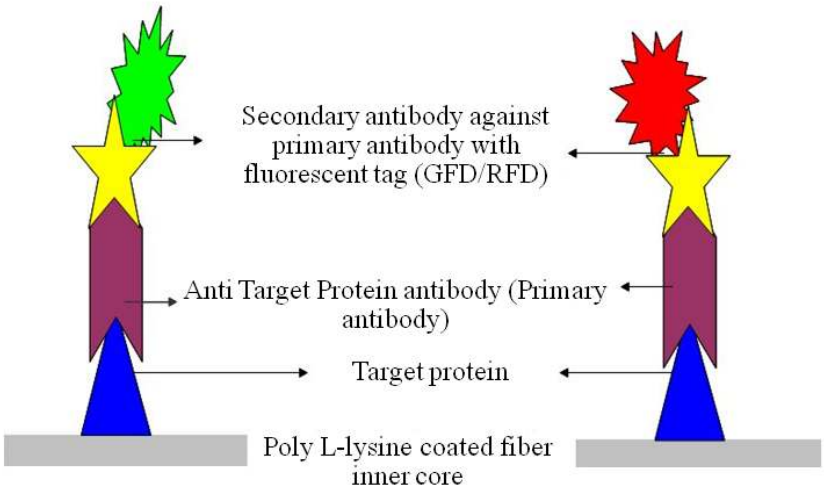

Figure 3.21: Cartoon showing specific protein binding by developed protocol.

The concentration of proteins in the cell lysates are quantified using western blot analysis. The western blot is a generally used analytical technique to detect specific proteins in a given sample of tissue homogenate or extract. The endogenous estrogen receptor levels in the positive cells were detected using the antibody raised against estrogen receptor alpha. To confirm the ER protein signal, the cells are analyzed using anti-ER-α antibody for cellular ER, and anti-β-actin antibody for β-actin. For this purpose, 10 μg protein is resolved by 4-12% gradient sodium dodecyl sulfate-polyacrylamide gel electrophoresis (SDS-PAGE) and is transferred to nitrocellulose membrane. The membrane is blocked in 1X Tris Buffered Saline with Tween-20 (TBST) containing 5% milk powder for 3 hours. The membrane is further incubated overnight in the same buffer containing anti-ERα antibody (Acris Antibodies, GmbH, Germany) at 4°C. The membrane is washed and incubated with the secondary anti-Rabbit antibody conjugated with horseradish peroxidase (HRP) enzyme for 2 hours. The washed membrane is incubated with chemiluminescent substrate for HRP and exposed to X-ray film and developed. The stripped membrane is detected for protein β-actin and used as internal loading control.

The obtained results for MCF-7 and MDA-MB-231 cells are shown in fig-

ure 3.20(a)&(b). As the β-actin is the house keeping gene, it acts as a protein internal standard. Hence it gives signal in both MCF-7 and MDA-MB-231 cell lines as shown in figure 3.20 (a). It is also clear from the figure that only MCF-7 cell line gives signal corresponds to ER-α. The absence of signal in MDA-MB-231 cell lines confirms the lack of ER-α receptor in it.

3.5.2.2 Protein immobilization

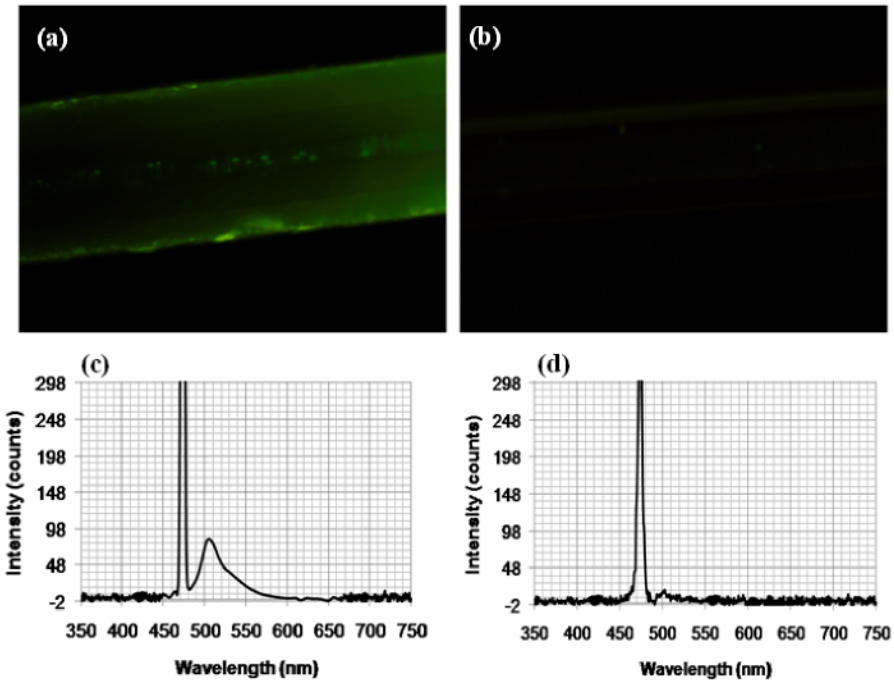

Figure 3.22: Fluorescent (Alexa Fluor 488 (Green fluorescent dye)) (a) & (b) Microscopic image and (c) & (d) spectral signature showing protein binding inside the fiber immobilized with ER alpha positive (MCF-7) cell lysate (sample fiber) & ER alpha negative (MDA-MB-231) cell lysate (control fiber).

The different steps involved in the process are schematically represented in figure 3.21. The binding of protein mainly depends upon the efficient surface attachment procedures which is crucial for biosensor application. Hence, the primary step of the experiment is to activate the silica inner core of the fiber to facilitate the detection of ER protein. Poly-L-lysine is used to pre coat the inner wall of the fiber and this activated surface provides a base for append the targeted protein to achieve this goal. The tip of the fiber is dipped in the 0.01% Poly L-lysine (*Sigma*

Aldrich, USA) solution for 3 minutes and the solution is allowed to get into the fiber by simple capillary forces. The fiber is permitted to dry out in room temperature for approximately one hour. After drying it is washed twice with PBS for 5 minutes, thus the inner core is prepared for further process.

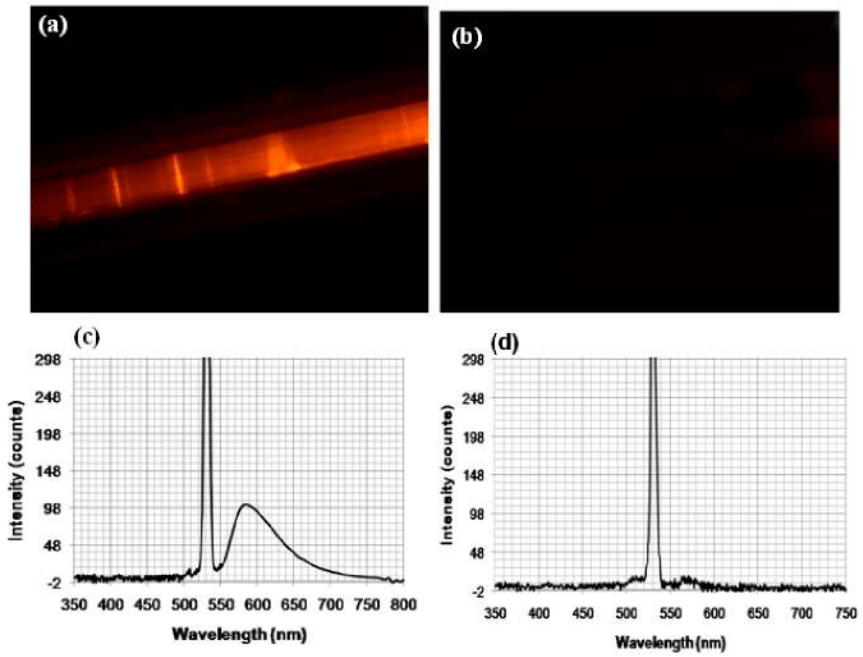

Figure 3.23: Fluorescent (Alexa Fluor 488 (Red fluorescent dye)) (a) & (b) Microscopic image and (c) & (d) spectral signature showing protein binding inside the fiber immobilized with ER alpha positive (MCF-7) cell lysate (sample fiber) & ER alpha negative (MDA-MB-231) cell lysate (control fiber).

In the next step, ER alpha positive (MCF-7) and negative (MDA-MB-231) cell lysates are allowed to stick inside different photonic crystal fibers for protein binding (3 minutes). After that the fibers are incubated at 4°C for two hours, then washed thrice briefly in TBST buffer. The primary antibody binding is done using anti-estrogen alpha (primary antibody-Acris antibodies, GmbH, Germany) solution diluted to a final concentration of 1:1000 (14 mg/ml) in TBS for 5-10 minutes and incubated for 3 hrs at 4°C. Concurrently sodium iodide symporter antibody (NIS primary antibody; Whatman) is also used to check the non-specific binding of the ER alpha protein. This is followed by TBST buffer wash (thrice) for 10 minutes and dried at 4°C for one hour. The experiment is completed by adding secondary antibody solution made in TBS containing Alexa^{TM} Fluor 488 (Green

fluorescent dye) and/or 555 (Red Fluorescent dye) labeled Goat anti-rabbit IgG Invitrogen^{TM} diluted to 1: 100, same way as that of the earlier step. Appropriate controls are performed simultaneously for both green/red dye detection. Now the immuno binding of the protein is completed inside the fiber core and it is ready for imaging/ sensing. The fibers are stored in dark ambience at 4°C.

The fluorescence fingerprints of the Estrogen Receptor alpha protein are observed under fluorescence microscope and its optical characteristics are also analyzed using the spectrophotometer. The cleaved end of the fiber carrying immobilized protein is focused under the microscope (*Olympus* fluorescence microscope CKX41) and checked for the fluorescence signal. Both the control fiber and sample fiber are analyzed for the emission signal. An abundant fluorescence signal is noticed in the centre core, due to the large size that allows fast and easy flow of more quantity of samples inside, compared to the surrounding holes in the case of fiber immobilized with ER alpha positive (MCF-7) cell lysate. The fluorescent signal is found to be increased linearly with the concentration of cell lysate as a result of more number of binding surfaces inside. The control fibers (MDA-MB-231 cell lysate immobilized) showed literally no fluorescent signal (see figure 3.22(b) and figure 3.23(b)) where as the green (see figure 3.22(a)) and red (see figure 3.23(a)) signals are observed for sample fibers (MCF-7 cell lysate immobilized) with secondary antibodies such as green (Alexa Fluor 488) and red (Alexa Fluor 555) dyes.

3.5.2.3 Spectroscopic Analysis

The presence of ER alpha protein inside the hollow-core is further confirmed through the spectroscopic method. The schematic set up used for the spectral analysis of fluorescent proteins are as shown in figure 3.8. A CW Diode-pumped solid-state (DPSS) laser (output power ≈10 mW) is coupled to the proximal end of the sample immobilized PCF using a high precision single mode fiber coupling (FC) unit (*Melles Griot Pte Ltd.*) with a microscope objective (20x, 0.65NA (L_1). The diverging beam emerging from the distal end of the sample immobilized fiber

is allowed to pass though a 2-f lens system, which is configured using two microscope objective (MO) lenses [Newport M-20X, 0.4 (L_2) and Olympus UMPLAN FI 50X/0.8 (L_3)]. The 2-f lens system focuses the beam into a high quantum efficiency spectrophotometer (Ocean Optics, QE65000). The spectrometer is coupled to a PC which displays the spectrum. In our study, lasers with wavelength of 473 nm and 532 nm are used for the Green Fluorescent dye and Red Fluorescent dye analysis respectively. Green emission is obtained at around 515 nm for sample fibers (MCF-7 cell lysate immobilized) (see figure 3.22(c)) with Alexa Fluor 488 as the secondary antibody. Similarly, red emission at around 585 nm is obtained for sample fibers with Alexa Fluor 555 as the secondary antibody as shown in figure 3.23(c). But in the both cases, control fibers are failed to show any fluorescence signals, figure 3.22(d) and figure 3.23(d). These spectral signatures authenticate the strong binding of ER alpha protein inside the HC-PCF.

3.5.2.4 Image processing method

The distribution of fluorescence in the fiber and the localized presence of protein are investigated by image processing means. In order to understand the distribution of fluorescence inside the fiber, the image is processed with *ImageJ*. The wavelengths corresponding to the red dye (Alexa Fluor 555) is extracted from the obtained fluorescence image. The distribution of the extracted intensity along the length of the sample fiber has been normalized and plotted as given in the figure 3.24(b). It is clear that the fluorescence is distributed along the central hollow-core where the cells are immobilized. It has concentrated towards the right end facet of the fiber through which the sample is adsorbed inside the fiber. These results strongly confirm the specific binding of ER alpha protein inside the hollow-core. The respective fluorescence microscopic image and normalized fluorescence intensity distribution along the length of the control fiber (negative cell line-MDA-MB-231 immobilized) are given in figure 3.25. The control fiber has failed to produce fluorescence signal due to lack of the receptor.

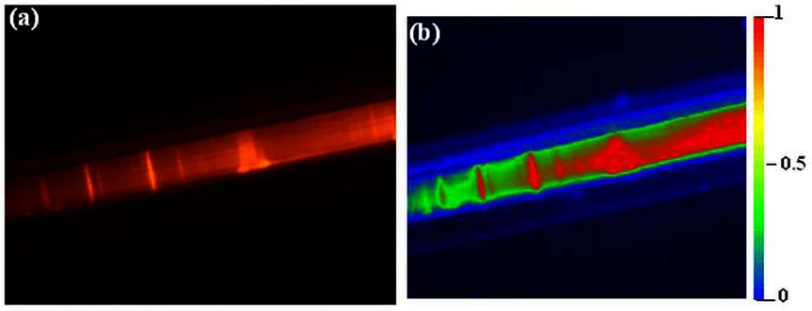

Figure 3.24: (a) Fluorescence microscopic image of Alexa Fluor 555 labelled MCF-7 cell immobilized inside the HC-PCF and (b) Normalized fluorescence intensity distribution along the length of fiber.

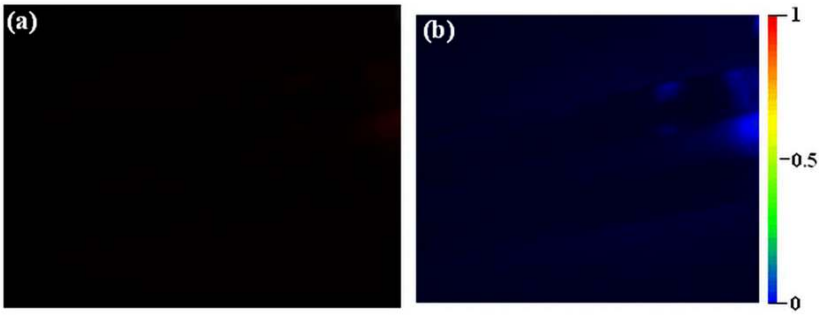

Figure 3.25: (a) Fluorescence microscopic image of Alexa Fluor 555 labelled MDA-MB-231 cell immobilized inside the HC-PCF and (b) Normalized fluorescence intensity distribution along the length of fiber.

3.6 Conclusion

In conclusion, an HC-PCF fluorescence sensor scheme has been demonstrated on the basis of refractive index scaling law. The variations in the central wavelength for different filling material indices are studied in the case of HC-PCFs with cladding made of pure fused silica with array of air holes running along the entire length of the fiber. A proof of concept study has been performed by infiltrating fluorescence sample volume inside HC-PCF and the quantification of fluorescence intensity is analyzed using spectroscopic method. The sensitivity has been compared for similar fiber with different dispersed media and different fibers with same dispersed medium. The obtained experimental results are in good agreement with the analytical results. Further, an antigen-antibody reaction method is employed to recognize the ER alpha protein. In general, this sensor can be applied for any other protein of interest too. The proposed methodology is implemented in array format

immuno recognition of specific protein using a hollow core photonic crystal fiber. The primary step of the experiment is to activate the silica inner core of the fiber to facilitate the detection of ER protein. Poly-L-lysine is used to pre-coat the inner wall of the fiber to create an activated surface that can bind the targeted protein effectively. In the second step, ER alpha positive (MCF-7) and negative cell (MDA-MB-231) lysates are allowed to stick inside different HC-PCF in order to bind with specified antibodies. The primary antibody raised against ER alpha protein (anti-rabbit) is subsequently used to recognize the bio molecule even in fragments, which is available on the core surface. In the current work, we used the Alexa^{TM} Fluor 488 (Green fluorescent dye) and/or 555 (Red Fluorescent dye) as a secondary antibody compatible to the anti ER alpha protein. Fluorescence signal is observed inside the fiber core under microscope in case of MCF-7 cell immobilized HC-PCF, whereas MDA-MB-231 cell immobilized fiber showed literally no signal. This result confirms the possible application of HC-PCF in specifically detecting the presence of protein at a very low sample volume. This method has an additional advantage that the immobilized sample can be analyzed spectroscopically using a simple optical set up. By using laser with wavelengths such as 473 nm and 532 nm, the fluorescence spectrum has been obtained for both positive and negative cell immobilized HC-PCF, which further confirms the ability of HC-PCF for the specific protein detection. The distribution of fluorescence inside the fiber immobilized with ER positive cell and the localization of protein across the length of the fiber has been investigated. The developed technique enables to recognize ≈20 pg of ER alpha protein specifically in a 50 nL sample volume, which is expected to offer great potential as biosensor for medical diagnostics applications.

Chapter 4

Transverse Optical trapping inside HC-PCF

This chapter illustrates a numerical investigation and experimental study carried out for optical trapping applications with transversely probed hollow-core photonic crystal fibers (HC-PCFs). The transmission intensity distribution, at the central core of liquid filled hollow-core photonic crystal fibers (HC-PCFs) with different central wavelengths, is monitored for both TE and TM modes with illumination in the Γ-M direction. Forces acting on the sphere located inside the central core along the transverse direction of these liquid-filled fibers are calculated and compared using Finite Difference Time Domain (FDTD) and Maxwell Stress Tensor based methods. An optical trapping system is designed where a near-infrared laser light is focused using a microscope objective to create an optical trap across a liquid-filled HC-PCF. A micron sized particle is loaded into the liquid-filled hollow-core by optical trapping method for analysis and subsequently moved to a different medium by translating the trap along the length of HC-PCF. Further, a multi-functional optical system is developed that is capable of trapping, manipulating, imaging and performing spectral signature characterizations.

4.1 Background

It is known that the electromagnetic waves (light) can exert radiation force on objects where it impinges. In situations where these objects have low mass and are in vacuum or fluid solution (such that frictional forces are low), these optical forces can actually be used to manipulate particles [9]. Then by using a loosely focused laser beam it is possible to push particles in the direction of laser propagation [23]. Alternatively, if the laser is tightly focused the particles tend to experience a strong gradient force that pushes them towards the region of high optical intensity. The

resultant photonic force depends on the laser beam parameters and the position of the particle within the beam. It is also found to depend on the size, shape and refractive index of the particle. This photonic force is found to be useful in applications such as optical tweezers, levitation of particles and near-field scanning optical microscopy [97, 98].

Hollow core photonic crystal fibers (HC-PCFs) are a group of silica waveguides distinguished by a microstructured cladding of periodic air holes surrounding a central air core [71], where light within certain wavelength bands is prevented from propagating through cladding region due to bandgap effects. The mode propagation properties strongly depend on wavelength, which in turn depends on the design configuration and the geometry of air holes. Unlike conventional fibers, photonic crystal fibers are made of pure silica glass (SiO_2) without any doping. Hence it is biocompatible and chemically inert. Apart from their primary function as waveguides, the HC-PCFs is utilized as biosensor [77, 99]; due to its better sensitivity arising from high light-matter interaction in the central hollow-core which in turn reduces the sample consumption rate. A few groups have examined the possibility of various ultra-small optical devices by transversely probing light across the length of microstructured HC-PCF [89, 100]. Transverse guidance through a solid-core photonic crystal fiber is already reported, numerically and experimentally, and the presence of partial bandgaps are observed [87].

There are mainly two types of trapping possible by employing HC-PCF. In the first case, laser beam propagates along the length of fiber to levitate the particles along the fiber axis using the radiation pressure of the guided mode [17, 101, 102]. Here the trapping is realized through the guided mode, hence the choice of fiber or laser wavelength is much easier. However, the control over positioning of particle along the length of fiber is little. In the second type of trapping using HC-PCF, as the one we considered in this study, laser beam propagates transversely through the PCF cladding and focuses onto the fiber axis (i.e. central core). In this transverse optical trapping method, a much better control over the positioning and manip-

ulation of the particle can be realized. But the influences of fiber microstructure and the infiltrated medium on the partial bandgaps have to be taken in to account for optimizing these fibers for specific transverse optical trapping applications.

In this perspective, we have examined the transmission characteristics at the central core of transversely probed HC-PCFs for Γ-M direction. The study examines the possible application of HC-PCFs in the field of optical tweezers where the sample particles are suspended in an aqueous medium. The wavelength of trapping beam is determined by the transverse partial bandgap existing in the HC-PCFs. Based on rigorous analysis method, numerical analysis is performed to investigate the transverse trapping mechanism inside the hollow-core. Transverse probing through a microstructured hollow-core photonic crystal fiber is considered and the presence of photonic stop bands is observed in the transmission spectrum. Wavelength of the trapping laser beam is defined by this transmission spectrum. The rigorous diffraction problem [103, 104] considered here consists of mainly two steps. In the initial step, the diffraction problem is solved and the field in the region of the particle is calculated rigorously. In the second step, the force acting on the particle is computed by applying Maxwells stress tensor. The nature of the force with the relative position and motion of the particle inside the hollow-core is studied. All the main physical aspects are included in this numerical study, which is expected to give more favorable results.

4.2 Theoretical model and simulations

4.2.1 Why FDTD for OT?

Currently, various numerical methods have been applied to solve Maxwell's equations such as finite element methods (FEMs), discrete dipole approximation (DDA) and T-matrix method. In FEMs, spatial discretization is performed to obtain a numerical solution to the system of differential equations [105]. But, the FEM method scales defectively with simulation volume. In DDA, the particle itself is

divided into small volumes. Each of the parts is treated as a simple dipole with polarizability depending on the composition of the particle [106]. The T-matrix method is more suitable for systems with high symmetry [107]. The electromagnetic field in objects with complicated configurations can be calculated conveniently by the finite-difference time-domain (FDTD) [108] method employing Maxwell's equations. In this context, the finite-difference time domain (FDTD) method is implemented here to study optical trapping of particle using Maxwell stress tensor. In the FDTD method, the analyzed region is divided into discrete grids of points, and the finite-difference representation of Maxwell's curl equations using a central-difference formulation and the Yee-cell notation is applied to each grid. FDTD method permits one to scale linearly with simulation volume. Moreover, it can handle arbitrary structures and has the ability to manage many types of materials under a single structure. As the whole computational domain is gridded, the grid's spatial discretization must be suitably fine to resolve both the minimum electromagnetic wavelength and the smallest geometrical feature in the computational domain. The calculation time will be longer when the computational domain is large and grid resolution is high.

Though a time consuming method for an electromagnetic problem, the FDTD has many unique advantages when considered for simulating optical trapping. The optical trap space is first converted into meshes, and then the FDTD is used to calculate the electric and magnetic fields of the optical traps in the spatial domain as a function of time steps. The momentum of light can be determined from $\vec{\mathbf{S}} = \vec{\mathbf{E}} \times \vec{\mathbf{H}}$ in the time domain [2]. Also, FDTD allows to analyze arbitrary shape scattering objects, and to easily induce a focused light source. The latter is very important because optical trapping experiments are usually demonstrated within the focused light field generated from a high numerical aperture (NA) objective lens within a microscope. In addition, the FDTD can give a scattering field in time domain, which is very useful to study optical trapping phenomena in ultra-fast optics and near field optical microscopy.

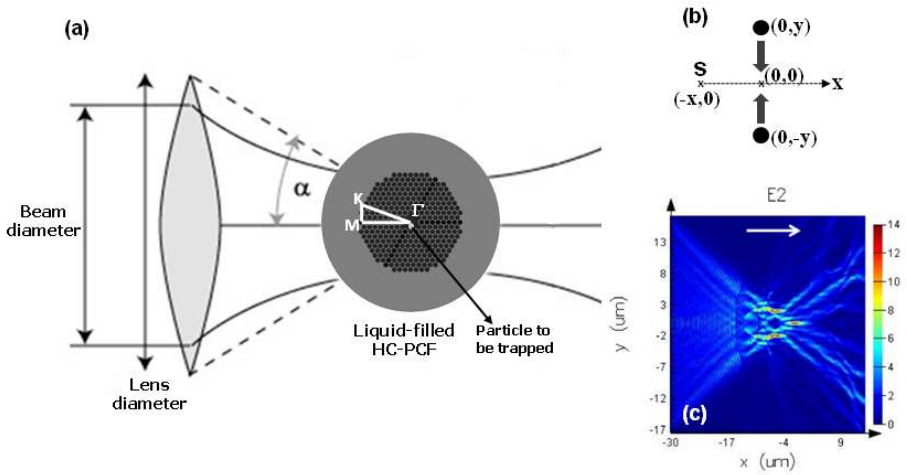

Figure 4.1: Schematic of using a thin lens for focusing a Gaussian light beam to a central hollow-core (b) considered geometry for the trapping and (c) Trapping field distribution displaced across the face of the water filled HC-PCF (arrow indicates the direction of beam propagation).

The fundamental analysis on the optical trapping across HC-PCF is demonstrated using FDTD method and Maxwell stress tensor. We employ the two dimensional FDTD (2D-FDTD) method to obtain the solution of the Maxwell equations [108]. In the FDTD method, the analyzed region is divided into distinct grids of points.

4.2.2 Theory

A thin lens is used for focusing the Gaussian beam to the central core of the fiber as shown in figure 4.1. The numerical aperture (NA) of the lens is defined by the refractive index (n) of the medium in which the source exists and α is the half angle of the radiation spread measured in the far-field as shown in the figure 4.1(a).

$$NA = n \sin \alpha \tag{4.1}$$

The optical forces involved in trapping inside hollow-core arise from the photon momentum transfer, which occurs when the transverse guided beam interacts with the particles inside the hollow-core. This momentum transfer can be expressed by solving the electromagnetic scattering problem. For smaller particles where

ray optics is inappropriate, rigorous electromagnetic expansions describing spheres near foci can be used. Here, the electromagnetic field scattered by the particle is calculated by solving Maxwell equations.

$$\vec{\nabla} \times \vec{E} = -\frac{\partial \vec{B}}{\partial t} \tag{4.2}$$

$$\vec{\nabla} \times \vec{B} = \mu \vec{J} + \frac{1}{c^2} \frac{\partial \vec{E}}{\partial t} \tag{4.3}$$

$$\vec{\nabla} \cdot \vec{E} = \frac{\rho}{\varepsilon} \tag{4.4}$$

$$\vec{\nabla} \cdot \vec{B} = 0 \tag{4.5}$$

where 'ε' and 'μ' represent the electric permittivity and the magnetic permeability of the dielectric medium, respectively. The electromagnetic force on a charged particle can be expressed as follows:

$$\vec{F} = q\left(\vec{E} + \vec{v} \times \vec{B}\right) = \int \left(\rho \vec{E} + \vec{J} \times \vec{B}\right) d\tau \tag{4.6}$$

According to Maxwell's equations, an electromagnetic field possesses a momentum $\vec{P}$ based on its field. Since the force is the time rate of change of momentum $\vec{P}$, equation (4.6) can be expressed as:

$$\frac{d\vec{P}}{dt} = \int \left(\rho \vec{E} + \vec{J} \times \vec{B}\right) d\tau \tag{4.7}$$

Substitute for '$\vec{J}$'and 'ρ' from equation (4.3) and equation (4.4), equation (4.7) can be written as follows:

$$\frac{d\vec{P}}{dt} = \int \left[\left(\varepsilon \vec{\nabla} \cdot \vec{E}\right) \vec{E} + \left(\frac{1}{\mu} \vec{\nabla} \times \vec{B} - \varepsilon \frac{\partial \vec{E}}{\partial t}\right) \times \vec{B}\right] d\tau \tag{4.8}$$

$$\frac{d\vec{P}}{dt} = \int \left[\varepsilon \left(\vec{\nabla} \cdot \vec{E}\right) \vec{E} + \frac{1}{\mu} \left(\vec{\nabla} \times \vec{B}\right) \times \vec{B} - \varepsilon \left(\frac{\partial \vec{E}}{\partial t} \times \vec{B}\right)\right] d\tau \tag{4.9}$$

$$\frac{\partial E}{\partial t} \times \vec{B} = \frac{\partial}{\partial t}\left(\vec{E} \times \vec{B}\right) - \left(\vec{E} \times \frac{\partial \vec{B}}{\partial t}\right) = \frac{\partial}{\partial t}\left(\vec{E} \times \vec{B}\right) + \vec{E} \times \left(\vec{\nabla} \times \vec{E}\right) \quad (4.10)$$

$$\frac{d\vec{P}}{dt} = \int \left\{ \varepsilon \left(\vec{\nabla} \cdot \vec{E}\right) \vec{E} + \frac{1}{\mu}\left(\vec{\nabla} \times \vec{B}\right) \times \vec{B} - \varepsilon \left[\mu \frac{\partial \vec{S}}{\partial t} + \vec{E} \times \left(\vec{\nabla} \times \vec{E}\right) \right] \right\} d\tau \quad (4.11)$$

where, $\vec{S} = \frac{\vec{E} \times \vec{B}}{\mu}$ is the Poynting vector.

$$\begin{aligned} \frac{d\vec{P}}{dt} &= \int \left\{ \varepsilon \left[\left(\vec{\nabla} \cdot \vec{E}\right) \vec{E} + \left(\vec{E} \cdot \vec{\nabla}\right) \vec{E} - \frac{1}{2}\vec{\nabla}\left(E^2\right) \right] + \frac{1}{\mu} \left[\left(\vec{\nabla} \cdot \vec{B}\right) \vec{B} \right. \right. \\ &\quad \left. \left. + \left(\vec{B} \cdot \vec{\nabla}\right) \vec{B} - \frac{1}{2}\vec{\nabla}\left(B^2\right) \right] \right\} d\tau - \varepsilon\mu \frac{d}{dt} \int \vec{S} d\tau \end{aligned} \quad (4.12)$$

By applying divergence theorem to equation (4.12)

$$\frac{d\vec{P}}{dt} = \int \vec{T} \cdot \hat{n} da - \frac{1}{c^2}\frac{d}{dt} \int \vec{S} d\tau \quad (4.13)$$

Where '$\vec{T}$' is known as the Maxwell stress tensor and is actually a derivation of the conservation laws of electromagnetic energy and momentum. '$\hat{n}$' is the unit vector perpendicular to the surface, and 'da' is an infinitesimal surface element. '$\vec{T}$' has units of force per unit area and its components are described as follows:

$$\vec{T}_{\alpha\beta} = \varepsilon \vec{E}_\alpha \vec{E}_\beta + \frac{1}{\mu}\vec{B}_\alpha \vec{B}_\beta - \frac{1}{2}\left(\varepsilon E^2 + \frac{1}{\mu}B^2\right)\delta_{\alpha\beta} \quad (4.14)$$

where '$\delta_{\alpha\beta}$' denotes the Kronecker delta function. It can be expressed as follows:

$$\delta_{\alpha\beta} = \begin{cases} 1 & \text{if } \alpha = \beta \\ 0 & \text{if } \alpha \neq \beta \end{cases}$$

The second term in equation (4.13) defines the momentum carried by elec-

tromagnetic field within the volume 'V'. The field momentum is zero when it is averaged over one oscillation period.

Hence, the change of the momentum inside of the surface can be determined by integrating Maxwell stress tensor on the surface surrounding the object. Since the momentum changes on the boundary of the object, the extinction amount of the momentum becomes the induced optical force ($\vec{F}_{induced}$) acting on the object [104, 109].

$$\left\langle \vec{F}_{induced} \right\rangle = \left\langle \oint \left(\vec{T} \cdot \hat{n} \right) ds \right\rangle \tag{4.15}$$

where $\langle ... \rangle$ represents the time average.

$$\vec{T} = \begin{bmatrix} T_{\alpha\alpha} & T_{\alpha\beta} & T_{\alpha\gamma} \\ T_{\beta\alpha} & T_{\beta\beta} & T_{\beta\gamma} \\ T_{\gamma\alpha} & T_{\gamma\beta} & T_{\gamma\gamma} \end{bmatrix} \tag{4.16}$$

Here, α, β and γ represent the Cartesian coordinate components of elemental surface. The α, β and γ are parallel to β-γ, α-γ, and α-β planes, respectively. Hence, $T_{\alpha\beta}$ represents the force per unit area on the α^{th} component of the surface along the α^{th} direction. Correspondingly, $T_{\beta\alpha}$, $T_{\beta\beta}$, and $T_{\beta\gamma}$ represent the surface force densities on the β^{th} component of the surface along the α, β, and γ directions, respectively.

The expansion of field components is carried out by making use of scalar potentials and a separation of variables in the coordinate system surrounding the sphere. Once the scattering electromagnetic field is known, the optical force acting on the particle can be determined in the second computational step by applying Maxwell's stress tensor (T).

All the analysis performed here is using two dimensional (2D) method. By considering so, the divergence of input and diffracted beams from the numerical structure into the third dimension (normal to the transverse geometry) is neglected. In the 2D simulation, the elements of the Maxwell stress tensor for harmonic fields

are $T_{\alpha\alpha}$, $T_{\alpha\beta}$, $T_{\beta\alpha}$ and $T_{\beta\beta}$, with $\vec{E}$ and $\vec{H}$ being the total electric and magnetic fields in spherical coordinates. In this study, we assume that E_z, H_x and H_y are nonzero.

For determining the steady-state motion of the sphere in the central liquid core of the HC-PCF, the Navier-Stokes viscous drag forces induced by a liquid flow on the sphere has to be considered. From Stokes law, the expression for viscous force is given as [110]:

$$\vec{F}_{vis} = -6\pi\eta r\vec{V} \tag{4.17}$$

The negative sign implies that viscous force is opposite to the velocity ($\vec{V}$) of the sphere. 'η' represents the viscosity of the surrounding fluid. The sphere considered in this study is immersed in water ($\eta = 1.002 \times 10^{-3}$Ns/m^2 at 20^0C). The other forces involved in the particle motion in the liquid are the force of gravity $\vec{F}_g$ and the buoyancy force $\vec{F}_b$ created by the liquid, these forces having opposite directions.

Hence the net optical force $\vec{F}_{total}$ acting on a given sphere can be determined by,

$$\vec{F}_{total} = m\vec{a} = \vec{F}_{induced} + \left(\vec{F}_b - \vec{F}_g\right) + \vec{F}_{vis} \tag{4.18}$$

where $m = \frac{4\pi r^3\rho}{3}$

Here, 'ρ' is the density and 'r' is the radius of the sphere. (For polystyrene sphere, ρ=1060 kg/m^3).

The equation (4.18) gives the initial force acting on the particle located inside water filled central core and can be used to analyze the optically induced particle motion. Once the force acting on the particle is known, the dynamic motion of the particle can be studied using the fundamental laws of motion.

$$\vec{V} = \vec{u} + \vec{a}t \tag{4.19}$$

$$\vec{x} - \vec{x_0} = \vec{u}t + \frac{1}{2}\vec{a}t^2 \tag{4.20}$$

The position at a later time is determined from the position, velocity and force

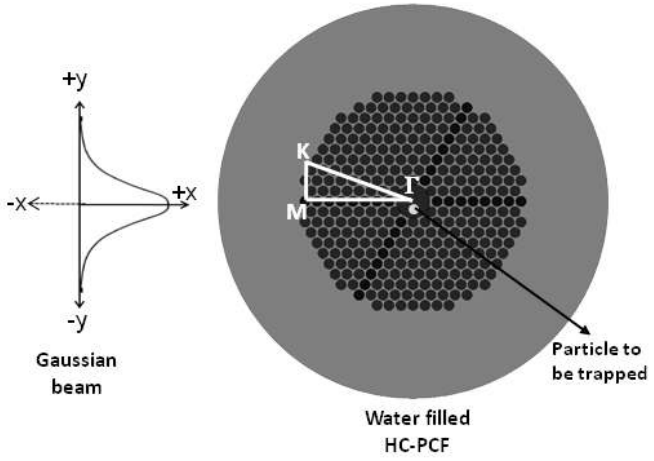

Figure 4.2: Schematic of the numerical configuration considered for focusing a Gaussian light beam to central hollow-core of HC-PCF.

at the previous step. The process can be repeated for several steps at short intervals of time which provide the trajectory of the particle inside the core.

4.2.3 Existence of partial bandgaps in HC-PCF

Bandgap characteristics of transversely probed hollow-core photonic crystal fibers (HC-PCFs) are numerically investigated by FDTD analysis. The transmission characteristic of the transverse trapping beam is described using concept of photonic partial bandgap. The field and intensity distribution are monitored at the central hollow-core for both TE and TM modes illuminated in the Γ-M direction. From the numerical results obtained, it is found that photonic stop bands are formed in the transmission spectrum. It is inferred that such partial bandgap studies are important for the application of HC-PCFs in the well-known area of optical tweezers where an efficient trapping can be performed inside the hollow-core.

4.2.3.1 Transmission intensity distribution

Figure 4.2 shows the considered numerical geometry to simulate transmission characteristics at the central core of HC-PCF. The PCF voids are filled with different infiltrated liquid-media against a background of silica ($n_b = 1.45$). The infiltrated liquid media considered in this study are ethanol (refractive index, n = 1.36),

Table 4.1: Comparison of the fiber parameters of HC-1060 and HC-1550 considered for numerical study

Fiber parameters	HC-1060	HC-1550
Central Wavelength (λ_0)	1060nm	1550nm
Core diameter (D)	9.7μm	10.9μm
Hole diameter (d)	2.5μm	3.42μm
Pitch (Λ)	2.75μm	3.8μm
Diameter of silica cladding	123μm	125μm
No. of rings surrounding core	8	8
Silica refractive index	1.45	1.45
Numerical aperture (NA)	0.12	0.2

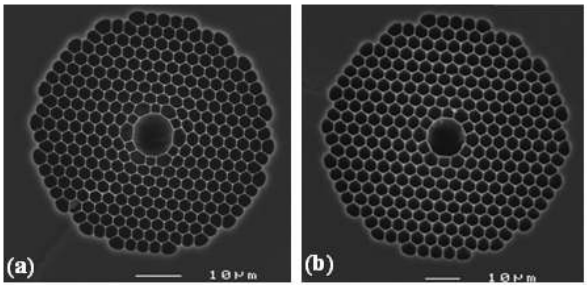

Figure 4.3: SEM images of the facets of HC-PCFs with central wavelength (λ_0) at (a) 1060 nm and (b) 1550 nm.

methanol (n = 1.34) and water (n = 1.33). The HC-PCFs (Crystal Fiber A/S) employed here are designed for air-filled operation at wavelengths 1550nm (HC-1550) and 1060nm (HC-1060) respectively. The scanning electron micrograph (SEM) images of the HC-PCF facets are shown in figure 4.3. The cross section of the PCF has a microstructure of circular inclusions in a triangular lattice. The details of the fiber parameters are given in Table 4.1. The computational domain is excited by a continuous-wave source with a Gaussian beam profile using a 0.7NA thin lens. To reduce the computational complexity, it is assumed that the fiber structure (see figure 4.2) is invariant to the z-direction.

HC-PCF can be considered as a 2D photonic crystal for illumination in the transverse direction. Initially, the simulation area is excited by a continuous-wave source with a Gaussian beam profile. The geometry of the HC-PCF is designed such that the trapping beam is propagated in the Γ-M direction. Two states of

polarizations are defined for the illuminating light: the transverse magnetic (TM) and transverse electric (TE) polarizations. TM polarization has its electric field parallel to the length of the fiber and TE polarization has its magnetic field parallel to the length of fiber. Three directions are defined as shown in figure 4.2, following the six fold symmetry of the fiber holes array where 'Γ' denotes the origin, 'K' is the nearest neighbour direction, and 'M' is the next-nearest-neighbour direction. In the HC-PCFs, the hole diameters are relatively large so that the analysis along the Γ-K direction is very complex. Hence in the present study, we consider the light propagation in the Γ-M direction. The geometry of the HC-PCF is designed such that the trapping beam is propagated in the Γ-M direction only. The frequency domain power monitor is used to get the transmission characteristics along the propagation directions.

Transmission spectrum are for HC-PCF with central wavelength 1060 nm (HC-1060) is obtained by varying free-space wavelength of the source between 500 nm and 2750 nm. The normalized transmission intensity distribution in the Γ-M direction for both TE and TM polarized light is presented in figure 4.4(a) and figure 4.4(b), respectively. It is clear from the intensity distribution that partial bandgaps exist in the transverse direction. The simulation predicts fundamental bandgap at wavelength near 1.84 μm and second order bandgap near 0.85 μm. These transverse partial bandgaps are present in the Γ-M direction for both TE and TM polarization. In order to probe the trapping beam transversely to the central core, the wavelength of the beam has to be outside this partial bandgaps. From the obtained result, it is concluded that the laser with wavelengths in the range of 660-690 nm will perform better as a trapping laser for this particular HC-PCF.

Further simulation is performed on liquid filled HC-PCF with central wavelength 1550 nm (HC-1550) by varying free-space wavelength of the source between 750 nm and 3000 nm, again, for both TE and TM polarized light. The obtained result for TE and TM polarization modes are as shown in figure 4.5(a) and figure 4.5(b), respectively. It is clear from the intensity distribution that partial

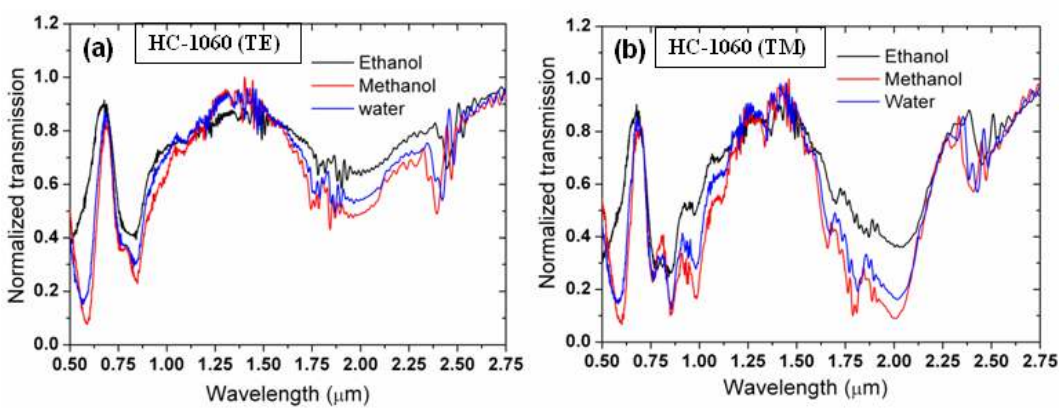

Figure 4.4: Transmission characteristics of the liquid-filled central core of HC-PCF (λ_0 = 1060 nm) for the Γ-M direction of (a) TE and (b)TM modes.

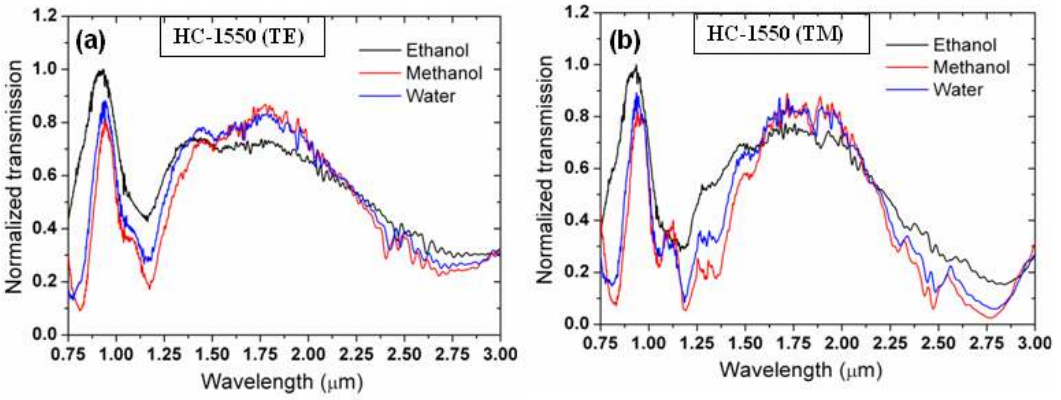

Figure 4.5: Transmission characteristics of the liquid-filled central core of HC-PCF with central wavelength at 1550 nm for the Γ-M direction of (a) TE and (b) TM modes.

bandgaps exist in the transverse direction. These transverse partial bandgaps are present in the Γ-M direction for both TE and TM polarization for this fiber as well. In this case, simulation predicts a fundamental gap near 2.68 μm, the second order near 1.17 μm. In order to probe the trapping beam transversely to the central core, the wavelength of the beam has to be outside this partial bandgaps. From the obtained simulation result, it is concluded that the laser with wavelengths in the range of 920-960 nm will perform better as a trapping laser for this particular HC-PCF. The comparison between transmission characteristics at the central core for water-filled HC-PCF with central wavelength 1060 and 1550 nm for Γ-M direction of TE mode is shown in figure 4.6.

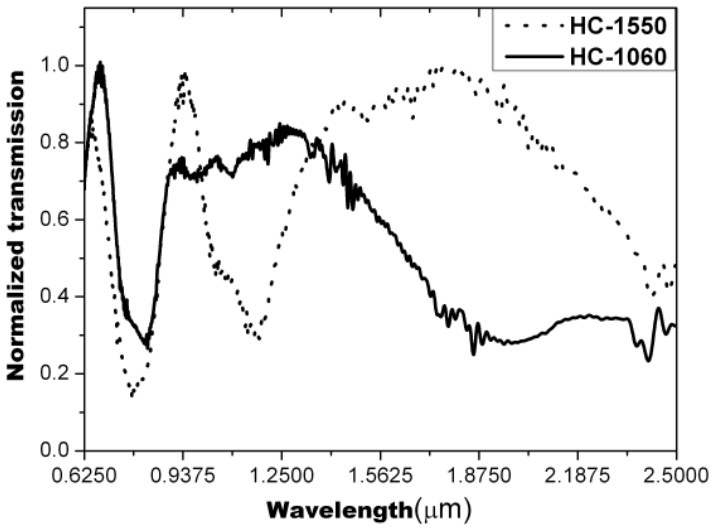

Figure 4.6: Normalized transmission inside the water filled central core of HC-PCF with central wavelength at 1060 nm (solid line) and 1550 nm (dotted line) for the Γ-M direction of TE mode.

Hence the partial bandgaps are function of fiber microstructure. The wavelength at which partial bandgaps exist does not change noticeably by filling the fiber holes with different liquid-samples. But the effect of partial bandgap is found to be suppressed by increasing the refractive index of filling liquid.

4.2.3.2 Field intensity distribution

The field distribution at the central core of water filled HC-PCF at various wavelengths is acquired by simulation. It is assumed that a silica (n=1.5) sphere of diameter 0.1 μm is at the central core. The fiber used in this study has the central wavelength of 1060 nm. The resultant field on the surface of the sphere is recorded using four 1D monitors that cover the sphere. The four analysis script located inside the group is used to obtain the field data. After the fields across the surface of the particle are calculated for each propagation direction, the entire field at an arbitrary point in the space is given by a superposition of the plane wave response times the appropriate amplitude coefficient. The field intensity distribution across the fiber facet in the direction perpendicular to the length of the HC-PCF is shown in figure 4.7. The central core of HC-PCF located at (0, 0) is marked as 'x' in the figure 4.7 (in both SEM image and simulation geometry). The field distribution

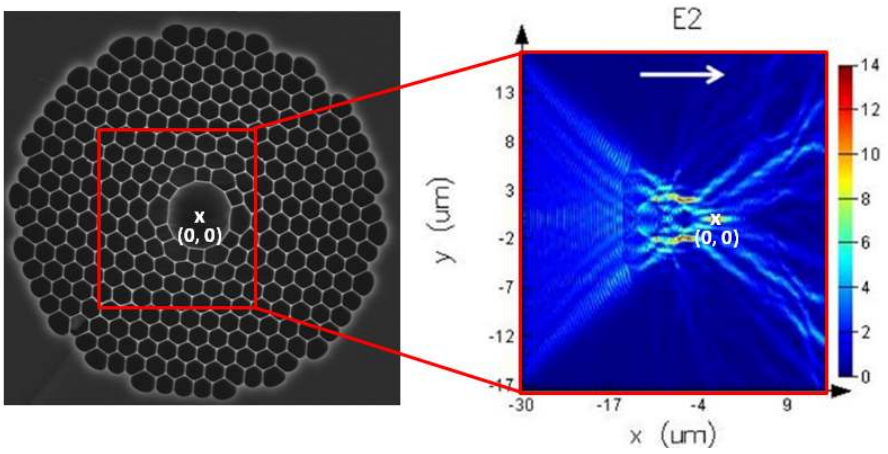

Figure 4.7: Field intensity distribution across the facet of the water-filled HC-PCF in the direction perpendicular to the length of the fiber (arrow indicates the direction of beam propagation).

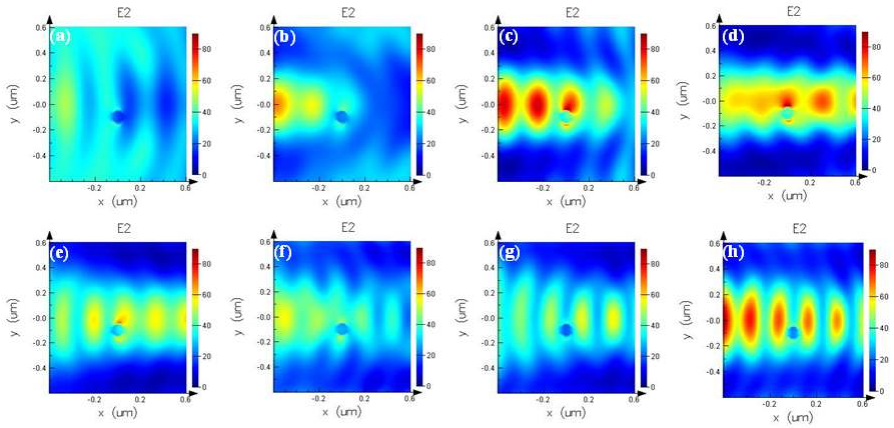

Figure 4.8: Field distribution surrounding the silica particle located at the water filled core of HC-PCF at wavelengths (a) 800 nm, (b) 750 nm, (c) 700 nm, (d) 650 nm, (e) 600 nm, (f) 550 nm, (g) 500 nm and (h) 450 nm.

on the right side is across the facet of the water-filled HC-PCF and corresponds to the region enclosed by the rectangular box in the left image. It can be seen from the field intensity profile that the laser propagating across the water filled fiber microstructure focuses to the central region of the core.

The existence of partial bandgap in the photonic bandgap fiber is further confirmed by figure 4.8, in which we present field information surrounding the silica core recorded over a range of wavelengths (450-800 nm). The field distribution surrounding the silica sphere is found to be a function of wavelength. At certain

wavelength range, 650-675 nm, the field distribution surrounding the silica sphere is maxima as expected from the transmission characteristics of water filled hollow-core PCF with central wavelength 1060 nm (see figure 4.4). The field intensity is found to be lower for a range of wavelength around 800 nm. This is consistent with second order bandgap obtained in this region in the intensity transmission characteristics.

4.2.4 Transverse optical trapping inside HC-PCF: Numerical study

4.2.4.1 Numerical geometry

A schematic diagram representing the focusing of Gaussian beam to the central core of HC-PCF using a thin lens is shown in figure 4.1(a). The HC-PCFs (Crystal Fiber A/S) employed here are designed for air-filled operation at wavelengths 1550 nm (HC-1550) and 1060 nm (HC-1060) respectively. The scanning electron micrograph (SEM) images of the HC-PCF end face is given in figure 4.3. The HC-1550 has a diameter of 10.9 μm surrounded by a microstructure comprised of eight periods of hexagonally packed cylinders with a period of 3.8 μm with filling fraction of around 90%. The external diameter of the HC-PCF is 125 μm. The HC-1060 has a centre core size of diameter 10 μm$\pm$ 1 μm surrounded by a microstructure comprised of eight periods of hexagonally packed cylinders with a period of 2.75 μm and a filling fraction of around 90%. The cladding diameter is 123 μm $\pm$ 5 μm. The silica of these fibers has a refractive index of 1.45. The particle considered in this study is polystyrene sphere (n = 1.59) of diameter 2 μm. The optical trapping beam is launched into the system using a 0.7 NA thin lens. Figure 4.1(b) shows the considered geometry for the trapping, where 'S' defines the laser source position. The trapping field intensity distribution across the fiber face in the direction perpendicular to the length of the HC-PCF is shown in figure 4.1(c). It can be seen from the field intensity profile that the laser propagating across the water filled fiber microstructure focuses to the central region of the core.

The two dimensional FDTD (2D-FDTD) method employed in this study uses four perfectly matched boundary layers to simulate the propagation of the optical trapping beam across the PCF. Since the PCF is much longer in the longitudinal direction than in the transverse, it can be considered as a 2D planar structure, neglecting the out of the plane beam divergence. A grid size of 70 μm $\times$ 20 μm is chosen as the overall simulation area, where a small region 1.2 μm $\times$ 1.2 μm surrounds the central region of the core (0, 0). This small region is having grid sizes of 10 nm along x- and y-directions. The larger mesh is chosen everywhere else to help minimize computation time. A total of 14400 (120 $\times$ 120) mesh points are used in the computation domain, with 4 perfectly matched layer (PML) cells on each side of the boundary. The PML layer allows the reflected light to escape the simulation volume. The overall simulation time is set to 300 fs. In order to determine the force exerted on the sphere by the focused Gaussian beam, the beam focal point is varied by keeping the sphere stable. The method can efficiently scan over a large range in the axial direction. In order to describe the dynamic motion of the particle inside the hollow-core, the beam focal point is kept constant and the motion is studied in steps of 100 μs time interval.

4.2.4.2 Force calculation using Maxwell Stress Tensor

The analytical approach used here is based on Maxwells stress tensor to decompose the illuminating beam into a plane wave spectrum and determine the field distribution for all illumination directions separately where the force is calculated at various positions relative to the waist of the trapping beam. A thin lens with NA of 0.7 was used to focus the Gaussian beam, of waist width 3 μm, to the central core of the fiber as depicted in figure 4.1(a). The focal point of the beam is adjusted so that the particle is trapped at the central core. The light entering the medium refracts through and reflect off the polystyrene sphere. The changes in photonic momentum cause a resultant force on the microsphere. The microsphere (S) used in our study is of diameter 2 μm with refractive index of 1.59. Four one

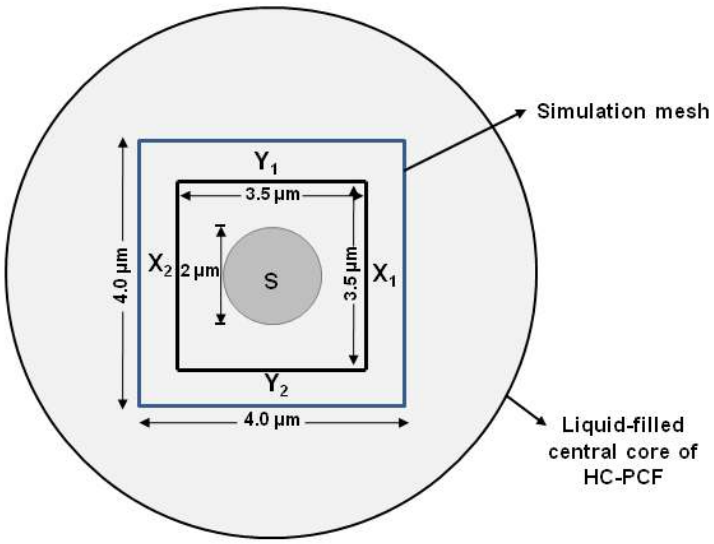

Figure 4.9: Schematic shows numerical geometry closest to microsphere (S) used in the FDTD simulation for calculating forces acting on it (X_1, X_2, Y_1 and Y_2 are frequency domain field and power monitors).

dimensional (1D) frequency domain field and power monitors such as X_1, X_2, Y_1 and Y_2 are used in the 2D simulation as shown in figure 4.9. Each of these monitors can record the electric and magnetic fields at its position. These monitors form a closed 2D box (3.5 μm $\times$ 3.5 μm) around the particle and provide the fields spatial distribution on the surface of the box. The monitors are surrounded by a small simulation mesh (4 μm $\times$ 4 μm) which is having grid sizes of 40 nm along x- and y-directions. The electric and magnetic components of the Maxwell stress tensor (T) are extracted from the four simulation monitors surrounding the sphere. The expression for T can be found in equation (4.14). In the two dimensional (2D) simulation the elements of the Maxwell stress tensor for harmonic fields are T_{11}, T_{12}, T_{21} and T_{22}. In this study, we assume that E_z, H_x and H_y are nonzero. The force components on a surface is obtained by integrating the dot product of the outwardly directed normal unit vector with the electric and magnetic components of the Maxwell stress tensor on the corresponding surface (using equation (4.15)).

In trapping experiment of biological sample, trapping laser with wavelength in the range 780-1100 nm is favourable as it corresponds to the region of minimum absorption of biological sample [30]. In this study, the wavelength of the laser is

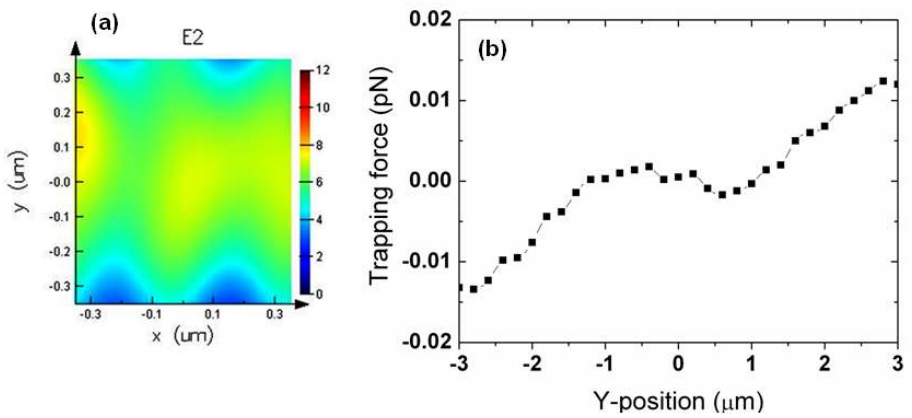

Figure 4.10: (a) Electromagnetic field distribution and (b) variation of force along transverse direction inside the centre core of HC-PCF in the absence of the sphere.

selected is that of the trapping laser employed in the experiment described in the section 4.3, *i.e.*, 800 nm. Also, the infiltrated medium considered is ethanol since the partial bandgap effect is found to be slighter from the transmission characteristics (section 4.2.3.1). Also, ethanol filled fiber is favourable for the further fluorescence spectroscopic analysis of these fibers as it can evaporate quickly.

In order to check the accuracy of our simulation, electromagnetic field distribution has been determined in the absence of sphere, and the force is calculated with Maxwell stress tensor. The results obtained are shown in figure 4.10. In the absence of the sphere, there is negligible field around the focal point of the beam when compared to the field distribution in the presence of the sphere (see figure 4.11). Theoretically, in the absence of sphere, the forces should be zero. The discrepancy here could be due to numerical errors. When compared to the obtained force values in the presence of the sphere, the corresponding values obtained in absence of the sphere are found to be negligibly small.

The forces are calculated for free sphere dispersed in ethanol for displacement in the transverse direction. The result obtained is depicted in figure 4.11. The result shows that a restoring force is acting on the particle directing it to reach the equilibrium position defined by the trapping beam. When the sphere shifts its position to either positive/negative axis along transverse direction, the optical forces act on the particle to attract it to the equilibrium position. The HC-PCFs

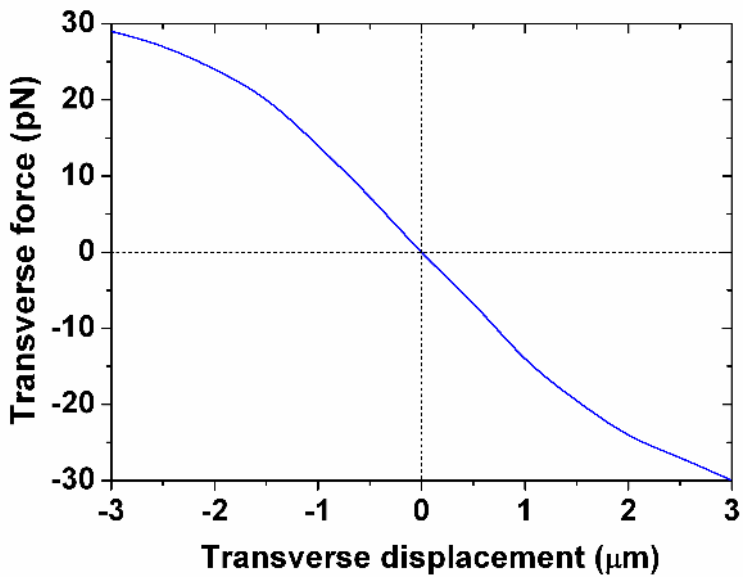

Figure 4.11: Transverse trapping force on a free particle dispersed in ethanol.

are designed such that the direction of propagation of the trapping beam is along the Γ-M direction in the photonic crystal axis as in figure 4.1. HC-PCFs with central wavelengths 1060 nm and 1550 nm are chosen for this simulation study as well. The nature of forces obtained in the transverse direction for the sphere inside the core of ethanol filled hollow-core fibers is simulated. Figure 4.12 compares the evolution of the trapping force acting on the particle across the transverse direction for both fibers. In both simulations, the beam parameters are kept the same.

From the obtained result (figure 4.12), it is clear that the force acting on the particle is repulsive at the central core region. But towards the edge of the core, the force is found to be restorative in nature. Hence trapping of micron sized particle is possible towards the edge of central core. This is quite different from the trapping force in the absence of HC-PCF where the transverse force is completely restorative in nature. The magnitudes of the restorative force in trapping across HC-PCFs are smaller when compared to the free particle case. This is expected from the loss caused by the propagation across the microstructured silica cladding. Also, the magnitude of the restorative force is found to be different for both fibers. The HC-PCF with central wavelength 1550 nm gives higher restorative force than one with central wavelength 1060 nm. This can be explained using the obtained transmission

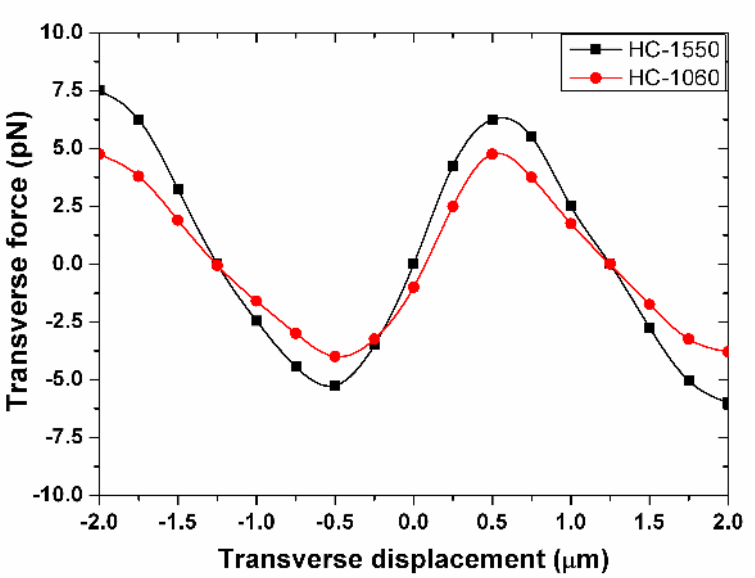

Figure 4.12: Transverse trapping force on a particle displaced across the facet of the ethanol-filled HC-PCFs with central wavelengths such as 1550 nm (HC-1550 (solid rectangle)) and 1060 nm (HC-1060 (solid circle)).

spectra at the central core for both these fibers (section 4.2.3.1). Partial bandgap is present around the wavelength of 800 nm in the fiber with central wavelength 1060 nm for both TE and TM polarization modes (Figure 4.4). However, for fiber with central wavelength 1550 nm, the wavelength of 800 nm is outside partial-bandgap region (Figure 4.5).

An optical trapping experiment is performed to attract and guide fluorescent microsphere sample in to the central core of liquid-filled HC-PCF using a laser beam wavelength of 800 nm which is probed transversely to the HC-PCF. The ethanol filled HC-PCF with central wavelength at 1550 nm is selected for experimental study since the restorative trapping force exerted on particle is found to be higher based on the numerical analysis described above (figure 4.12). The details on the experiment is described in the next section.

4.3 Transverse optical trapping inside HC-PCF: Experimental study

Optical manipulation, separation and detection of biological cells have immense potential biomedical applications, for example, in disease detection. In this section, we present optical manipulation and detection of micron sized fluorescent particles inside hollow-core photonic crystal fiber (HC-PCF) by transverse optical trapping. An optical trapping system is designed where a near-infrared laser light is focused using a microscope objective to create an optical trap across a liquid-filled HC-PCF. Here, trapping laser beam propagates transversely through the liquid-filled HC-PCF cladding and focuses to the fiber axis (i.e. central core). The sample particles get attracted into the central core of HC-PCF due to the laser induced optical force and undergo different analyses. These particles are consequently moved into a different medium by translating the trap along the length of fiber. This study may lead to consider HC-PCFs as being ideal platforms for the investigation into optical manipulation and detection of biological species inside the central core. The proposed method will be particularly advantageous for biosensing application where the reagent use is limited, such as analysis of rare or precious cells, and the sample environment is to be changed after study.

4.3.1 Experimental Set Up

The schematic of the experimental setup for transverse optical trapping inside HC-PCF is shown in figure 4.13(a). The photograph of experimental set up is given in figure 4.14. Trapping light was delivered by a continuous-wave Ti: Sapphire laser (Coherent Mira 900B, pumped by a Coherent Verdi V10 frequency-doubled Nd: YVO_4 laser (532 nm)). The wavelength of the Ti: Sapphire laser is centered at 800 nm and has a repetition rate of 80 MHz when operated in femto-second pulse mode. Gaussian laser beam (TEM_{00} profile) is passed through a beam collimator unit, which allows controlling the divergence of the laser beam, and fills the back

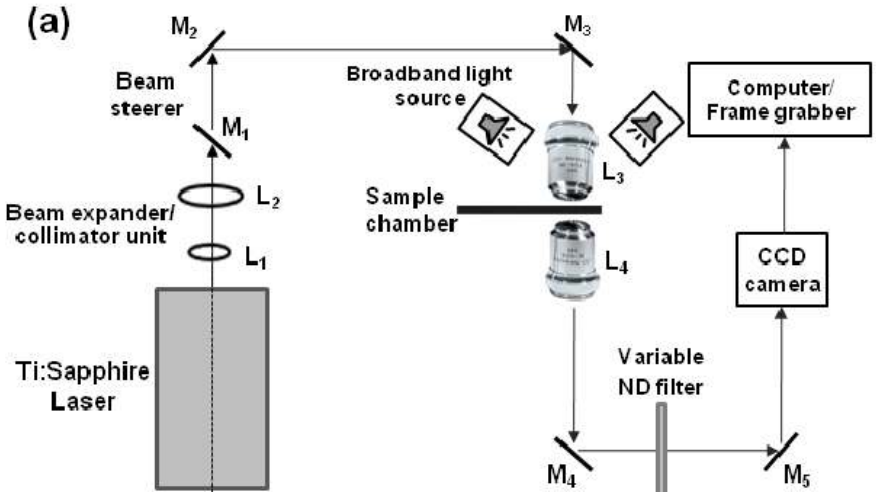

Figure 4.13: Schematic of optical trapping set up consider for transverse optical trapping inside HC-PCF.

pupil of microscope objective lens (Newport M-40X/0.65 (L_3)) to form an optical trap inside a sample chamber. The laser power was 220 mW, measured before the focusing objective lens (L_3).

The picture of sample chamber is shown in figure 4.15(a). The sample chamber is formed by placing two pieces of double sided sticky tape across the center of a standard microscope slide to form a 2-3 mm wide channel. A cover slip is positioned over the top of the tape, at right angles to the microscope slide, and tightly sealed, forming a channel with volume of a few microlitres. A portion of the sample chamber is expanded in figure 4.15(b). The end face of HC-PCF and the microsphere sample are visible here. The sample chamber is mounted on a three-axis translational stage. The deposition of sample solution is done on one side of the channel and then drawing in of the solution is performed from the other side. The hollow-core PCF is introduced through the side of channel. Now the sample chamber and the axis along the length of fiber are perpendicular to the probing laser beam. The image of the trapped particles is projected through a different objective lens (Newport, M-20X/0.4 (L_4)). The digital CCD camera (PL-A741; PixeLINK, Ottawa, Canada) is used for acquiring data, and is triggered under computer control to take bright field videos or images of the sample at a desired sampling rate.

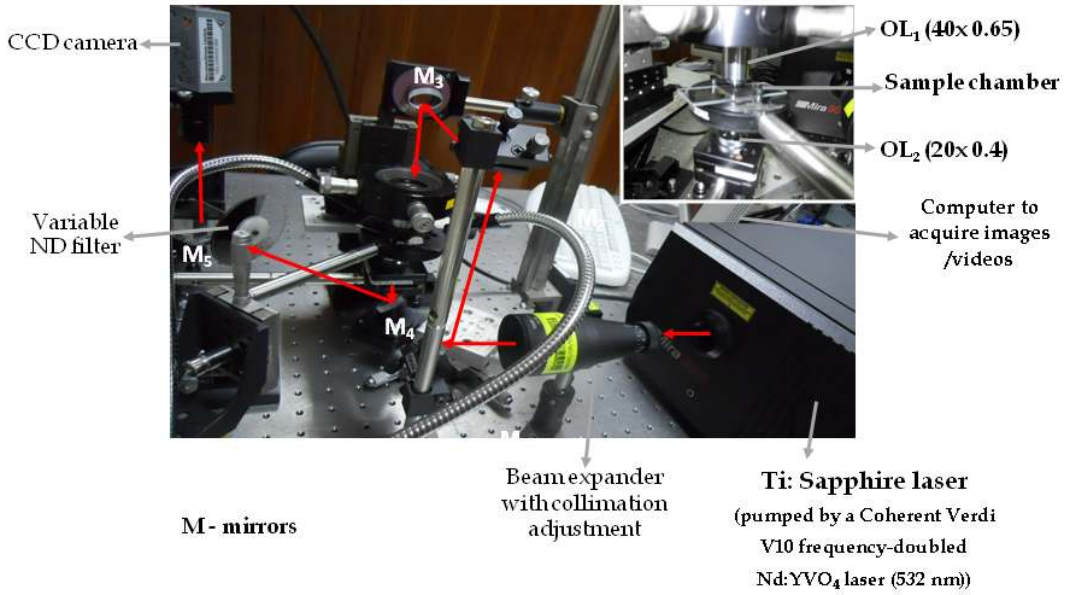

Figure 4.14: Experimental set up for transverse optical trapping inside HC-PCF (laser beam propagation direction is shown in red arrows) [inset: Trapping region is expanded]

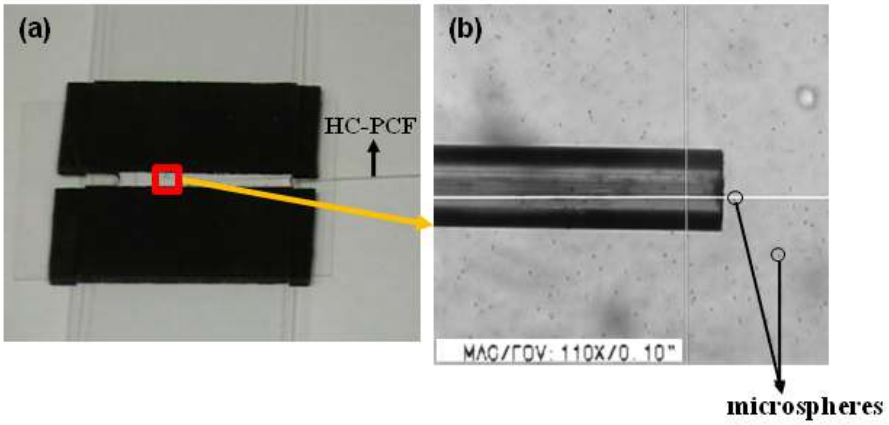

Figure 4.15: (a) picture of the sample chamber containing fluid media with fluorescent microsphere sample and HC-PCF and (b) Microscopic view of a portion of the channel.

4.3.2 Results and Discussion

4.3.2.1 Materials and methods

The HC-PCF with central wavelength at 1550 nm is selected for this study based on the simulation carried out. The hollow core has a diameter of 10.9 μm surrounded by a microstructure comprised of eight periods of hexagonally packed cylinders

with a period of 3.8 μm with filling fraction of around 90%. The silica of the fiber has a refractive index of 1.45 and the cladding diameter is 125 μm. The fiber is cut into segments of ≈6 cm length and one end of the fiber is cleaved carefully using a fiber cleaver to produce a flat surface. The cleaved end of the HCPCFs segments were dipped into the ethanol to allow the solution to drawn into the fiber holes due to the capillary effect. The filling of liquid solution to the fiber holes is to ensure that effect of capillary force to attract the particle towards the fiber core is least. The sample solution containing fluorescent microspheres is transferred to the sample chamber through the sides of the channel formed. Sample used in this study is fluorescent microsphere dispersed in ethanol. Green fluorescent microspheres (*Duke Scientific Corp.*) of diameter ≈2 μm employed in this study are internally-dyed polymer beads. A broadband light source is employed to view the channel formed in the sample chamber as shown in figure 4.13.

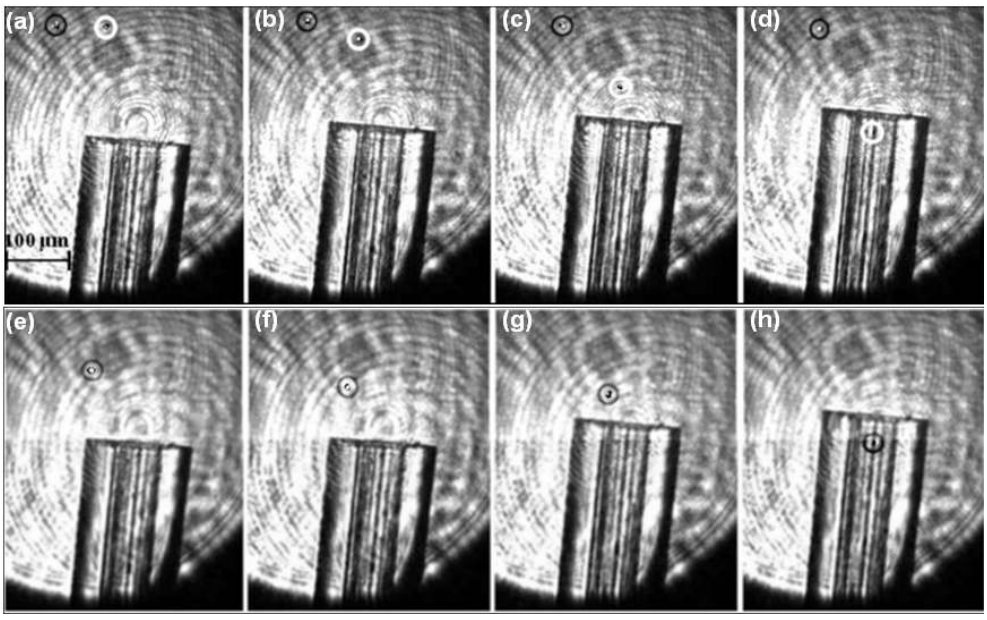

Figure 4.16: Sequential images (1 s interval), (a) to (h), showing the movement of two microparticles (solid black and white line encircling particles positions) to the central core of HC-PCF by means of optical trap formed by focusing laser light.

Higher viscosity (η) of the liquid medium would impede the motion of the particle with a force (viscous drag force) that is proportional to the instantaneous velocity. In the case of optical trapping inside HC-PCF, the viscous drag force helps to attract and track particle into the core of HC-PCF by dissipating the

kinetic energy gained by the particle as it falls into the traps potential energy well. In our study, the fluorescent microspheres are dispersed in water ($\eta = 0.001002$ Pas for water at room temperature). The local increase in temperature would result in an increase in kinetic energy of the particle, if the particle in trap is absorbing. Conversely, if the medium itself is absorbing the increase in temperature would result in decrease in local viscosity of the medium.Since the wavelength of laser beam (800 nm) is within the low absorption region and the particle is not trapped for long, the effect of local heating due to absorption is significantly less.

Now the ethanol-filled HC-PCF is introduced into the chamber through sideways and the positioning is performed by adjusting sample chamber stage. The positioning of cleaved fiber end is performed by translating XYZ stage. When the laser is ON, the position of the fiber is further adjusted so that the beam is probing exactly towards the cleaved end of the fiber, in the transverse direction. Trapping laser is focused through a 40X 0.65 NA microscope objective lens. Real-time monitoring was executed with a charge-coupled device (CCD) camera mounted on top of the microscope and connected to a computer. We found that once the laser is switched on and focused to the cleaved end of the fiber, the microspheres around the fiber end get initially attracted laterally and trapped and guided to the core of HC-PCF. Figure 4.16(a)-figure 4.16(h) is a series of eight consecutive pictures showing position of two particles in optical trap, taken by the CCD camera. Images are taken at 1 s intervals of time.

The fiber is permitted to dry out in room temperature for approximately 30 minutes. The fiber containing sample is then checked for fluorescent signal using an optical set up. Schematic diagram of optical set up is shown in figure 4.17. A continuous wave (CW) diode-pumped solid-state (DPSS) 404 nm laser (output power $\approx$5 mW) is coupled into the proximal end of PCF immobilized with fluorescence sample using a high precision single mode fiber coupling unit. The beam emerging from the distal end of the fiber is focused to a high quantum efficiency spectrophotometer (Ocean Optics, QE65000) using a microscope objective (20X,

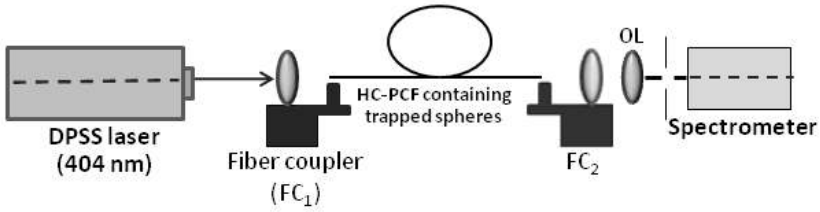

Figure 4.17: Schematic diagram of the experimental set-up used for checking the fluorescent signature inside HC-PCF.

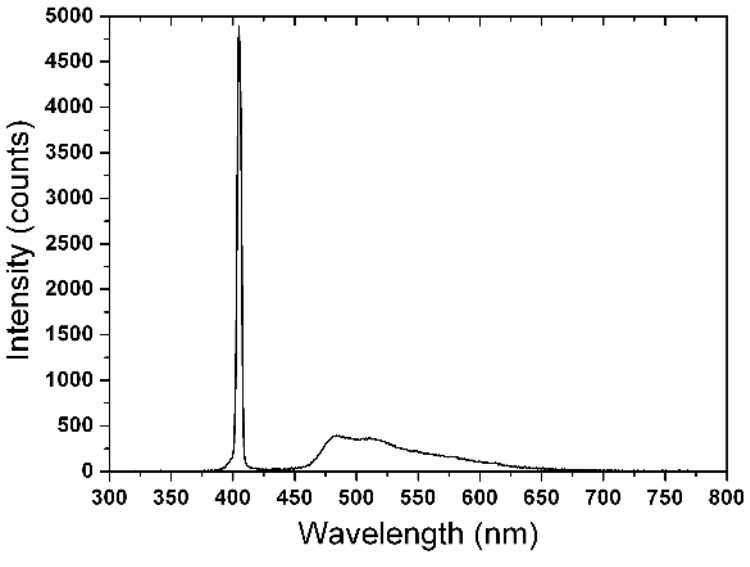

Figure 4.18: Fluorescence signal obtained from the HC-PCF at 404 nm excitation.

0.65NA). The spectrometer is coupled to a PC which displays the spectrum. From the obtained fluorescence spectrum shown in figure 4.18, it is evident that the emission signal represents the presence of sample microspheres.

4.3.3 Reversible trap inside HC-PCF

A further experiment is performed where the fluorescent microsphere particles trapped into the core of HC-PCF using the laser induced optical force undergoes imaging and fluorescence spectroscopic analysis. It is illustrated that the proposed method can track the particle into a different medium using the optical trap as well. The optical setup used in this study is same as shown in figure 4.13. The beam coming out of the laser is expanded and collimated and is directed to the back aperture of the trapping objective (L_3) using three mirrors (M_1, M_2 and M_3).

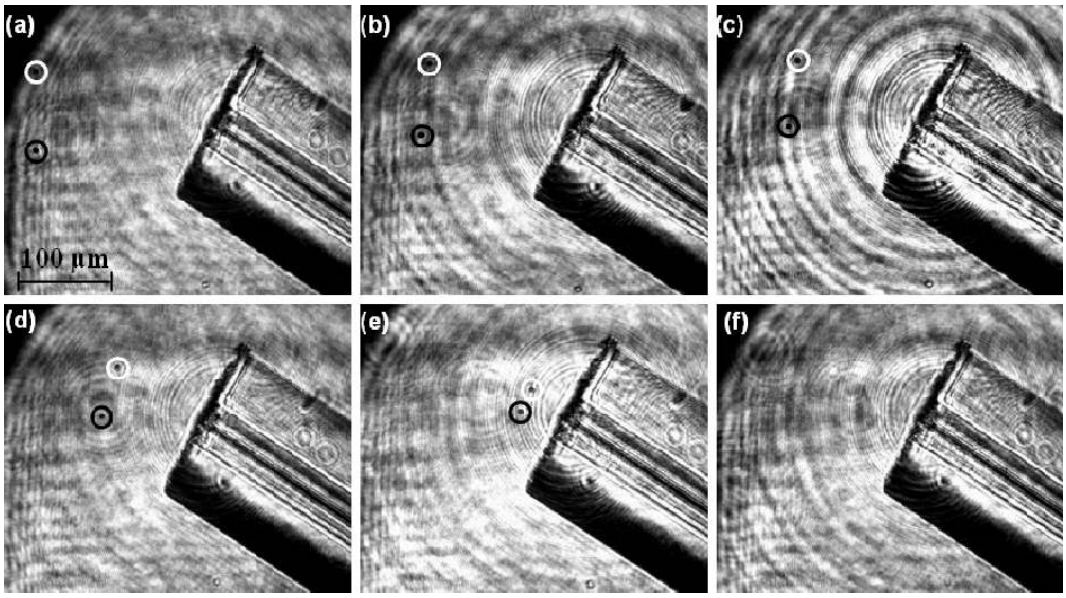

Figure 4.19: Sequentially captured images at 3.5 s intervals of time, (a) to (f), showing the movement of two microparticles (solid black and white line encircling particles positions are guide to the eyes) to the central core of HC-PCF by means of optical trap formed by focusing laser light. Images were cropped to show important features.

The beam is expanded for overfilling the back aperture of the trapping objective. The laser power measured before the objective lens is 180 mW. The fiber in the sample chamber is adjusted such that the probing beam points exactly towards the cleaved end of the fiber, (*i.e.,* in the transverse direction). The microparticles around the fiber end are initially attracted laterally and trapped and guided to the core of HC-PCF. Movement of particle close to the fiber end is imaged through the objective (L_4) onto a CCD camera. Figure 4.19 shows the sequential images obtained through the camera. Images are taken at 3.5 s intervals of time. The result shows that microparticles are flowing into the core region of HC-PCF due to the laser induced trapping force.

The fiber containing fluorescent microsphere is removed from the sample chamber and washed externally, using methanol, without disturbing the microsphere inside the core of liquid filled fiber. The presence of particle inside the central core of HC-PCF is examined using a microscope and the obtained image is shown in figure 4.20(a). In order to enhance the particle images from background, the acquired image is filtered by image processing means and the result is shown in

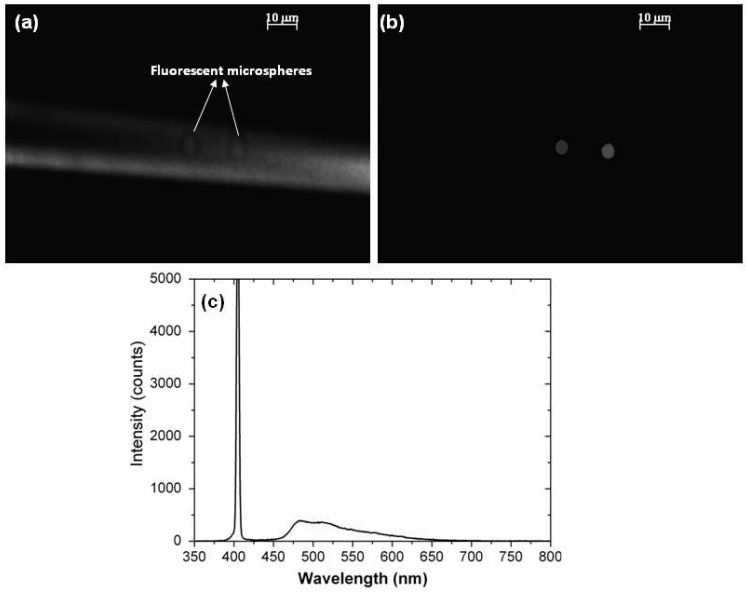

Figure 4.20: (a) Microscopic image showing the trapped fluorescent microspheres inside the HC-PCF (imaged with 50X/0.5NA objective lens), (b) processed image and (c) fluorescence signal obtained from the same fiber.

figure 4.20(b). The fiber containing fluorescent microsphere sample is then checked for fluorescence signature characterisation and analysis using an optical set up as shown in figure 4.17. A continuous wave (CW) diode-pumped solid-state (DPSS) 404 nm laser (output power ≈5 mW) is coupled into the proximal end of PCF, immobilized with fluorescence sample, using a high precision single mode fiber coupling (FC) unit (Melles Griot Pte Ltd). The beam emerging from the distal end of the fiber is focused to a high quantum efficiency spectrophotometer (Ocean Optics, QE-65000) using a microscope objective (20X, 0.65NA). The spectrometer is coupled to a PC which displays the spectrum. The obtained spectrum is given in figure 4.20(c).

A further experiment was performed to show that our experimental platform using HC-PCF also allows for transferring the trapped sample from fiber to a different fluid medium. This was done by translating optical trap along the length of fiber. The fiber containing microsphere sample is positioned as in figure 4.13(a). The approximate position of the microsphere sample is spotted under white light illumination with the imaging objective lens (L_4 in figure 4.13(a)). Now the laser beam is switched ON and the translational motion along the axis of the fiber is

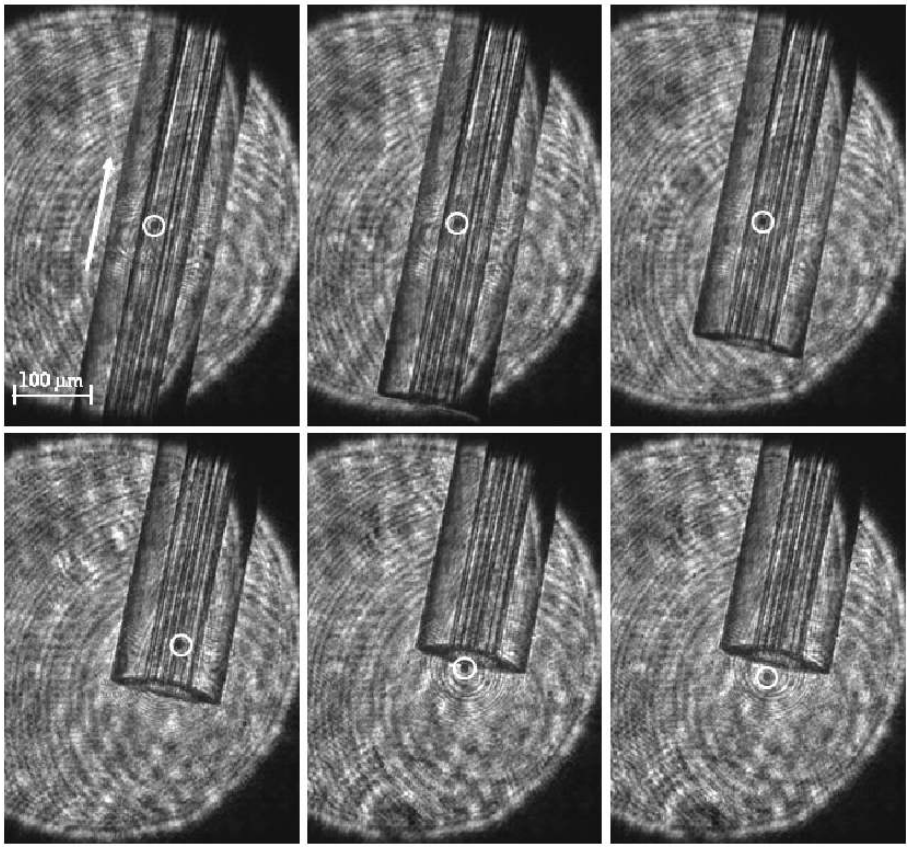

Figure 4.21: Sequential images (1 s interval), (a) to (f), showing the movement of microsphere from the central core to the liquid medium by translating optical trap along the length of fiber (white arrow shows the direction of fiber movement and white line encircling particles position is guide to the eyes). Images were cropped to show important features.

achieved by manually translating the sample chamber stage. The movement is monitored throughout using the CCD camera. The particle is found to be coming out of the fiber holes to the liquid medium due to the laser induced optical force. The sequence of images of the particle coming to the medium, shown in figure 4.21, is taken at time intervals of one second.

4.4 Multi-functional trap

Other than component miniaturization, it is also advantageous in exploring multi-functional trapping system with the incorporation of additional optical functions such as imaging, diagnosis, and sensing into the basic trapping scheme. This section details the proposed concepts and experimental demonstration carried out

with respect to multi-functional trapping employing hollow-core photonic crystal fiber (HC-PCF. Illustration of multi-functions (optical modalities) such as imaging, position sensing and fluorescence detection are carried out sequentially and simultaneously with micron-sized fluorescent beads as samples. The use of multi-functional optical system may have high potential within single-cell analysis since parallel measurements provide good statistics.

A 2-3 mm wide channel, tightly sealed on top with a cover-slip, with a volume of a few microlitres is formed on a standard microscope slide. The picture of the sample chamber is as same as shown in figure 4.15. The sample chamber is mounted on a three-axis translational stage that provides a stable and smooth translation mount for the sample chamber. The HC-PCF with central wavelength at 1550 nm is selected for this study as well. The sample chamber and the axis along the length of fiber are adjusted to be perpendicular to the probing laser beam. The sample solution containing 2 μm sized green fluorescent micro spheres (internally-dyed polymer beads) dispersed in water and is transferred to the sample chamber through the sides of the channel.

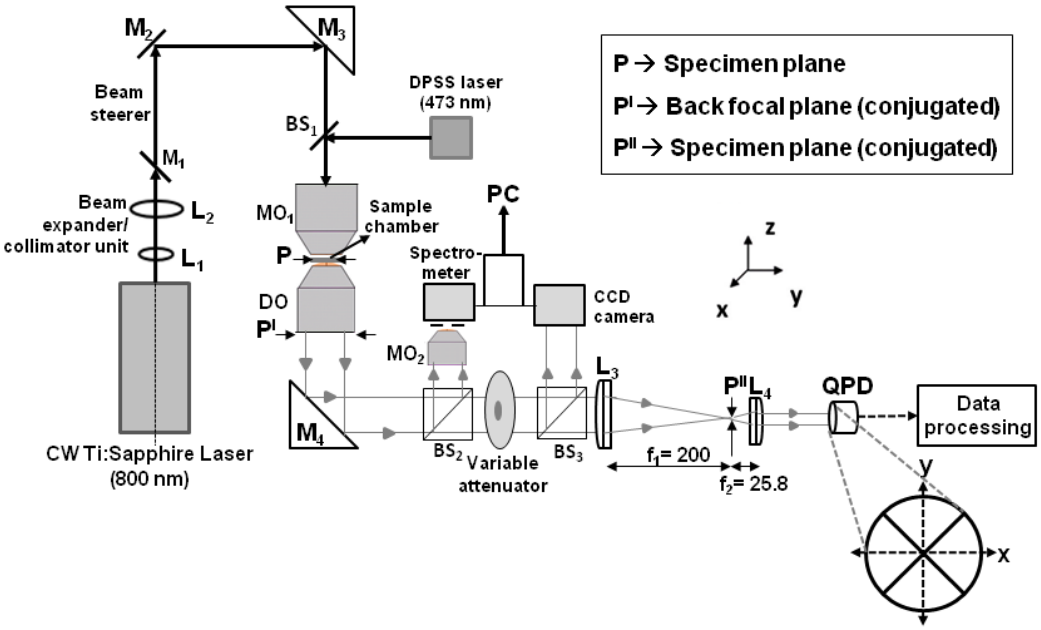

Figure 4.22: Schematic of experimental setup employed for the multi-functional optical trap system.

The schematic diagram of the experimental setup for the multi-functional opti-

cal trap employing HC-PCF is shown in figure 4.22. Trapping light was delivered by a continuous-wave Ti: Sapphire laser (Coherent Mira 900B, pumped by a Coherent Verdi V-10 frequency-doubled Nd: YVO_4 laser (532 nm)). The wavelength of the Ti: Sapphire laser is centered at 800 nm and has a repetition rate of 80 MHz when operated in femto-second pulse mode. Gaussian laser beam (TEM_{00} profile) passed through a beam collimator unit, which allowed controlling the divergence of the laser beam, is expanded and collimated and is directed to the back aperture of the trapping objective (MO_1, Newport M-40X/0.65) using a beam steering unit (formed by mirrors M_1 and M_2) and mirror M_3. A fiber coupled diode-pumped solid-state (FC-DPSS) laser (output power≈3 mW) with wavelength 473 nm was employed for fluorescence excitation. The fluorescence excitation light is directed to MO_1 using a pellicle beamsplitter (BS_1). The signal emerging from the sample chamber is collected using a detection objective (DO, Newport, M-20X/0.4) at its back focal plane and is transmitted by a mirror (M_4). A low NA DO is chosen in order to collect more light over a larger depth of focus.

Three sets of planes are defined: specimen plane (P), conjugated back focal plane (P^{I}) and conjugated specimen plane (P^{II}). The trapping and the fluorescence excitation laser beams are probed through the sample chamber as shown in figure 4.22. The signal emerging from the DO is directed towards a high quantum efficiency spectrometer (QE 65000, Ocean Optics), operating with a spectral range of 200 to 1100 nm and optical resolution within range of 0.14-7.7 nm FWHM, using a microscope objective lens (MO_2). The digital CCD camera (PL-A741; *PixeLINK*, Ottawa, Canada) is used for acquiring images and is triggered under computer control to take bright field videos or images of the sample at a desired sampling rate. The detection signal is also demagnified using a pair of lenses (plano-convex lens (L_3) and objective lens (L_4)) to project it onto a position detector. The focal distances of L_3 and L_4 are 200 mm and 25.8 mm, respectively. The QPD detects the changes in the forward scattered light pattern with the changes in the particles position and these changes are measured using a PC oscilloscope and analysed us-

ing PicoScope 3204 (*Pico Technology Ltd.*, UK) software installed in a PC. The obtained digital signals can be acquired and stored for further analysis using the said software. The specifications of QPD and PC oscilloscope are given in **Appendix A**. The QPD outputs a voltage signal corresponding to the displacement of the bead along the x- and y-axes (V_x and V_y), thereby indicating the position/ location of the bead.

4.4.1 Results and discussions

The central wavelength of the Ti: Sapphire laser is tuned to be at 800 nm. The beam is expanded as explained in the earlier section for filling the back pupil of microscope objective lens. The laser power measured before the objective lens is 220 mW. The fiber in the sample chamber is adjusted such that the probing beam points exactly towards the cleaved end of the fiber (*i.e.,* in the transverse direction). The microparticles around the fiber end are initially attracted laterally and trapped and guided to the core of HC-PCF. Movement of particle close to the fiber end is collected through detection objective and is directed to CCD camera, spectrometer and quadrant Photodetector as shown in figure 4.22. Figure 4.23 shows the images of particle being trapped and guided into the core of HC-PCF, acquired with CCD camera by probing the laser beam transversely to the central core.

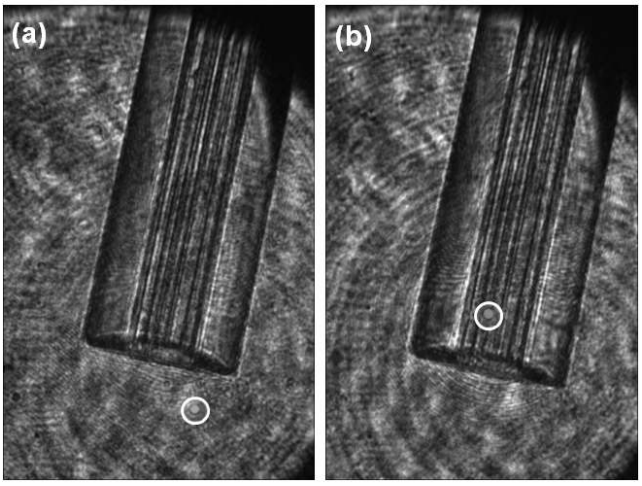

Figure 4.23: (a) & (b) shows images of a particle being trapped within an HC-PCF (solid white line encircling particles positions are guide to the eyes).

4.4.1.1 Fluorescence measurements

The fluorescence at the trapped region was measured and characterized simultaneously by exciting the region with a fiber-coupled blue laser (wavelength, λ = 473 nm) as shown in the figure 4.22. Here, the excitation laser is directed to the trapping region using a pellicle beam splitter (BS_1). The spectrometer collects the light emerging from the microscope objective (DO) through the transfer optics as represented in figure 4.22. When there is no particle in the core of HC-PCF, the collected spectra have peaks corresponding to the trapping light beam (λ = 800 nm) and fluorescence excitation source (λ = 473 nm) only. With the fluorescent polymer bead trapped and guided to the trapping region inside the central core of HC-PCF, the collected spectra also contain the emitted fluorescent signal. In our experiment, spectra are acquired at the time interval of 2 seconds and the obtained result is shown in the figure 4.24.

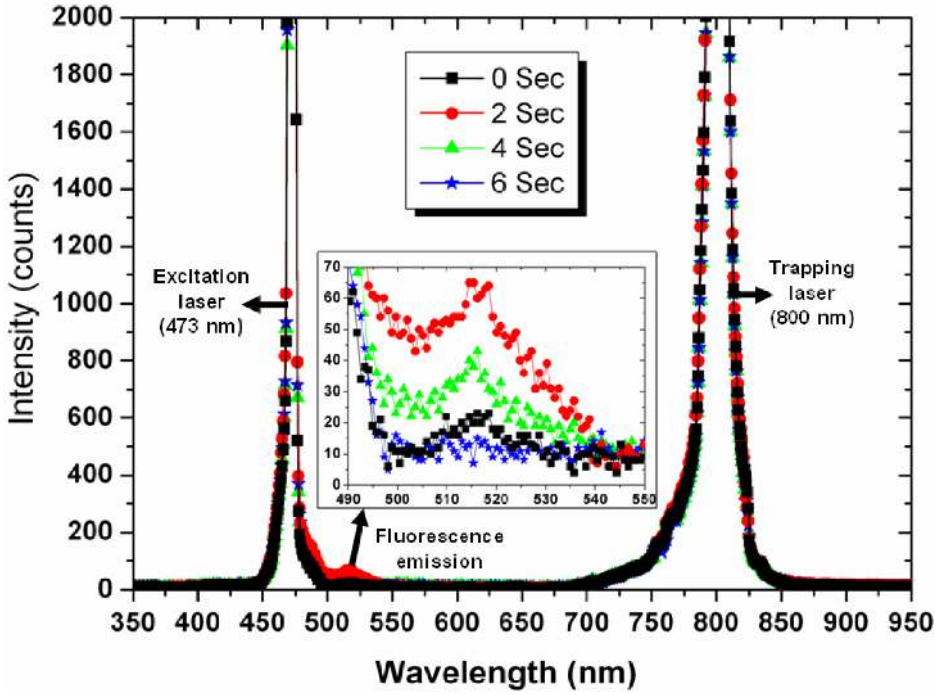

Figure 4.24: Optical spectrometer data obtained at the back focal plane of detection objective at time intervals of 2 seconds. In this configuration, an 800 nm laser is used to trap the bead. The 473 nm laser is used as the fluorescence excitation source [Inset: Fluorescence emission region is enlarged].

The variations in the fluorescent signal intensity with respect to wavelength at

different intervals of time are expanded in the inset of figure 4.24. The scattered trapping light from the sample chamber, the fluorescence excitation and emission lights are clearly observed in the presence of particle. The fluorescence intensity measurements are carried out continuously during the trapping process. For convenience, the data at instances t = 0, 2, 4 and 6 seconds are shown in figure 4.24. The fluorescent intensity is related to the location of particle with respect to the optical axis. As particle gets trapped and reaches extremely close to the optical axis, fluorescent intensity becomes a maximum (at t = 2 seconds in fig. 4.24). As particle moves away from the optical axis, the emitted fluorescent signal decreases gradually and there is no significant fluorescent emission (e.g. at t = 6 seconds in figure 4.24) as the particle moves completely away from the trapping region. Hence the fluorescent signal gives an indication about the position of the particle around the trapping region with respect to the optical axis.

4.4.1.2 Particle tracking using QPD

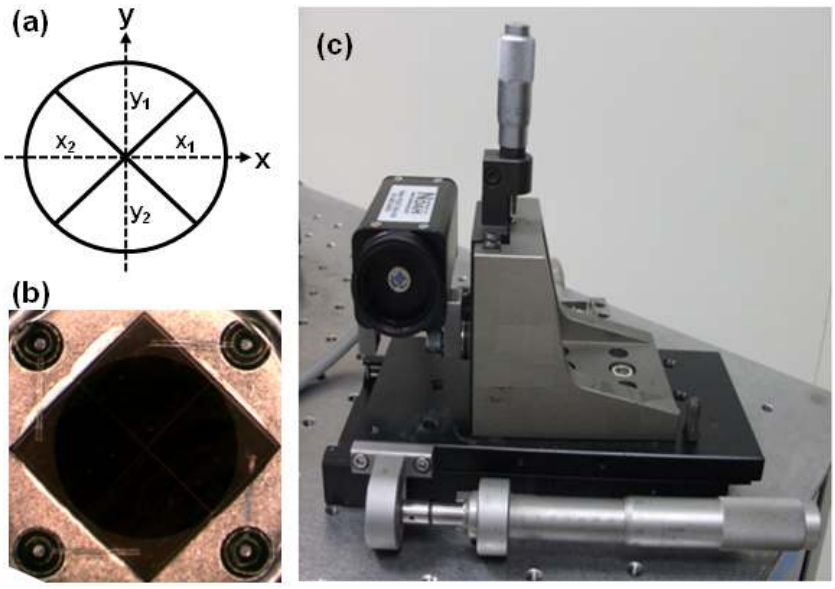

Figure 4.25: (a) schematic representation, (b) microscopic image of detector surface and (c) QPD positioned by an X-Y micrometer translator.

Position measurement of the trapped particle in the proposed scheme is carried out by employing quadrant photodiode (QPD) based on back-focal plane (BFP)

scheme. The quadrant photodiode (QPD) is the foremost way of gathering information on the position of the trapped particle relative to the center of the trap. The details about the QPD circuit and working principle can be found in section 2.1.4 and **Appendix B**. Focused light beam from the microscope objective (MO_1) passes through the sample chamber containing microspheres where the diffracted light from the microsphere interferes with the undiffracted light. The light pattern at the BFP of the detection objective (DO) is projected onto the QPD detector by associated collection optics as detailed in figure 4.22. The analog circuitry inside QPD forms voltages V_x and V_y corresponding to real X and Y positions of the trapped particle with respect to the centre of trap. The linear position sensor module (*Noah Corp.*) employed in our experiment is based on a PSD and outputs a position in terms of voltage. Figure 4.25 (b) shows the microscopic image of the detector. In order to convert the voltage signals to the actual displacement units, the QPD must be calibrated. The calibration experiment is described in the next section.

Position calibration

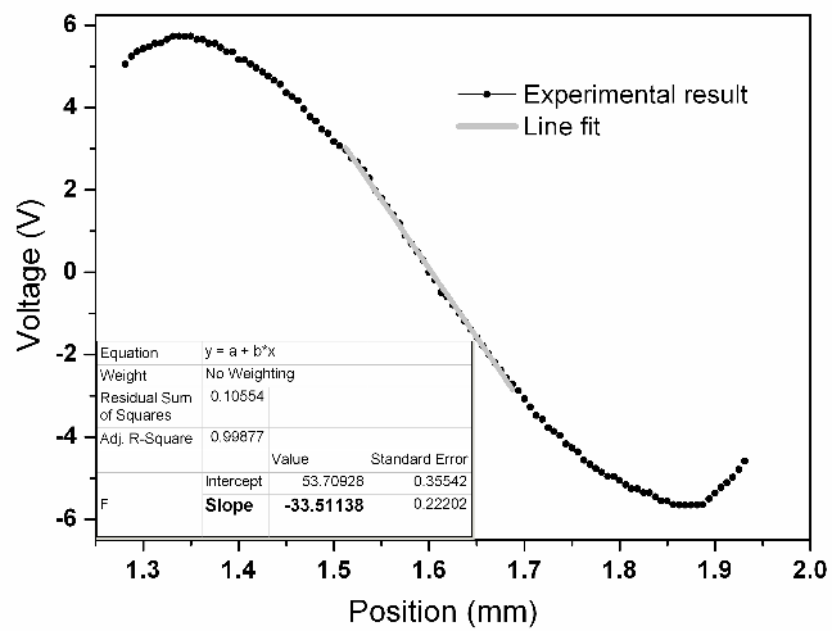

Figure 4.26: Output voltage signal acquired by moving the QPD at steps of 10 μm in X-direction versus displacement of the microsphere imaged to QPD.

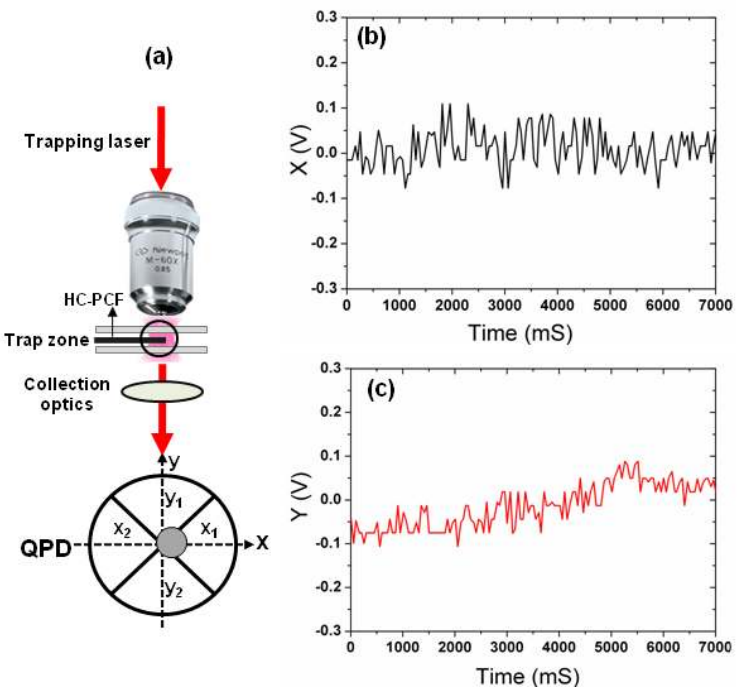

Figure 4.27: (a) Schematic of the setup employing QPD for particle detection, yielding electrical signals proportional to the particle displacements. Quadrant photodiode signals corresponding to the particle positions along the (b) X and (c) Y directions.

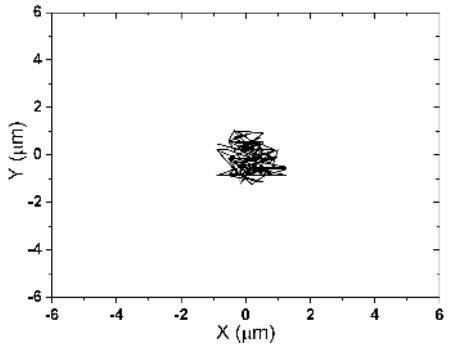

Figure 4.28: Brownian motion of the trapped bead projected on the x-y plane.

A 1 μm polymer microsphere bead attached to the glass surface (the high-salt buffer of this sample makes the bead stick to the glass by hydrophobic interaction) is used as the sample. The QPD is scanned along X-direction at steps of 10 μm and the related displacement is of a trapped sphere imaged to the QPD is indicated by the corresponding QPD voltage. The obtained result is shown in figure 4.26. Here, the X-axis represents the reading on the micrometer stage in x-direction of QPD and corresponding voltage reading from the QPD is represented on Y-axis. It is

clear from the figure 4.26 that output voltage changes linearly with displacement of the microsphere in certain region. Hence the detection signal is linear for small bead displacements within that region. The slope of linear fit for this region provides the ratio of output voltage to the displacement of the bead. The ratio obtained is about 33.5 mV/μm. The ratio of the voltage to the real displacement of the bead is obtained by multiplying the magnification of bead with this value. In our experiment the ratio is about 2.58, so the ratio of output voltage to the real displacement is about 86.43 mV/μm.

The particle tracking system employing QPD is schematically represented in figure 4.27. The forward scattering beam from the sample chamber is collected with the collection optics. Details on the collection/transfer optics can be seen in figure 4.22. The collection optics project the forward scattered beam onto a quadrant photodiode which is used to track the motion of the trapped particle in the transverse (x-y) plane. Hence, the X and Y voltage signals are acquired using QPD concurrently with imaging (figure 4.23) and fluorescence measurements (figure 4.24) while the particle is being trapped to the central core of HC-PCF. The obtained signals are shown in figure 4.27(b). These voltage signals correspond to the particle positions along the X and Y directions. The X and Y voltage signals are converted to the displacement values based on the position calibration data. The Brownian motion of the trapped bead is reconstructed using the positional data as shown in figure 4.28.

4.5 Conclusion

A novel optical manipulation and detection method is proposed and illustrated in this chapter by combining an optical trap methodology, HC-PCF and detection techniques. The transmission characteristics of the probe beam at the central core are numerically studied for HC-PCFs with different central wavelengths. The presence of fundamental and higher-order partial bandgaps is observed in the transmission spectrum. We have further studied the field intensity distribution

surrounding the silica microsphere particle located at the central core of the water filled fiber. The variation of field distribution surrounding the sphere with wavelength is found to be in accordance with the partial bandgaps observed in the transmission characteristics. Such a pseudo-bandgap must be considered for HC-PCF based transverse trapping applications since the wavelength of the trapping beam should not be within these stop bands. A 2D-FDTD simulation based on rigorous diffraction analysis method is carried out to numerically illustrate optical trapping of small sized particle inside the hollow-core of an HC-PCF using an external beam focused transversely along Γ-M direction. The intensity distribution is monitored at the central hollow-core for both TE and TM modes and photonic partial bandgap effects are observed in the transmission spectrum for both polarizations. The evolution of transverse forces acting on the particle along the transverse direction is calculated using Maxwells stress tensor for free particle suspended in water and for particle inside water filled HC-PCF. Though the nature of force acting on the particle located inside water filled HC-PCF is quite different from that on the free particle suspended in water, it is possible to give complete control over the particle kept close to the wall of HC-PCF. From the obtained force data, the dynamic motion of the sphere inside the hollow-core is also simulated. The results show that the central hollow-core can be used as an efficient trapping medium by employing transverse beam.

Further, an optical trapping system is designed where a near-infrared laser light is focused using a microscope objective to create an optical trap across a liquid-filled HC-PCF. The fluorescent microsphere particles loaded into the hollow-core by optical trapping methods can be maneuvered by translating the trap along the length of HC-PCF. The particle is subjected to multiple characterizations such as imaging and fluorescence signature characterization. The liquid-filled HC-PCF is washed externally without disturbing the sample trapped inside the core and the sample particle is subsequently moved to a different medium by translating the trap along the length of HC-PCF. Further, a multi-functional optical system has been

proposed and developed based on the above principle that have much functionalities in terms of trapping, imaging, position sensing and fluorescence signature characterization from a cell-like particle, sequentially or simultaneously. The proposed methodology with the miniature size offers a disposable, sterile and highly sensitive platform for detection and separation of cell like particles in a very low sample volume. Such results are expected to be a driving force towards an efficient integrated trapping platform employing HC-PCF for biomedical applications.

Chapter 5

Conclusions and Future Research Directions

This chapter concludes the thesis highlighting the salient and original contributions made. The future research directions are explained by highlighting the potential research challenges ahead.

5.1 Conclusion

5.1.1 Major Contributions

The major contributions of this research thesis, in this context, can be summarized as follows:

- Analytical investigation and experimental verification of fluorescence sensing studies employing HC-PCFs based on refractive index (RI) scaling law.
- Conceptualization, design and development of a sensor for detection of protein in an extremely low sample volume [such as $\approx$ 20 pg of ER alpha protein specifically in a 50 nL sample volume].
- Fundamental research into the transverse optical trapping mechanism inside the HC-PCF.
- Proposed and illustrated a multi-functional optical trapping system configuration for transverse optical trapping of micron sized samples inside HC-PCF. The system is expected to perform multi-functional analysis for cell like particles in terms of trapping, imaging, position sensing and fluorescence signature characterization.

Novel optical manipulation and detection techniques based on microstructured photonic crystal fiber have been proposed and illustrated in this thesis. Such a system can ultimately be integrated into a device such as a heterogeneous biochip with built-in microfluidic delivery and other non-optics based analysis and synthesis functionalities. The unique guiding mechanism and other structural and dispersion properties of the photonic crystal fibers offer variety of advantages over conventional optical fiber. The high light-matter interaction and ability to hold fluids or fluid borne particles enable HC-PCFs function as ideal platforms for optical manipulation and detection of micron scaled inorganic or biological species inside the central core.

In order to understand light guidance and transmission at various wavelengths, near-field imaging of the hollow-core fiber was carried out. It was found that the major portion of the optical power is located in the hollow-core or in the first few rings of cladding. By filling all holes with test samples, the light is guided in the fiber walls itself and only an evanescent interaction occurs between sample and light. The evanescent sensing in the hollow-core photonic crystal fiber (HC-PCF) is having many advantages over the conventional fiber, whose guidance is based on total internal reflection. Major advantages are the higher light-matter interaction, easier fiber preparation (no need to remove cladding as in conventional fiber), broader bandwidth, access certain wavelength regimes which are difficult to explore using conventional fiber etc. In order to understand the sensitive detection of bio-chemical solutions using photonic crystal fiber based evanescent-wave sensor, a proof of concept study of the technique was carried out. The fluorescent sample was introduced as a solution into the air holes of the fibers that function as cladding.

An efficient fluorescence sensing scheme based on HC-PCF has been demonstrated on the basis of refractive index scaling law. On filling the air holes with fluid medium, there is a shift in photonic bandgap edge (PBE) and change in refractive index sensitivity. The dependence of the shift in the photonic bandgap edge on the background and the ambient indices are studied analytically. It was found that

in a water filled fiber, the effect of background index on shift in central wavelength (PBE Shift) is much significant than that of the ambient index. The variations in the central wavelength for different filling material indices are studied in the case of HC-PCFs with cladding made of pure fused silica with array of air holes running along the entire length of the fiber. A proof of concept study has been performed by infiltrating fluorescence microsphere sample volume inside HC-PCF and the quantification of fluorescence intensity is analyzed using spectroscopic method. The sensitivity has been compared for similar fiber with different dispersed media and different fibers with same dispersed medium. This result promises the possible application of HC-PCF in specifically detecting the presence of biomolecules in a very low sample volume. Immobilization of biorecognition elements on the inner surface of the holey region of the fiber could provide a new class of PBGF-based fluorescent biosensors with high sensitivity which requires low volume of sample.

An optical method using hollow core photonic crystal fiber for protein detection is described. An antigen-antibody binding method to detect ER alpha protein in ultra small quantity of sample is demonstrated. In general this sensor can be applied for any other protein of interest too. The proposed methodology is implemented in array format immuno recognition of specific protein using a hollow core photonic crystal fiber. The primary step of the experiment is to activate the silica inner core of the fiber to facilitate the detection of ER protein. Poly-L-lysine is used to pre-coat the inner wall of the fiber to create an activated surface that can bind the targeted protein effectively. In the second step, ER alpha positive (MCF-7) and negative cell (MDA-MB-231) lysates are allowed to stick inside different HC-PCF in order to bind with specified antibodies. The primary antibody raised against ER alpha protein (antirabbit) is subsequently used to recognize the bio molecule even in fragments, which is available on the core surface. In the current work we used the Alexa Fluor 488 (Green fluorescent dye) and Alexa Fluor 555 Goat anti-rabbit IgG (Red fluorescent dye) as a secondary antibody compatible to the anti-ER alpha protein. The fluorescence fingerprints of the Estrogen Receptor alpha protein

were observed under fluorescence microscope and its optical characteristics were also analyzed using the spectrophotometer. Fluorescence signal was observed inside the fiber core under microscope in case of fluorescent protein labelled MCF-7 cell immobilized HC-PCF, whereas fluorescent protein labelled MDA-MB-231 cell showed literally no signal. This method has an additional advantage that the immobilized sample can be analyzed spectroscopically using a simple optical set up. The distribution of fluorescence inside the fiber immobilized with ER positive cell and the localization of protein across the length of the fiber has been investigated by image processing means. The developed technique enables to recognize $\approx$ 20 pg of ER alpha protein specifically in a 50 nL sample volume, which is expected to offer great potential as biosensor for medical diagnostics applications. This method holds great promise in that the hollow-core photonic crystal fiber can be used as a potential biosensor for medical diagnosis and therapeutics.

The strong interaction between the guiding light and the sample inside the core can lead to HC-PCFs being considered as ideal platforms for the research on the manipulation and characterization of micron-scale inorganic or biological samples. Optical trapping of small sized particle inside the hollow-core of liquid-filled HC-PCFs are numerically demonstrated using FDTD method and Maxwell stress tensor for employing theses fibers for trapping fluorescent sample. The transmission intensity distributions at the central hollow-core of liquid-filled HC-PCFs are monitored using an external beam focused transversely along Γ-M direction for both TE and TM modes. The presence of fundamental and higher-order partial bandgaps is observed in the transmission spectrum for both polarizations. Such a pseudo-bandgap must be considered for HC-PCF based transverse trapping applications since the wavelength of the trapping beam should not be within these stop bands. The evolution of transverse forces acting on the particle along the transverse direction is studied for particle inside HC-PCFs. Based on the numerical study, ethanol filled HC-PCF with central wavelength 1550 nm is selected for experiment. The results show that the central hollow-core can be used as an efficient trapping

medium by employing transverse beam configuration.

Optical trapping inside HC-PCF is performed by probing laser beam across the length of fiber experimentally as well. Micron sized particles guided and trapped into the hollow-core by optical trapping methods can be moved by translating the trap along the length of HC-PCF. The trapped particles are subjected to multi-optical modality analysis (multiple characterizations) such as imaging and spectroscopic analysis. The liquid-filled HC-PCF is washed externally so as not to affect the fluorescent sample trapped inside the core. Then it is placed on another sample cell to which sample is to be guided using the optical trap. After developing the above mentioned novel trapping, imaging or spectroscopic methods by making use of microstructured PCF, thesis targets at the integration of it into a multi-functional optical trap. The multi-functional optical system has much functionality in terms of trapping, motion control, and position sensing and signature characterization from a cell-like particle, sequentially or simultaneously. The multi-functional trap incorporating PCF is expected to have much significance in the biomedical fields in terms of system performance and multiple functionalities.

In our traverse optical trapping experiment using HC-PCF, fluorescent microspheres dispersed in water was employed as the sample with which the optical manipulation and detection studies were performed. Such dielectric spheres can serve as first simple models of living cells in biological trapping experiments and also as basic particles in physical trapping experiments. In typical biophysical experiments, a polystyrene bead chemically attached to the biomolecule or cell under study is optically trapped, and the analysis of its dynamics allows one to gain insights into the mechanics of the object it is attached with [111, 112]. Appropriate modification of our developed system/concept can lead to optical trapping application of biological objects including cells which are also in our near-future research interests. The trapping force acting on biological cell is much smaller than that of polystyrene beads (refractive index, n $\approx$ 1.59) due to the lower average refractive index of cells (n $\approx$ 1.36-1.4). This relative reduction in total force can

be overcome by using more light to create a stronger trap; but it should be noted that the increase in light intensity may damage the cell. Also, the cells shape may deviate from a perfect sphere that can also reduce trap stiffness. The modulations in amplitude and phase of trapping light will allow trapping low-index particles or cells with improved trap stiffness for the future experiments [113]. With the proposed concepts, it is expected to achieve transportation, manipulation and isolation of cells in a sample volume as small as the order of a few nanolitres. Though the thesis proves the proposed concepts only with fluorescent particles, the derived system and concepts can be applied to cells and relevant biomedical applications. Further, the proposed optical configuration has the advantage that it can be used to separate/sort smaller number of cells and yet deliver a high yield. For example, identification of specific cell types in a cell sample derived from a subject can indicate the presence of a disease (e.g. cancer) or predisposition to such a disease while isolation of adult stem cells (e.g. mesenchymal stem cells-MSCs) can be used in subsequent cell therapy [114].

A small and inexpensive device such as the proposed one may offer a disposable, sterile and highly sensitive platform for detection and separation of cell like particles in a very low sample volume that will be highly promising in the future translational medicine. Such results are expected to be a driving force for developing new types of optical manipulation techniques for potential biomedical and lab-on-a-chip applications. These proposed concept and method are favoured over other reported/ conventional methods in case of rare or precious cells, for example, primary cells that may not lead to large cell populations. Reagent use is limited in such a small environment. A small and inexpensive device such as the proposed one may offer a disposable, sterile platform for cell separation that would bring the technology of cell separation to a wider number of researchers in the field of biosciences.

5.2 Future research directions

The developed optical manipulation and detection system can be improved further for specific applications in the future. The future work in this context can be focussed to enhance the performance of the system in terms of flexibility and functionality. The control over laser beam movement and sorting are the important functionalities to be incorporated for immediate practical application of the developed system.

Currently the developed system has limited control on moving trap and is not possible to construct groups of traps. This necessitates scanning laser beam over a range of angles, or to control the output angle of a laser beam with high precision. The incorporation of acousto-optic deflector (AOD) to the system can provide such functionalities [34, 115]. The flexibility, accuracy, and speed of AODs will facilitate to create large arrays of optical traps which can be changed dynamically. By means of AOD, a single laser beam can be divided among hundreds of optical tweezers in the focal plane. The laser beam can be scanned rapidly from point to point in the sample using AODs to produce arrays of tweezers with great control over the position of the traps. Hence by incorporating custom-made driving electronics, single or even groups of traps can be created that will be controlled by the PC or repeatedly by programs.

The optical trapping in the proposed system is achieved with a high NA objective. The need for a high NA objective to achieve the optical trap considerably limits the field of view of the device (restricted to few hundreds of micrometers). Also the degree of freedom from the restriction of motion is found to be small. In order to avoid such difficulties, fiber optic probe based trapping principle is introduced [116, 117, 118]. The fiber optic trap system relies on the same working principle as the optical trapping but the laser beam is delivered through an optical fiber instead of objective. In absence of any lenses, the light beam emerging from fiber will be diverging. In the case of single lensed fiber trap, lens tip will act as a focusing (converging) point for the high optical gradient trap. By incorporating

lens ended fiber instead of objective lens, improved functionality of the optical manipulation beyond that of conventional optical trapping and sorting methods can be achieved.

In a single lensed fiber trap, the trapped objects can be moved easily and freely, in coordination with the trapping fiber. Also the trapping point can be easily located. The smallest transmission window was one of the major concerns in the case of conventional single mode fiber based fiber optic trap. The emergence of photonic crystal fiber can revolutionize the area of bio-imaging or trapping due to its novel properties. For example, photonic crystal fiber can support multiple wavelengths. In particular, endlessly single mode photonic crystal fiber can transmit any wavelength of light in a single-mode. Hence they offer simple and effective means for trapping particles or cells with light of a particular wavelength and simultaneous spectroscopic measurements with light of a different wavelength. In a probe based scheme, double-clad photonic crystal fiber (DC-PCF) has many advantages over the conventional fibers because of its unique properties- the single-mode central core and the high NA multimode inner cladding. Further, endlessly single mode core of DC-PCF has a hexagonal shaped output mode and consequently the mode output does not propagate with a Gaussian dependency as in the case of conventional fiber. The mode profile comes to a focus at a finite distance away from the end faces of the fiber. This property will be particularly advantageous in the application of DC-PCF based fiber probe for optical trapping and manipulation applications.

A double-clad photonic crystal fiber (DC-PCF) based dual-modality probe is designed to obtain simultaneous image and spectrum from a sample surface. The details of this study are explained in **Appendix C**. The comparison in collection efficiencies of these microstructured fibers, hollow-core and double-clad PCFs, is performed. The SEM images of the fibers under study are shown in Figure 5.1(a) & 5.1(b). The DC-PCF (DC-165/16-Passive, Crystal-fibre A/S) has a core diameter of 16 μm, an inner cladding with a diameter of 165 μm and NA of 0.6 at wavelength

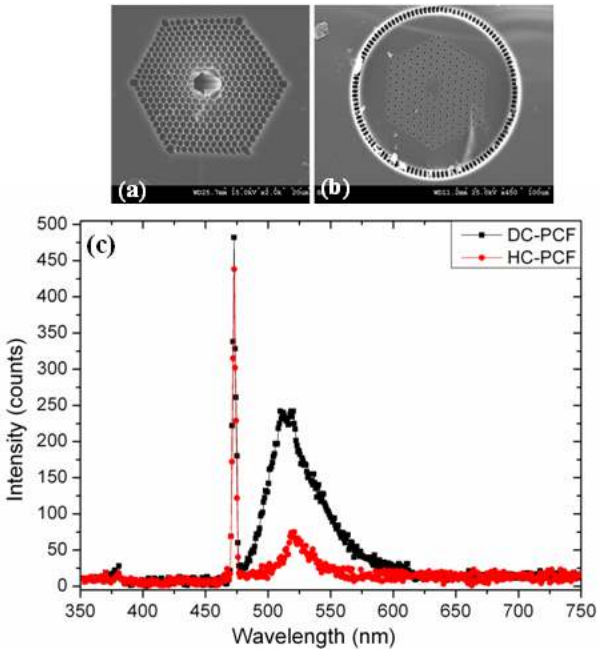

Figure 5.1: The SEM images of the used (a) hollow-core PCF and (b) double-clad PCF in the probe configuration. (c) The collected intensity spectra of Green wop dye using hollow-core PCF and double-clad PCF based fiber probe at constant illumination.

600 nm. Within the outer cladding region of 350 μm in diameter, a ring of air holes is used to efficiently guide and collect light in the pure silica multimode inner cladding. The hollow-core fiber has a core size of 6 μm, cladding diameter of 122 μm and NA of 0.2. The sample used in this study is a phantom tissue stained with green wop fluorescent dye. The excitation light source used in this study is a 473 nm Diode-Pumped-Solid-State (DPSS) laser (output power $\approx$10 mW) and is delivered to the sample surface from the probe distal end. The reflected and fluorescence light from the surface plane of the target specimen is collected and focused at the hollow-core/double-clad photonic crystal fiber plane. A 20X objective lens with 20 mm working distance is placed at the proximal end of probe which collects the emitted light and is directed to the high quantum efficiency spectrometer using a pellicle beam splitter. The collected intensity spectra using these two fibers are shown in figure 5.1(c) for comparison. The large numerical aperture of the outer core in the DC-PCF can enhance collection of emitted fluorescence when compared to the hollow-core fiber. This promises the application of this fiber for optical trapping.

Stand-alone self-aligned microlenses have been fabricated in our recent study for fiber probe imaging [119]. Details about this study are described in **Appendix D**. This work focuses on the stand alone microlenses along with custom-fabricated specialty optical fiber, such as imaging fiber. Stand-alone self-aligned microlenses have been fabricated employing micro-compression molding and are then attached at the end facet of specialty fiber optics. By properly adjusting the distal end of the lensed fiber probe, the particle can be attracted and trapped near the tip. The fiber could be translated to arbitrary locations so as to transport the trapped particle for further sorting applications. Hence, the integration of trapping using fiber probe with the developed hollow-core fiber trap scheme, it is able to manipulate particle inside the core and sort them to a different channel based on the emitted fluorescence. The sorting application is possible with the improved orientation control obtained through the movement of the mechanical manipulator holding the fiber probe. Incorporation of recent advancement in R & D in light sources, detectors and AOD to the multiple trap and subsequent selective manipulation of individual micro particles may enhance the performance of developed multi-functional optical system to a great extent.

In brief, the microstructured HC-PCF can act as a biocompatible, chemically inert and disposable platform for sensing and trapping of cell/micron sized particle. The sample consumption rate is reduced through assay miniaturization. The optical manipulation and sorting of micron sized particle with the ultimate goal of a low-cost portable instrument for point of care diagnosis can be achieved by incorporating AOD and lens-ended fiber probe based trapping principles. It can lead to an all-fiber optic, miniaturized system that can be employed for optical manipulation, fluorescence detection, imaging, sorting and/or assembly of microscopic particles and biological cells in an extremely low sample volume with optical forces from a focused laser beam (optical tweezers).

Appendices

Appendix A

Specifications of QPD and PC oscilloscope

Table A.1: QPD Specifications

Spectral range	190 - 1100 nm
Transimpedence Gain	104 or 105 (selectable)
Bandwidth	DC to 30 kHz
Output Signal Range:	
X, Y Position	0 to ±10 V
SUM	0 to 10 V
DC Supply Requirement	±15 V, 50 mA
Nominal Beam Power Range	0.001 to 1 mW

Table A.2: Oscilloscope Specifications

Bandwidth	50 MHz
Sampling rate (repetitive signals)	2.5 GS/s
Sampling rate (single shot)	50 MS/s
Channels	2 + Ext trigger
Oscilloscope time bases	5 ns/div to 50 s/div
Time-base accuracy	50 ppm
Spectrum ranges	0 to 25 MHz
Dynamic range	50 dB
Signal generator	Fixed 1 kHz square wave
Trigger modes	Free Run, Auto, Repeat, Single and Save To Disk On Trigger
Pre/post trigger	-100% to +100%
Buffer size	256 kS
Resolution	8 bits
Accuracy	3%
Ranges	±100 mV to ±20 V
Input impedance	1 MΩ

Appendix B

QPD for position detection

The Quadrant photodiode (QPD) consist of four photodiodes arranged in quadrant form in order to allow calculation of X and Y position. The voltages of the photodiodes vary linearly with the amount of light incident upon it in a certain range of light intensities. Each quadrant in QPD generates a voltage corresponds to light intensity incident upon it. The analog circuit forms voltages V_x and V_y corresponds to real X and Y position of the trapped particle with respect to the centre of trap.

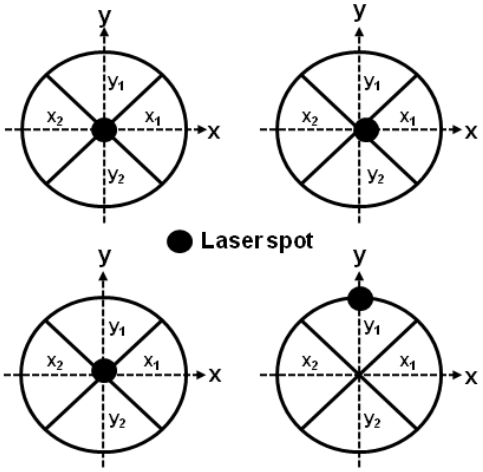

Figure B.1: Schematic of optical trapping and position measurement using the quadrant photodiode detector (QPD).

Let x_1, x_2, y_1 and y_2 are the individual Photodetector element signals. There are three outputs such as *Sum*, X and Y. The Sum signal corresponds to the total light level incident on the quadrant Photodetector. The X and Y position signals are normalized such that their values are independent of the total light level, and are functions of position only. This is true as long as the Sum value is between 0.1 and 10 volts.

$$Sum = x_1 + x_2 + y_1 + y_2 \tag{B.1}$$

$$X = 10 \times \frac{(x_1 - x_2)}{(x_1 + x_2)} \tag{B.2}$$

$$Y = 10 \times \frac{(y_1 - y_2)}{(y_1 + y_2)} \tag{B.3}$$

When there is nothing in the trap or the trapped bead is exactly at the centre of trap (figure B.1(a)), the laser beam is focused at the centre of QPD resulting zero signals along X and Y direction. The sum voltage (maximum *sum*) should be adjusted so that it is less than 10 volts. While the trapped particle moves slightly away from the trap centre, the laser spot moves on the QPD results a nonzero values of X and Y position signals. For example, If the spot falls on the right side of detector (as in figure B.1(b)), the X voltage is positive. Alternatively, X voltage is negative if the spot falls on left side. In similar way, Y voltage is positive when the spot falls on the upper side (see figure B.1(c)) and negative while it is on the lower side. If the spots go out of the four elements of detectors active area, the *Sum* voltage is lesser than the maximum *Sum* voltage.

Appendix C

Dual-modality scanning probe using Double-clad PCF

Initial experimental analyses were also carried out for a probe based system using photonic crystal fiber. It describes the use of photonic crystal fiber (PCF) and a commercial micro-camera to construct a dual mode endoscope aimed at bio-medical applications. Hollow-core and double-clad are tested and the latter found to have superior performance. The double-clad PCF combined with a micro-camera and tested using a fluorophores stained phantom.

C.1 Fiber based fluorescence probe

In a single fiber based fluorescence probe, the effective fluorescence detection volume from a region adjacent to its tip is determined by both its illumination and collection volumes. To be detecting a particle at a given point P, it has to get excited and simultaneously a photon emitted from this point has to be collected by the same fiber. In a double-clad fiber, the excitation mode is single. The illumination intensity distribution adjacent to the tip of the flat cleaved fiber is assumed to be axis symmetric. Hence the excitation intensity distribution is approximated by a TEM_{00} Gaussian beam.

$$I(r,z) = \frac{2}{[\pi\omega^2(z)]} exp\left[\frac{-2r^2}{\omega^2(z)}\right] \tag{C.1}$$

$$\omega(z) = \omega_0 \left[1 + \left(\frac{z\lambda}{\pi\omega_0^2}\right)^2\right]^{1/2} \tag{C.2}$$

The illumination intensity distribution adjacent to the tip of the flat cleaved fiber is assumed to be axis symmetric. The probability of collection is given by the

probability of a photon emitted from the sample reaching the fiber end, provided the angle of incidence is less than or equal to the maximum acceptance angle () of the fiber. Where, n denotes the refractive index of outside medium and NA denotes the numerical aperture.

$$\alpha = sin^{-1}\left(\frac{NA}{n}\right) \tag{C.3}$$

C.2 Comparison of collection efficiencies of Hollow-core and Double-clad PCF

Photonic crystal technology offers new types of fibers which can remove most of the limitations while using the conventional silica fibers[75]. In photonic crystal fibers light guidance is possible even through air[76]. The possibility of guidance mechanism in air allows the suppression of back ground noise signal. The double-clad fiber is another type of photonic crystal fiber, where the central single mode core is surrounded by a lower index cladding region. This cladding region is further surrounded by a region of even lower index so that light can be confined and propagated. Thus Double-clad PCFs made of pure silica have attracted research in biosensing and bioimaging to improve the system efficiency because of their dual function of single-mode and multimode delivery through the central core and the inner cladding region of high numerical aperture (NA), respectively[39, 77]. By utilizing an optical fiber having double claddings we could deliver an excitation beam through the small diameter conventional core of a fiber and subsequently collect the excited fluorescence light signal using the large diameter inner cladding of the same fiber. Due to small diameter of the fiber, it can be easily incorporated into the existing endoscopy equipment.

The performance of two different types of photonic crystal fibers, double clad and hollow-core, for beam delivery/collection have been analyzed. In a single-fiber based fluorescence probe, the effective fluorescence detection volume from a region adjacent to tip of the fiber is determined by both its illumination and

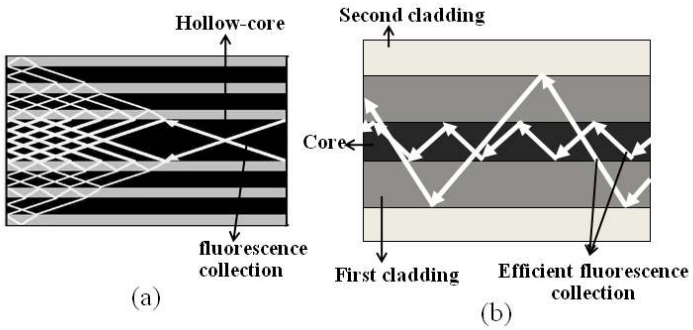

Figure C.1: Illustration of fluorescence collection in a (a) hollow-core PCF and (b) Double-clad PCF.

collection volumes. For a particle to be detected at a given point it has to get excited and simultaneously a photon emitted from this point has to be collected by the same fiber. The hollow-core PCF guide light in a hollow-core by means of photonic bandgap effect achieved using a holey structure around the core. These fibers guide light in single mode with greatly improved power delivery compared to conventional single mode fibers. Double-clad fibers are characterized by a central single-mode core surrounded by an inner and an outer cladding region. Here, the excitation mode is single.

The figureC.1 illustrates the efficient fluorescent collection in a double clad fiber compared to the hollow-core fiber. Here, the single mode core is surrounded by a larger numerical aperture outer core (also acts as cladding of the inner core) which can collect the emitted fluorescence. Since the fluorescent emission is assumed to be constant in every direction, the collection probability is proportional to solid angle subtended by the area of intersection at the point where the particle to be detected is placed. Since double-clad fiber can propagate light in the inner cladding region by total internal reflection, enhanced fluorescence collection is possible. The NA of the inner cladding is generally twice as large as that of conventional single-mode fibers. Thus efficient fluorescence collection is possible in double-clad fiber along with single mode excitation. The diverging beam from 473 nm DPSS Laser (output power = 10mW) was collimated by a lens and was diverted to the fiber coupling unit [Newport F-91TS Coupler] using a pellicle beam splitter (B.S). The microscope

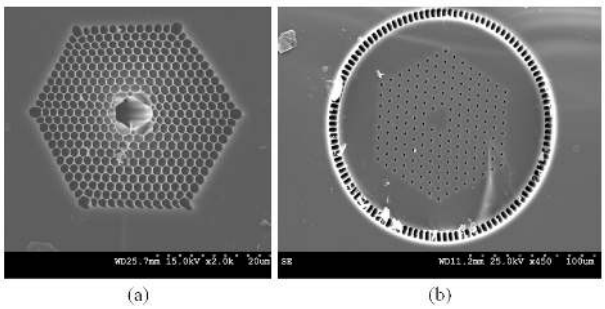

Figure C.2: The SEM images of the used (a) hollow-core and (b) double-clad fibers in the probe configuration.

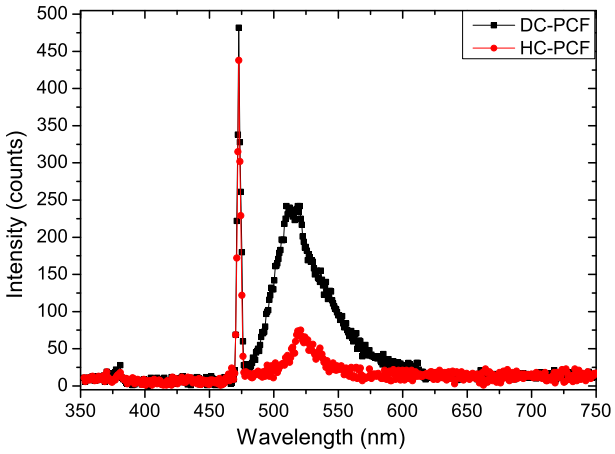

Figure C.3: The collected intensity spectra of Green wop dye using hollow core and double-clad fiber probe at constant illumination.

objective (MO) lens (Newport M-20X, 0.4NA) integrated with the FC coupler at the proximal end of double-clad/hollow-core PCF performs the illumination as well as the collection duties. The double-clad PCF ((DC-165/16-Passive, Crystal-fibre) has a core diameter of 16 μm, an inner cladding with a diameter of 165 μm and NA of 0.6 at wavelength 600 nm. Within the outer cladding region of 350 μm in diameter, a ring of air holes is used to efficiently guide and collect light in the pure silica multimode inner cladding. The hollow-core fiber (Air-6-800, Crystal-fibre) has a core size of 6 μm, cladding diameter of 122 μm and NA of 0.2. The SEM images of the fibers under study are shown in figureC.2.

The sample used is a phantom tissue (Simulab Corp.), stained with Green wop fluorescent dye. The source light is delivered to the sample surface from the probe

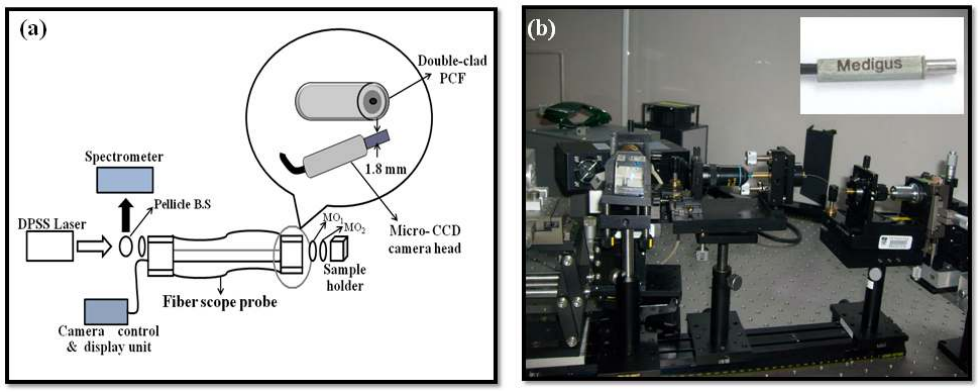

Figure C.4: (a)Schematic diagram of integrated dual-modality fiber probe based on double-clad fiber and micro camera and (b) Actual prototype (inset: Image of camera head of diameter 1.8 mm)

distal end. The test phantom sample was placed on the XYZ scanning stage as shown in the figure C.4. The reflected and fluorescence light from the surface plane of the target specimen will be collected and focused at the hollow-core/double-clad photonic crystal fiber plane. A 20x objective lens with 20 mm working distance is placed at the proximal end of probe which collects the emitted light and is directed to the high quantum efficiency spectrometer using a pellicle beam splitter. The large numerical aperture of the outer core in the double-clad photonic crystal fiber can enhance collection of emitted fluorescence when compared to the hollow-core fiber. The collected intensity spectra using these two fibers are shown in figureC.3 for comparison. The collection efficiency of the double-clad fiber is found to much higher than that of the hollow-core fiber.

C.3 Dual-modality probe using Double-clad PCF and Micro-camera based system

A dual-modality scanning probe has been designed by exploring the properties of double-clad fiber and micro CCD based system. The main advantage of dual-modality approach is that it is capable of acquiring the information (both spatial and chemical, simultaneously) from the targeted tissue site by replacing the diagnostic test and methodology. The incorporation of two modalities into a single

fiber scope will definitely increase the diagnostic accuracy and will provide more favourable results.

The double-clad PCF has a core diameter of 16 μm, an inner cladding with a diameter of 165 μm and NA of 0.6 at wavelength 600 nm. The fiber core is surrounded by air holes with a hole to hole pitch ratio of 0.26. Within the outer cladding region of 350 μm in diameter, a ring of air holes is used to efficiently guide and collect light in the pure silica multimode inner cladding. The 1.8mm x 1.8mm CCD camera includes a micro camera head that has high quality optics and a shielded camera cable. The picture of camera used for the study is given in figure C.4. It also includes control unit including a video processor and keypad for operating the camera. The small packaging of the camera head is specially designed for small diameter endoscopes. The camera is found to be highly applicable in endoscopy imaging due to its small head size and its high performance.

The fiberscope probe has been developed with distal end consists double-clad fiber and micro-camera. Again, the sample used is a phantom tissue (Simulab Corp.), stained with fluorophores. In this study, Green wop and red wop fluorescent dyes were selected as the staining agent (fluorochrome) for the phantom tissue. The sample is placed over a 3-axis scanning stage which acts as the sample holder. The stage can be varied over few centimetres with micrometer resolution, which effectively increases the scanning range of the fiber probe. The purpose of such kind of stage is for ex-vivo studies.

The DPSS laser (473 nm), which is diverted through a pellicle B.S is coupled to the proximal end of double-clad fiber. The diverging beam emerging from the distal end of the image fiber was allowed to pass though the 2-f lens system, which is configured using two microscope objective (M.O) lenses [Newport M-20X, 0.4 (MO_1) and Olympus UMPLAN FI 50X/0.8 (MO_2)]. The reflected and fluorescence light from the target specimen surface will be collected at the double-clad fiber, which can transmit light through the core as well as the inner cladding. This light is collected through a M.O and is transmitted to high quantum efficiency

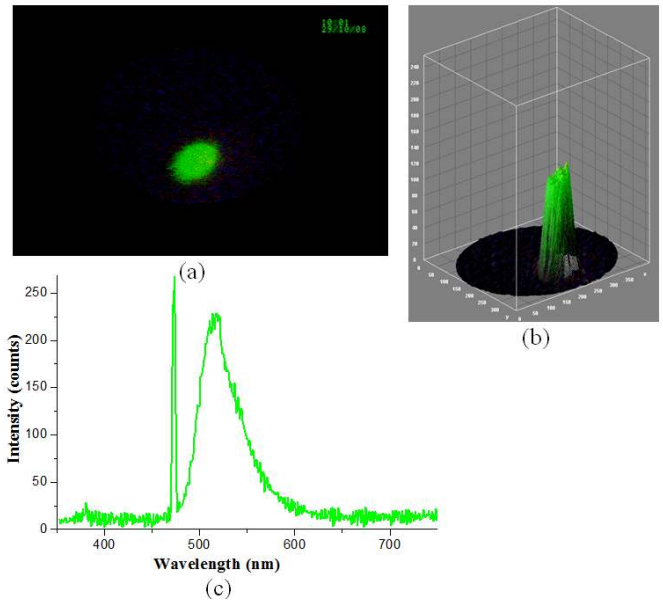

Figure C.5: (a) Spatial information (image), (b) corresponding interactive 3D surface plot and (c) Chemical information (Spectrum) of the phantom tissue sample coated with Green wop fluorescent dye

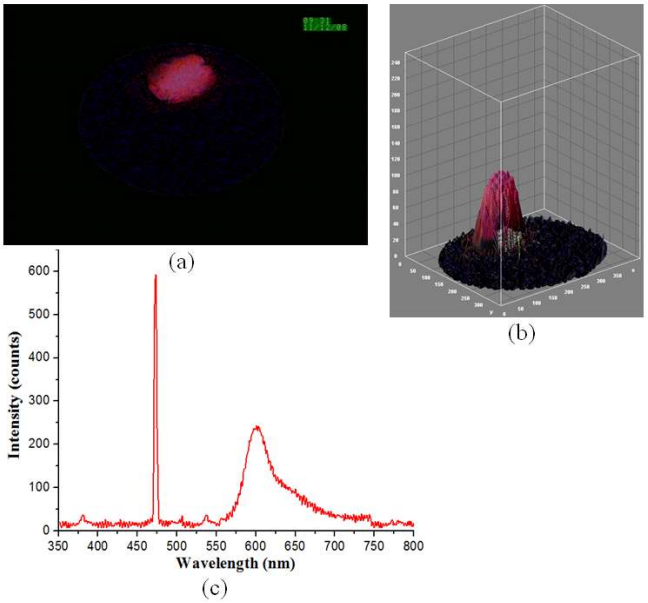

Figure C.6: (a) Spatial information (image), (b) corresponding interactive 3D surface plot and (c) Chemical information (Spectrum) of the phantom tissue sample coated with Red wop fluorescent dye

(QE) spectrometer using a pellicle beam-splitter. The spectrometer attached to a personal computer which displays the chemical information (spectrum) of the sample under study. Simultaneously the spatial information (image) about the object is obtained through the micro camera which is configured as shown in figure C.4 . The obtained image and spectra of the tissues stained with green wop and red wop fluorescent dyes are given in figure C.5 and figure C.6 respectively. The interactive 3D surface plot of the obtained images is also given.

C.4 Conclusion

A dual-modality probe for measuring spatial and chemical information simultaneously by exploring the properties of photonic crystal fiber and a micro-CCD camera is demonstrated. Both hollow-core and double-clad PCFs were incorporated in the probe configuration and the collection efficiencies were compared. Then the probe was designed with distal end consisting of highly efficient double clad PCF and micro-CCD camera. The designed probe configuration has only been used in ex-vivo conditions, where the sample was placed over a XYZ stage which allows an extremely large scanning range. But it can be employed in in-vivo diagnostics too. The main advantage of dual-modality approach is that it is capable of simultaneously acquiring both the spatial and chemical information from the targeted tissue site. The incorporation of two modalities into a single fiber scope can increase the diagnostic accuracy and provide more favourable results. This proposed probe and methodology is expected to find potential applications in the area of bio-medical diagnostics.

Appendix D

Micro-lens-ended fiber optic probe for fluorescence imaging and sensing application

A double-clad PCF based dual-modality fiber scope probe that can simultaneously obtain the spectroscopic signature and images was proposed and demonstrated in **Appendix C**. However, the use of microscope objective lenses for signal collection at the distal end makes this probe unsuitable for in-vivo applications. Microlens-ended fibers, which have found tremendous interest in the recent past, find potential biomedical applications, in particular, in endoscopic imaging. This work focuses on the stand alone microlenses along with custom-fabricated specialty optical fiber, such as imaging fiber, for probe imaging applications. Stand-alone self aligned microlenses have been fabricated employing micro-compression molding and then attached at the end facet of imaging fiber. The details of the fabrication process can be found in reference [120]. The schematic of how the molded lens is attached on the top of an image fiber (Fujikura 15-600N, 600 μm diameter, 15000 Pixels) is shown in figure D.1(a). The distal end is designed so that it can be used for the working distances raging from 1.3 mm to several millimeters. The distance between the microlens and the fiber is adjustable.

D.1 Fluorescence Collection and Imaging efficiency

Schematic of experimental set up used for imaging and collection efficiency of fluorescent signal is shown in figure D.1(b). The whole system consists of a coherent light source (473 nm, DPSS laser), intermediate optical elements, tissue sample and the detector (high resolution CCD). The sample used is microspheres (glass microbubbles (GMB) from 3M Scotchlite) of approximate size of 10 μm doped in polyvinyl alcohol (PVA) matrix. Rhodamine6G dye is added as fluorescence

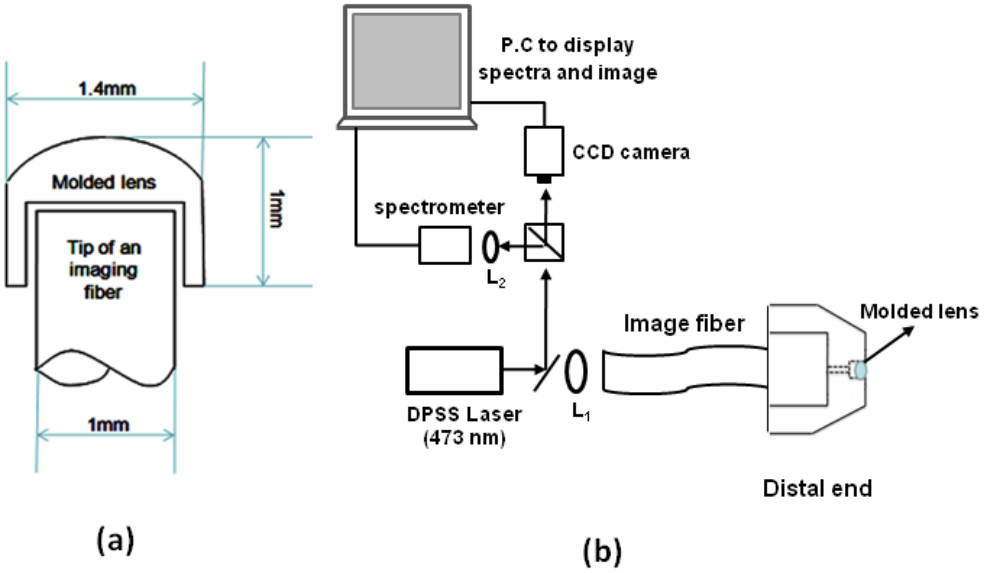

Figure D.1: (a) schematic showing arrangement of molded lens and imaging fiber and (b) schematic of optical set up used for analyzing the fluorescence collection efficiency and imaging efficiency of micro-lens-ended image fiber.

material in the glass microbubbles (GMB)-polyvinyl alcohol (PVA) composite.

The diverging beam from Laser was collimated by a lens and was diverted to the micro-lens-ended image fiber using a dichroic filter. The reflected and fluorescence light from the surface plane of the target specimen will be collected by the same fiber. A 20x objective lens with 20 mm working distance is placed at the proximal end of probe which collects the emitted light and is directed to the high quantum efficiency spectrometer (QE 65000, Ocean Optics) and CCD camera as shown in figure D.1(b). The spectrometer and camera are connected to the PC.

The fluorescence collection efficiency of the molded lens is verified by comparing the collected spectra and images of micro-lens-ended image fiber probe with a bare image fiber. Figure D.2 shows the collected spectra from the fluorescent target with and without microlens. It is clear that the collection of fluorescence light is enhanced in the presence of microlens. The image of the microsphere sample obtained at a working distance of 10 mm is also compared for lens-ended fiber and bare fiber. The obtained result is depicted in figure D.3. This result further confirms that micro-lens enhances the imaging ability of the image fiber and the

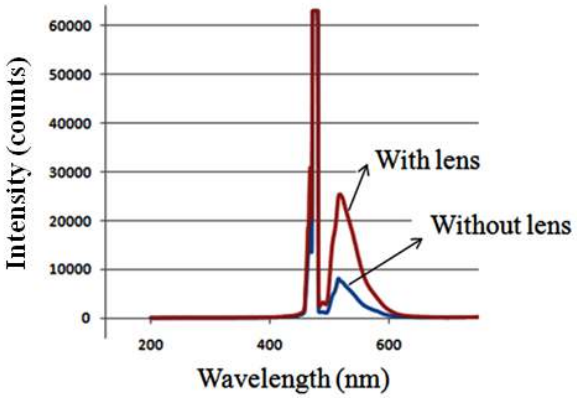

Figure D.2: Comparison between fluorescent signals collected using micro-lens-ended image fiber and bare image fiber.

working distance is also increased. In summary, we have shown that the microlens

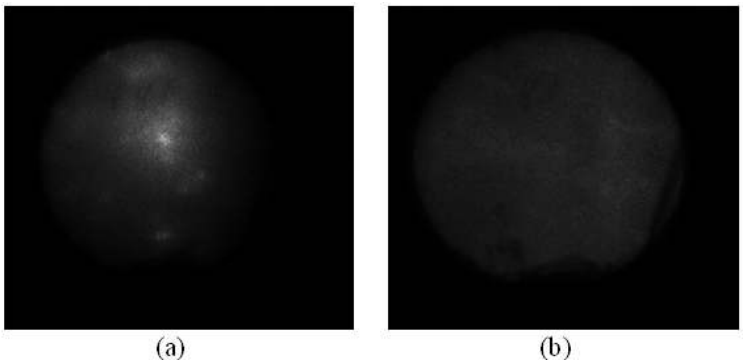

Figure D.3: Images taken from the micro-sphere sample at working distance of 10 mm, (a) micro-lens-ended fiber and (b) bare fiber.

fabricated by employing micro-compression molding method can enhance the performance of optical-fiber-based endoscopic imaging. A comprehensive study of the said microlens-ended fibers has been performed in order to substantiate the improvement in different performance parameters, such as focusing ability, efficiency of fluorescence collection and imaging.. The imaging system in fluorescence detection mode shows the suitability of the lens-ended fiber in imaging of micro-spheres smaller than the size of the nuclei of human epithelial cells. This is expected to find applications in the area of bio-medical diagnostics. Further research will be focused on improving both the lateral and axial resolution of the system by optimizing the fiber and lens parameters.

Publications list

List of International Journals

1. **V K Shinoj** and V M Murukeshan, "An HC-PCF based multi-functional optical system for trapping, position sensing and detection of fluorescent particles", *Optics Letters*, Volume 37, Issue 9 (2012).

2. **V K Shinoj** and V M Murukeshan, "An integrated HC-PCF transverse optical trapping system for optical manipulation and detection", *Journal of Applied Physics*, Volume 111, Issue 2, 023106 (1-5) (2012).

3. **V K Shinoj** and V M Murukeshan, "An HC-PCF fluorescence spectrocopy for detection of microsphere samples based on refractive index scaling law", *Optics & Photonics Journal*, Volume 1, Issue 2, 85-90 (2011).

4. **V K Shinoj** and V M Murukeshan, "Numerical investigation and optimization of Hollow-core photonic crystal fiber for optical trapping of fluorescent micro particles", *Micro & Nano Letters*, Volume 6, Issue 9, 785-789 (2011).

5. Saraswathi P, **V K Shinoj**, V M Murukeshan, and P Padmanabhan, "Highly sensitive optical detection of specific protein in breast cancer cells using Micro structured fiber in extremely low sample volume", *Journal of Biomedical Optics*, Volume 15, Issue 1, 017005 (1-6), 2010. (Also included in the March 1, 2010 issue of *Virtual Journal of Biological Physics Research*).

6. **V K Shinoj**, V M Murukeshan, Saraswathi P and P Padmanabhan, "Dual-modality probe based on photonic crystal fiber and micro-CCD camera for simultaneous sensing and imaging applications", *Optical Engineering*, Volume 48, Issue 10, 103601 (1-4), 2009.

List of International Conferences

1. **V K Shinoj** and V M Murukeshan, "Numerical study on Transverse Optical Trapping Inside Hollow-core PCF", *ICOPEN 2011* (Poster presentation), Singapore, March 23-25, 2011.

2. **V K Shinoj** and V M Murukeshan, "Finite-Difference Time-Domain analysis of bandgap characteristics of transversely probed Hollow-core photonic crystal fibers", *IEEE Photonics Global 2010* (Oral Presentation), Singapore, December 14-16, 2010.

3. **V K Shinoj** and V M Murukeshan, "Imaging and spectroscopic investigation of localized fluorescent particles inside HC-PCF for biomedical applications", *ICCMB2* (Oral Presentation), Singapore, August 2-4, 2010.

4. V M Murukeshan, Saraswathi P, **V K Shinoj** and P Padmanabhan, "Photonic crystal probe for specific protein detection using in extremely low sample volume", *World Molecular Imaging Congress* (Poster presentation), Montreal, Canada, September 23-26, 2009.

Bibliography

[1] H. Li, L. Ying, J. J. Green, S. Balasubramanian, and D. Klenerman. Ultrasensitive coincidence fluorescence detection of single DNA molecules. *Anal. Chem*, 75(7):1664–1670, 2003.

[2] A. Dorfman, N. Kumar, and J. Hahm. Highly sensitive biomolecular fluorescence detection using nanoscale ZnO platforms. *Langmuir*, 22(11):4890–4895, 2006.

[3] A. Manz, N. Graber, and H. M. Widmer. Miniaturized total chemical analysis systems: a novel concept for chemical sensing. *Sens. Actuators, B*, 1(1-6):244–248, 1990.

[4] D. R. Reyes, D. Iossifidis, P. A. Auroux, and A. Manz. Micro total analysis systems. 1. Introduction, theory, and technology. *Anal. Chem.*, 74(12):2623–2636, 2002.

[5] H. Andersson and A. Van den Berg. Microfluidic devices for cellomics: a review. *Sens. Actuators, B*, 92(3):315–325, 2003.

[6] A. Ashkin, JM Dziedzic, and T. Yamane. Optical trapping and manipulation of single cells using infrared laser beams. *Nature*, 330:769–771, 1987.

[7] J. Voldman, M. L. Gray, M. Toner, and M. A. Schmidt. A microfabrication-based dynamic array cytometer. *Anal. Chem.*, 74(16):3984–3990, 2002.

[8] A. R. Wheeler, W. R. Throndset, R. J. Whelan, A. M. Leach, R. N. Zare, Y. H. Liao, K. Farrell, I. D. Manger, and A. Daridon. Microfluidic device for single-cell analysis. *Anal. Chem.*, 75(14):3581–3586, 2003.

[9] A. Ashkin. Acceleration and trapping of particles by radiation pressure. *Phys. Rev. Lett.*, 24(4):156–159, 1970.

[10] H. Zhang and K. K. Liu. Optical tweezers for single cells. *J. R. Soc. Interface*, 5(24):671, 2008.

[11] C. Creely, G. Volpe, G. Singh, M. Soler, and D. Petrov. Raman imaging of floating cells. *Opt. Express*, 13(16):6105–6110, 2005.

[12] M. Ericsson, D. Hanstorp, P. Hagberg, J. Enger, and T. Nystrom. Sorting out bacterial viability with optical tweezers. *J. Bacteriol.*, 182(19):5551, 2000.

[13] F. Arai, C. Ng, H. Maruyama, A. Ichikawa, H. El-Shimy, and T. Fukuda. On chip single-cell separation and immobilization using optical tweezers and thermosensitive hydrogel. *Lab Chip*, 5(12):1399–1403, 2005.

[14] S. Weiss. Fluorescence spectroscopy of single biomolecules. *Science*, 283(5408):1676, 1999.

[15] A. Castro and E. B. Shera. Single-molecule detection: applications to ultrasensitive biochemical analysis. *Appl. Opt.*, 34(18):3218–3222, 1995.

[16] M. J. Lang, P. M. Fordyce, A. M. Engh, K. C. Neuman, and S. M. Block. Simultaneous, coincident optical trapping and single-molecule fluorescence. *Nat. Methods*, 1(2):133–139, 2004.

[17] S. Mandal and D. Erickson. Optofluidic transport in liquid core waveguiding structures. *Appl. Phys. Lett.*, 90:184103, 2007.

[18] Philip Russell. Photonic Crystal Fibers. *Science*, 299(5605):358–362, 2003.

[19] T. N. Buican, M. J. Smyth, H. A. Crissman, G. C. Salzman, C. C. Stewart, and J. C. Martin. Automated single-cell manipulation and sorting by light trapping. *Appl. Opt.*, 26(24):5311–5316, 1987.

[20] A. Ashkin and J. M. Dziedzic. Optical trapping and manipulation of viruses and bacteria. *Science(Washington)*, 235(4795):1517–1517, 1987.

[21] A. Chiou, M. T. Wei, Y. Q. Chen, T. Y. Tseng, S. L. Liu, A. Karmenyan, and C. H. Lin. Optical Trapping and Manipulation for Biomedical Applications. *Biophotonics*, pages 249–273, 2008.

[22] A. Ashkin and J. M. Dziedzic. Optical levitation by radiation pressure. *Appl. Phys. Lett.*, 19(8):283–285, 2009.

[23] A. Ashkin, J. M. Dziedzic, J. E. Bjorkholm, and Steven Chu. Observation of a single-beam gradient force optical trap for dielectric particles. *Opt. Lett.*, 11(5):288–290, 1986.

[24] A. Ashkin. History of optical trapping and manipulation of small-neutral particle, atoms, and molecules. *IEEE J. Sel. Top. Quantum Electron.*, 6(6):841–856, 2002.

[25] A. Ashkin. Forces of a single-beam gradient laser trap on a dielectric sphere in the ray optics regime. *Biophys. J.*, 61(2):569 – 582, 1992.

[26] Yasuhiro Harada and Toshimitsu Asakura. Radiation forces on a dielectric sphere in the Rayleigh scattering regime. *Opt. Commun.*, 124(5-6):529 – 541, 1996.

[27] K. Visscher and G. J. Brakenhoff. Theoretical study of optically induced forces on spherical particles in a single beam trap. I: Rayleight scatterers. *Optik*, 89(4):174–180, 1992.

[28] P. A. Neto and H. M. Nussenzveig. Theory of optical tweezers. *Europhys. Lett.*, 50:702, 2000.

[29] K. C. Neuman and S. M. Block. Optical trapping. *Rev. Sci. Instrum.*, 75:2787, 2004.

[30] K. Svoboda and S. M. Block. Biological applications of optical forces. *Annu. Rev. Biophys. Biomol. Struct.*, 23(1):247–285, 1994.

[31] R. Roy, S. Hohng, and T. Ha. A practical guide to single-molecule FRET. *Nat. Methods*, 5(6):507–516, 2008.

[32] M. W. Allersma, F. Gittes, M. J. deCastro, R. J. Stewart, and C. F. Schmidt. Two-dimensional tracking of ncd motility by back focal plane interferometry. *Biophys. J.*, 74(2):1074–1085, 1998.

[33] J. Gelles, B. J. Schnapp, and M. P. Sheetz. Tracking kinesin-driven movements with nanometre-scale precision. 1988.

[34] R. M. Simmons, J. T. Finer, S. Chu, and J. A. Spudich. Quantitative measurements of force and displacement using an optical trap. *Biophys. J.*, 70(4):1813–1822, 1996.

[35] G. Hong-Lian, L. Chun-Xiang, L. Zhao-Lin, D. Jian-Fa, H. Xue-Hai, C. Bing-Ying, and Z. Dao-Zhong. Displacement and force measurements with quadrant photodetector in optical tweezers. *Chin. Phys. Lett*, 20:950, 2003.

[36] S. Keen, J. Leach, G. Gibson, and M. J. Padgett. Comparison of a high-speed camera and a quadrant detector for measuring displacements in optical tweezers. *J. Opt. A: Pure Appl. Opt.*, 9:S264, 2007.

[37] F. Gittes and C. F. Schmidt. Interference model for back-focal-plane displacement detection in optical tweezers. *Opt. Lett.*, 23(1):7–9, 1998.

[38] S. F. Tolic-Norrelykke, E. Schaffer, J. Howard, F. S. Pavone, F. Jülicher, and H. Flyvbjerg. Calibration of optical tweezers with positional detection in the back focal plane. *Rev. Sci. Instrum.*, 77:103101, 2006.

[39] K. C. Neuman, E. H. Chadd, G. F. Liou, K. Bergman, and S. M. Block. Characterization of photodamage to Escherichia coli in optical traps. *Biophys. J.*, 77(5):2856–2863, 1999.

[40] H. Liang, K. T. Vu, P. Krishnan, T. C. Trang, D. Shin, S. Kimel, and M. W. Berns. Wavelength dependence of cell cloning efficiency after optical trapping. *Biophys. J.*, 70(3):1529–1533, 1996.

[41] U. Mirsaidov, W. Timp, K. Timp, M. Mir, P. Matsudaira, and G. Timp. Optimal optical trap for bacterial viability. *Phys. Rev. E*, 78(2):021910, 2008.

[42] G. Leitz, E. Fallman, S. Tuck, and O. Axner. Stress response in Caenorhabditis elegans caused by optical tweezers: wavelength, power, and time dependence. *Biophys. J.*, 82(4):2224–2231, 2002.

[43] Kerstin Ramser, Jonas Enger, Mattias Goksor, Dag Hanstorp, Katarina Logg, and Mikael Kall. A microfluidic system enabling Raman measurements of the oxygenation cycle in single optically trapped red blood cells. *Lab Chip*, 5:431–436, 2005.

[44] K. Ramser, K. Logg, M. Goksör, J. Enger, M. Käll, and D. Hanstorp. Resonance Raman spectroscopy of optically trapped functional erythrocytes. *J. Biomed. Opt.*, 9:593, 2004.

[45] A. M. Maxam and W. Gilbert. Sequencing end-labeled DNA with base-specific chemical cleavages. *Methods Enzymol.*, 65(1):499, 1980.

[46] Z. Li, K. Li, and S. Tong. Determination of nucleic acids in acidic medium by enhanced light scattering of large particles. *Talanta*, 51(1):63–70, 2000.

[47] J. R. Lakowicz and B. R. Masters. Principles of fluorescence spectroscopy. *J. Biomed. Opt.*, 13:029901, 2008.

[48] T. P. Thomas, M. T. Myaing, J. Y. Ye, K. Candido, A. Kotlyar, J. Beals, P. Cao, B. Keszler, A. K. Patri, T. B. Norris, et al. Detection and analysis of tumor fluorescence using a two-photon optical fiber probe. *Biophys. J.*, 86(6):3959–3965, 2004.

[49] H. M. Shapiro and R. C. Leif. *Practical flow cytometry.* Wiley Online Library, 2003.

[50] R. Y. Tsien. The green fluorescent protein. *Annu. Rev. Biochem.*, 67(1):509–544, 1998.

[51] M. Chalfie, Y. Tu, G. Euskirchen, W. W. Ward, and D. C. Prasher. Green fluorescent protein as a marker for gene expression. *Science*, 263(5148):802, 1994.

[52] T. Chishima, Y. Miyagi, X. Wang, H. Yamaoka, H. Shimada, A. R. Moossa, and R. M. Hoffman. Cancer invasion and micrometastasis visualized in live tissue by green fluorescent protein expression. *Cancer Res.*, 57(10):2042, 1997.

[53] S. Boutrus, C. Greiner, D. Hwu, M. Chan, C. Kuperwasser, C. P. Lin, and I. Georgakoudi. Portable two-color in vivo flow cytometer for real-time detection of fluorescently-labeled circulating cells. *J. Biomed. Opt.*, 12:020507, 2007.

[54] J. Novak, I. Georgakoudi, X. Wei, A. Prossin, and C. P. Lin. ¡ i¿ In vivo¡/i¿ flow cytometer for real-time detection and quantification of circulating cells. *Opt. Lett.*, 29(1):77–79, 2004.

[55] J. I. Peterson and G. G. Vurek. Fiber-optic sensors for biomedical applications. *Science*, 224(4645):123, 1984.

[56] C. Cordeiro, M. A. R. Franco, G. Chesini, E. Barretto, R. Lwin, C. H. Brito Cruz, and M. C. J. Large. Microstructured-core optical fibre for evanescent sensing applications. *Opt. Express*, 14(26):13056–13066, 2006.

[57] S. Smolka, M. Barth, and O. Benson. Highly efficient fluorescence sensing with hollow core photonic crystal fibers. pages 181–182, 2008.

[58] JC Knight, J. Broeng, TA Birks, and P.S.J. Russell. Photonic band gap guidance in optical fibers. *Science*, 282(5393):1476, 1998.

[59] K. Sott, E. Eriksson, E. Petelenz, and M. Goksör. Optical systems for single cell analyses. *Expert Opin. on Drug Discovery*, 2008.

[60] K. Ramser and D. Hanstorp. Optical manipulation for single-cell studies. *J. Biophotonics*, 3(4):187–206, 2010.

[61] W. Wang, Y. Liu, G. J. Sonek, M. W. Berns, and R. A. Keller. Optical trapping and fluorescence detection in laminar flow streams. *Appl. Phys. Lett.*, 67:1057, 1995.

[62] J. D. Joannopoulos and J. N. Winn. *Photonic crystals: molding the flow of light*. Princeton Univ Pr, 2008.

[63] M. Notomi. Theory of light propagation in strongly modulated photonic crystals: Refractionlike behavior in the vicinity of the photonic band gap. *Phys. Rev. B*, 62(16):10696–10705, 2000.

[64] A. Mekis, J. C. Chen, I. Kurland, S. Fan, P. R. Villeneuve, and J. D. Joannopoulos. High transmission through sharp bends in photonic crystal waveguides. *Phys. Rev. Lett.*, 77(18):3787–3790, 1996.

[65] S. Lin, J. G. Fleming, D. L. Hetherington, B. K. Smith, R. Biswas, K. M. Ho, M. M. Sigalas, W. Zubrzycki, S. R. Kurtz, and J. Bur. A three-dimensional photonic crystal operating at infrared wavelengths. *Nature*, 394(6690):251–253, 1998.

[66] H. Kosaka, T. Kawashima, A. Tomita, M. Notomi, T. Tamamura, T. Sato, and S. Kawakami. Superprism phenomena in photonic crystals: toward microscale lightwave circuits. *J. Lightwave Technol.*, 17(11):2032, 1999.

[67] R. Wang, X. H. Wang, B. Y. Gu, and G. Z. Yang. Effects of shapes and orientations of scatterers and lattice symmetries on the photonic band gap in two-dimensional photonic crystals. *J. Appl. Phys.*, 90:4307, 2001.

[68] M. A. Arnold. Fiber-optic biosensors. *J. Biotechnol*, 15(3):219–28, 1990.

[69] J. Jensen, P. Hoiby, G. Emiliyanov, O. Bang, L. Pedersen, and A. Bjarklev. Selective detection of antibodies in microstructured polymer optical fibers. *Opt. Express*, 13(15):5883–5889, 2005.

[70] J. C. Knight, T. A. Birks, P. S. J. Russell, and D. M. Atkin. All-silica single-mode optical fiber with photonic crystal cladding. *Opt. Lett.*, 21(19):1547–1549, 1996.

[71] R. F. Cregan, B. J. Mangan, J. C. Knight, T. A. Birks, P. S. J. Russell, P. J. Roberts, and D. C. Allan. Single-mode photonic band gap guidance of light in air. *Science*, 285(5433):1537, 1999.

[72] F. Helmchen, D. W. Tank, and W. Denk. Enhanced two-photon excitation through optical fiber by single-mode propagation in a large core. *Appl. Opt.*, 41(15):2930–2934, 2002.

[73] M. T. Myaing, J. Y. Ye, T. B. Norris, T. Thomas, J. R. Baker Jr, W. J. Wadsworth, G. Bouwmans, J. C. Knight, and P. S. J. Russell. Enhanced two-photon biosensing with double-clad photonic crystal fibers. *Opt. Lett.*, 28(14):1224–1226, 2003.

[74] D. Yelin, B. E. Bouma, S. H. Yun, and G. J. Tearney. Double-clad fiber for endoscopy. *Opt. Lett.*, 29(20):2408–2410, 2004.

[75] L. Fu, X. Gan, and M. Gu. Nonlinear optical microscopy based on double-clad photonic crystal fibers. *Opt. Express*, 13(14):5528–5534, 2005.

[76] J. M. Fini. Microstructure fibres for optical sensing in gases and liquids. *Meas. Sci. Technol.*, 15:1120, 2004.

[77] J. B. Jensen, L. H. Pedersen, P. E. Hoiby, L. B. Nielsen, T. P. Hansen, J. R. Folkenberg, J. Riishede, D. Noordegraaf, K. Nielsen, A. Carlsen, et al. Photonic crystal fiber based evanescent-wave sensor for detection of biomolecules in aqueous solutions. *Opt. Lett.*, 29(17):1974–1976, 2004.

[78] T. Birks, D. Bird, T. Hedley, J. Pottage, and P. Russell. Scaling laws and vector effects in bandgap-guiding fibres. *Opt. Express*, 12(1):69–74, 2004.

[79] G. Antonopoulos, F. Benabid, T. A. Birks, D. M. Bird, J. C. Knight, and P. S. J. Russell. Experimental demonstration of the frequency shift of bandgaps in photonic crystal fibers due to refractive index scaling. *Opt. Express*, 14(7):3000–3006, 2006.

[80] J. Sun and C. C. Chan. Photonic bandgap fiber for refractive index measurement. *Sens. Actuators, B*, 128(1):46–50, 2007.

[81] S. H. Aref, R. Amezcua-Correac, J. P. Carvalho, O. Frazão, J. L. Santos, F. M. Araújo, H. Latifi, F. Farahi, L. A. Ferreira, and J. C. Knight. Spectral characterization of a photonic bandgap fiber for sensing applications. *Appl. Opt.*, 49(10):1870–1875, 2010.

[82] L. Rindorf, P. E. Høiby, J. B. Jensen, L. H. Pedersen, O. Bang, and O. Geschke. Towards biochips using microstructured optical fiber sensors. *Anal. Bioanal. Chem.*, 385(8):1370–1375, 2006.

[83] T. M. Monro, W. Belardi, K. Furusawa, J. C. Baggett, N. G. R. Broderick, and D. J. Richardson. Sensing with microstructured optical fibres. *Meas. Sci. Technol.*, 12:854, 2001.

[84] Y. L. Hoo, W. Jin, C. Shi, H. L. Ho, D. N. Wang, and S. C. Ruan. Design and modeling of a photonic crystal fiber gas sensor. *Appl. Opt.*, 42(18):3509–3515, 2003.

[85] B. J. Mangan, L. Farr, A. Langford, P. J. Roberts, D. P. Williams, F. Couny, M. Lawman, M. Mason, S. Coupland, R. Flea, et al. Low loss (1.7 dB/km)

hollow core photonic bandgap fiber. In *Optical Fiber Communication Conference, 2004. OFC 2004*, volume 2, page 3. IEEE, 2004.

[86] J. B. Jensen, P. E. Hoiby, L. H. Pedersen, A. Carlsen, L. B. Nielsen, A. Bjarklev, and T. P. Hansen. Evanescent wave sensing using a hollow-core photonic crystal fiber. In *Proceedings of SPIE*, volume 5317, page 139, 2004.

[87] Hong Nguyen, Peter Domachuk, Benjamin Eggleton, Michael Steel, Martin Straub, Min Gu, and Mikhail Sumetsky. A new slant on photonic crystal fibers. *Opt. Express*, 12(8):1528–1539, Apr 2004.

[88] Kazuaki Sakoda. Symmetry, degeneracy, and uncoupled modes in two-dimensional photonic lattices. *Phys. Rev. B*, 52(11):7982–7986, Sep 1995.

[89] J. Tuominen, H. J. Hoffrén, and H. Ludvigsen. All-optical switch based on liquid-crystal infiltrated photonic bandgap fiber in transverse configuration. *J. Eur. Opt. Soc., Rapid Publ.*, 2, 2007.

[90] P. Domachuk, N. Wolchover, M. Cronin-Golomb, and F. G. Omenetto. Effect of hollow-core photonic crystal fiber microstructure on transverse optical trapping. *Appl. Phys. Lett.*, 94:141101, 2009.

[91] E. C. Mägi, P. Steinvurzel, and B. J. Eggleton. Transverse characterization of tapered photonic crystal fibers. *J. Appl. Phys.*, 96:3976, 2004.

[92] A. S. Webb, F. Poletti, D. J. Richardson, J. K. Sahu, et al. Suspended-core holey fiber for evanescent-field sensing. *Opt. Eng.*, 46:010503, 2007.

[93] D. Mogilevtsev, T. A. Birks, and P. S. J. Russell. Group-velocity dispersion in photonic crystal fibers. *Opt. Lett.*, 23(21):1662–1664, 1998.

[94] P. N. Prasad. Introduction to biophotonics. *J. Biomed. Opt.*, 10:039901, 2005.

[95] P. B. Luppa, L. J. Sokoll, and D. W. Chan. Immunosensors–principles and applications to clinical chemistry. *Clin. Chim. Acta*, 314(1-2):1–26, 2001.

[96] M. M. Bradford. A rapid and sensitive method for the quantitation of microgram quantities of protein utilizing the principle of protein-dye binding. *Anal. Biochem.*, 72(1-2):248–254, 1976.

[97] M. Gu, J. B. Haumonte, Y. Micheau, J. W. M. Chon, and X. Gan. Laser trapping and manipulation under focused evanescent wave illumination. *Appl. Phys. Lett.*, 84:4236, 2004.

[98] G. Pesce, A. C. Luca, G. Rusciano, P. A. Netti, S. Fusco, and A. Sasso. Microrheology of complex fluids using optical tweezers: a comparison with macrorheological measurements. *J. Opt. A: Pure Appl. Opt.*, 11:034016, 2009.

[99] S. Padmanabhan, V. K. Shinoj, V. M. Murukeshan, and P. Padmanabhan. Highly sensitive optical detection of specific protein in breast cancer cells using microstructured fiber in extremely low sample volume. *J. Biomed. Opt.*, 15:017005, 2010.

[100] P. Domachuk, H. C. Nguyen, and B. J. Eggleton. Transverse probed microfluidic switchable photonic crystal fiber devices. *IEEE Photonics Technol. Lett.*, 16(8):1900–1902, 2004.

[101] Michael J. Renn, Robert Pastel, and Heather J. Lewandowski. Laser Guidance and Trapping of Mesoscale Particles in Hollow-Core Optical Fibers. *Phys. Rev. Lett.*, 82(7):1574–1577, Feb 1999.

[102] F. Benabid, J. Knight, and P. Russell. Particle levitation and guidance in hollow-core photonic crystal fiber. *Opt. Express*, 10(21):1195–1203, 2002.

[103] C. Rockstuhl and H. P. Herzig. Rigorous diffraction theory applied to the analysis of the optical force on elliptical nano-and micro-cylinders. *J. Opt. A: Pure Appl. Opt.*, 6:921, 2004.

[104] V. Yannopapas. Optical forces near a plasmonic nanostructure. *Phys. Rev. B*, 78(4):45412, 2008.

[105] D. A. White. Numerical Modeling of Optical Gradient Traps Using the Vector Finite Element Method. *J. Comput. Phys.*, 159(1):13–37, 2000.

[106] B. T. Draine and P. J. Flatau. Discrete-dipole approximation for scattering calculations. *J. Opt. Soc. Am. A*, 11(4):1491–1499, 1994.

[107] S. H. Simpson and S. Hanna. Numerical calculation of interparticle forces arising in association with holographic assembly. *JOSA A*, 23(6):1419–1431, 2006.

[108] J. D. Jackson and R. F. Fox. *Classical Electrodynamics*, volume 67. 1999.

[109] J. P. Barton, D. R. Alexander, and S. A. Schaub. Theoretical determination of net radiation force and torque for a spherical particle illuminated by a focused laser beam. *J. Appl. Phys.*, 66(10):4594–4602, 2009.

[110] C. C. Huang, C. F. Wang, D. S. Mehta, and A. Chiou. Optical tweezers as sub-pico-newton force transducers. *Opt. Commun.*, 195(1-4):41–48, 2001.

[111] K. Visscher, M. J. Schnitzer, and S. M. Block. Single kinesin molecules studied with a molecular force clamp. *Nature*, 400(6740):184–189, 1999.

[112] Z. Bryant, M. D. Stone, J. Gore, S. B. Smith, N. R. Cozzarelli, C. Bustamante, et al. Structural transitions and elasticity from torque measurements on DNA. *Nature*, 424(6946):338–341, 2003.

[113] K. Dholakia and T. Čižmár. Shaping the future of manipulation. *Nat. Photonics*, 5(6):335–342, 2011.

[114] D. Gazit, B. Rubinsky, G. Pelled, and Z. Gazit. Systems And Methods For Analyzing And Manipulating Biological Samples, June 28 2007. WO Patent WO/2007/072,472.

[115] S. M. Block, C. L. Asbury, J. W. Shaevitz, and M. J. Lang. Probing the kinesin reaction cycle with a 2D optical force clamp. *Proc. Natl. Acad. Sci. U. S. A.*, 100(5):2351, 2003.

[116] K. Taguchi, H. Ueno, T. Hiramatsu, and M. Ikeda. Optical trapping of dielectric particle and biological cell using optical fibre. *Electron. Lett*, 33(5):413–414, 1997.

[117] Z. Hu, J. Wang, and J. Liang. Manipulation and arrangement of biological and dielectric particles by a lensed fiber probe. *Opt. Express*, 12:4123–4128, 2004.

[118] N. K. Metzger, E. M. Wright, W. Sibbett, and K. Dholakia. Visualization of optical binding of microparticles using a femtosecond fiber optical trap. *Opt. Express*, 14(8):3677–3687, 2006.

[119] M. Mirkhalaf, V. M. Murukeshan, S. B. Tor, V. K. Shinoj, and K. Sathiyamoorthy. Characteristics of stand-alone microlenses in fiber-based fluorescence imaging applications. *Rev. Sci. Instrum.*, 82:043110, 2011.

[120] M. Mirkhalaf, S. B. Tor, V. M. Murukeshan, N. H. Loh, and S. W. Lye. Fabrication of a stand-alone polymer microlens: design of molding apparatus, simulation and experimental results. *J. Micromech. Microeng.*, 19:095005, 2009.